An experimental study on the hydraulic conductivity of compacted bentonites in geoenvironmental applications

Claire Bennett

Geoenvironmental Research Centre

Cardiff School of Engineering

Cardiff University

Thesis submitted in candidature for the degree of Doctor of Philosophy at Cardiff University

April 2014

Acknowledgements

I would like to thank my supervisors Professor Hywel Thomas and Dr. Snehasis Tripathy for their guidance, support and motivation throughout this thesis. I am also extremely grateful to the Engineering and Physical Sciences Research Council for their financial support, without which this work would not have been possible.

I am extremely grateful to the technical staff of the School of Engineering, in particular Harry, Len, Ian, Brian, Carl, Steff, Des, Paul, Jeff and Ravi. I am thankful not only for their assistance but also for their friendship and encouragement. I would also like to thank a number of lecturers in the School of Engineering, in particular Dr. Diane Gardner and Dr. Michael Harbottle for their constant support, and Dr. Alan Kwan for his continuing encouragement.

I am so grateful to all those who I have shared an office with during my PhD - Ram, Shakil, Hesham, Panos and Majid - to who I will never be able to thank enough for their efforts and encouragement during this work. I would also like to thank all those in the GRC, including Rob, Alex, Phil, Jamie, Lee, Sanjana, Renato, Alessandro, Vaisilis, Richard, Dan, Ben, Eleni, Manju, Irfan and Mojgan.

I owe so much of the completion of this to my friends. To my wonderful girls, Emma, Becci, Alyssa, Mog and Ellen, who have been there from the beginning. To those who I have met at school and university - Brian, Ruth, Jen, Ben, Tash, Dave, Abby, Debbie, Gareth, Flora, Richard, Poorav, Matt, Owain, Owen, Rich, Rob, Joe, Mark and Julie - and all those who have shared this work with me - Iulia, Rob, Tina, Phil, Kate, Dan, Reza, Aki, Rhys, Fay and Caroline. I am especially grateful to Kat, who has contributed so much towards the final stages of this thesis.

I am grateful for the support of my family - my mum Cheryl, my brother Grant, my grandma Vera and my aunty Sandra, who have always been there for me when I have needed them. I would also like to thank Ellie, Jake, Denzel, Oscar, Bert, Alfie, Doug, Darwin, Chip and Henry for always listening, and Nick, who has been there through the highs and the lows.

I dedicate this thesis to my father, Graham, who I hope would be proud of me.

Abstract

Compacted bentonites and compacted sand-bentonite mixtures have been proposed as suitable barrier and backfill materials for the disposal of municipal solid waste and high level radioactive waste. Although unsaturated on placement, the barrier and backfill materials can become saturated subject to the availability of fluid. Detailed understanding of the saturated hydraulic conductivity of compacted bentonites and sand-bentonite mixtures is essential to ensuring the integrity of the waste disposal facility and the long-term protection of the geoenvironment.

This thesis is concerned with the experimental determination of the hydraulic conductivity of compacted MX80 bentonite and sand-bentonite mixtures (30% MX80 bentonite to 70% sand). A high capacity fixed ring modified swelling pressure cell was used for carrying out the hydraulic conductivity tests. High precision pressure-volume controllers were used to apply a range of hydraulic gradients between about 1250 and 12500 under constant head conditions. The expansion of the measuring system was studied to account for differences between inflow and outflow water volumes during the hydraulic conductivity tests. The hydraulic gradient was increased and decreased during the hydraulic conductivity tests. Chemical analysis of fluid samples collected from the inflow and outflow reservoirs after each hydraulic conductivity tests provided information about the type and amount of exchangeable cations expelled from the specimens. The inflow volume was calculated based on the system expansions. The hydraulic conductivities were calculated from Darcy's law. The saturated hydraulic conductivity of compacted bentonite and sand-bentonite specimens were also calculated based on the consolidation tests results. The gas permeability of compacted unsaturated bentonites was determined. The saturated hydraulic conductivity of compacted bentonites was assessed using various existing models. A model based on parallel plate flow was proposed in the current study. The proposed model considered the viscosity of water in the inter-platelet region and its influence on the hydraulic conductivity of compacted bentonites.

The correction of the water inflow volume by accounting for the system expansion during the hydraulic conductivity tests provided good compatibility between the inflow and outflow water volumes. The equilibrated inflow and outflow rates were found to be similar during the hydraulic conductivity tests. A linear relationship was noted between hydraulic gradient and hydraulic flux indicating the validity of Darcy's law for calculating the hydraulic conductivity of compacted bentonites. An expulsion of exchangeable cations from the compacted bentonite specimens occurred during the hydraulic conductivity tests. The amount of expelled cations was found to be less than about 6% of the total exchangeable cations present in the bentonite. The gas permeability of compacted unsaturated bentonite was found to decrease within an increase in compaction dry density. The calculated hydraulic conductivity of compacted unsaturated bentonite based on the measured intrinsic permeability was found to be greater than the measured hydraulic conductivity of compacted saturated bentonite indicating that swelling reduces the hydraulic flow paths. The saturated hydraulic conductivities calculated from the Kozeny-Carman model were found to better describe the measured saturated hydraulic conductivities than the other available models. The model proposed in this study did not satisfactorily establish the hydraulic conductivity of compacted saturated bentonite due to uncertainties associated with the assumptions made regarding the viscosity of the bulk fluid.

Table of Contents

Contents

Chapter 3 Materials and Methods

Chapter 4 Compliance of the hydraulic conductivity experimental set up

Chapter 5 Saturated hydraulic conductivity of compacted MX80 bentonite

List of Figures

List of Tables

CHAPTER 1

INTRODUCTION

1.1 Introduction

The safe disposal of waste materials, both radioactive and domestic, requires a detailed geoengineered solution. The isolation of the waste material and the protection of the geoenvironment are important considerations. The use of swelling clays in the containment and isolation of waste materials requires a better understanding of the materials to be used (Pusch and Yong, 2005).

One application of geoengineered barriers is the safe disposal of radioactive waste (Thomas et al., 1998). Deep geological repositories have been proposed as a suitable method for disposing of high level radioactive waste. The repositories will consist of a tunnel system located at a minimum depth of 500 m underground (Pusch, 1982). Engineered barriers composed of highly compacted swelling clays are proposed to isolate the radioactive waste (Sun et al., 2008). Bentonite has been selected for the engineered barriers due to its low permeability, high swelling capacity and retention properties (Villar and Lloret, 2007).

The high level radioactive waste will be stored in deposition holes at regular intervals along the tunnel network (Bucher and Muller-Vonmoos, 1989). The multi-barrier system consists of the canister which encapsulates the spent fuel surrounded by the bentonite buffer (Karnland et al., 2007). Compacted unsaturated bentonite blocks will form the bentonite barrier (Villar, 2007). The bentonite is required to serve a number of functions, including ensuring structural integrity of the canister and a high level of water tightness (Muller-Vonmoos, 1986).

Compacted bentonites have also been proposed as a suitable material for geosynthetic clay liners. These liners are a composite material comprising of bentonite and geosynthetics. Geosynthetic clay liners have been proposed as an alternative to soil barriers in the cover and bottom lining of waste containment facilities (Bouazza and Vangpaisal, 2003). A number of studies have been conducted previously in geosynthetic clay liners (Bouazza et al., 1996; Gilbert et al., 1996; Daniel et al., 1998; Shackelford et al., 2000; Didier et al., 2000). The geosynthetic clay liners are 5-10 mm thick, and contain approximately 5 kg/m^2 of bentonite (Bouazza and Vangpaisal, 2003).

When the bentonite is placed at the hygroscopic water content, it initially has a very high suction (Villar, 2007). Saturation of the bentonite barrier by the surrounding environment will therefore occur. During hydration and under restrained boundary conditions, compacted bentonites exhibit swelling pressures. Swelling pressure tests have been carried out on compacted bentonites by a number of authors (Pusch, 1982; Dixon and Gray, 1985; Bucher and Muller-Vonmoos, 1989; Komine and Ogata, 1994; Villar and Lloret, 2007; Karnland et al, 2007; Schanz and Tripathy, 2009).

Geoenvironmental barriers are widely used to limit the movement of water and contaminants (Dixon et al., 1999). The hydraulic conductivity of the clays depends on a number of factors, including soil composition, permeant characteristics, void ratio and structure (Lambe, 1954). The saturated hydraulic conductivity of compacted bentonite has been determined in a controlled laboratory environment (Komine and Ogata, 1994; Petrov et al., 1997; Cho et al., 1999; Dixon et al., 1999; Jo et al., 2001; Lee and Shackelford, 2005; Komine, 2008). It has also been reported that the saturated hydraulic conductivity is affected by compaction dry density, temperature, montmorillonite content, and type of exchangeable cation.

In the past, a range of applied hydraulic gradients have been considered for determining the hydraulic conductivity of compacted saturated bentonites. Usually larger hydraulic gradients have been shown to result in shorter testing durations. Differences between the saturated hydraulic conductivities determined in rigid- and flexible-walled permeameters haves been reported to be insignificant (Daniel, 1994).

A number of experimental factors can affect the determination of the saturated hydraulic conductivities. These include temperature fluctuations in the laboratory, dissolved air in the fluid, incomplete specimen saturation, biological action in the specimen, system expansion, leakage in the system and microstructural changes in the specimen. These factors are often not considered during hydraulic conductivity tests (Chapius, 2012). The effect of these factors on the saturated hydraulic conductivity can be quantified by assessing the inflow and outflow behaviour during hydraulic conductivity tests. Limited studies on the compatibility of inflow and outflow during hydraulic conductivity tests have been reported in literature.

Bentonite mixtures are widely used as geoenvironmental barriers to control the movement of liquid from waste disposal facilities (Stewart et al., 2003). Bentonite is blended with sand or crushed rock to reduce shrinkage cracks and to increase strength and volume stability (Kleppe and Olsen, 1985). The hydraulic conductivity of bentonite-enhanced mixtures can be controlled by the percentage of bentonite in the bentonite-enhanced mixture (Chapius, 1989; Sivapullaiah et al., 2000; Stewart et al., 2003; Komine, 2008).

The backfill material proposed to be used in deep geological disposal is required to create a zone of low permeability around the high level radioactive waste (Komine, 2010). The hydraulic conductivity is required to be between 10^{-11} and 10^{-12} m/s (Japan Nuclear Cycle Development Institute, 1999). Mixtures of 0-30% bentonite and 100-70% ballast material (crushed rock or sand) have been proposed for backfilling material in the Swedish repository concept (Borgesson et al., 2003). The backfilling material in the UK repository concept will consist of 30% bentonite and 70% crushed rock (Nirex, 2005). The hydraulic conductivity of compacted sand-bentonite prepared to these percentages has been reported

previously for different compacted bentonites (Sivapullaiah et al, 2000; Komine, 2008; Sun et al., 2008).

Once saturated, water may flow through the compacted bentonite under a hydraulic gradient. A number of transport mechanisms will be present in the bentonite-water system. The flow of water through the specimen may result in ion expulsion (Mitchell and Soga, 2005). Ions may diffuse due to the chemical concentration gradient between the compacted saturated bentonite and the adjacent fluid. Additional coupled processes may occur in the bentonite-water system.

Geosynthetic clay liners may also provide an important role in landfill covers as a gas barrier (Bouazza and Vangpaisal, 2003). The liner is required to prevent the migration of landfill gas to surrounding areas (Didier et al., 2000). In the case of deep geological repositories, gases may be produced due to canister corrosion (Horseman et al., 1999; Gens et al., 2001; Alonso et al., 2002).

Darcy's law can be used to calculate the gas permeability of compacted bentonites (Tanai, 1996; Bouazza and Vangpaisal, 2003; Alonso, 2006). Previous studies in the literature (Didier et al., 2000; Bouazza and Vangpaisal, 2003) have determined the gas permeability of compacted bentonite at increasing water content. Detailed study of the effect of dry density on gas permeability at low water contents has not been reported.

The experimental determination of saturated hydraulic conductivity can be time-intensive, due to the low permeability of compacted bentonites. Analytical models have been proposed to determine the saturated hydraulic conductivity of compacted bentonites. The

hydraulic conductivity of compacted bentonites can be calculated from the compressibility behaviour. The Kozeny-Carman model has been widely used for predicting the hydraulic conductivity in soils, and has been employed for compacted bentonite (Dixon, 1999; Chapius and Aubertin, 2003; Singh and Wallender, 2008). Achari et al. (1999) calculated the hydraulic conductivity from the cluster model proposed by Olsen (1962). Komine (2004) determined the hydraulic conductivity from parallel plate flow.

1.2 Scope and objectives of the research

Considering the use of compacted bentonites as geotechnical barriers in high level radioactive waste disposal repositories and geo-liners, the primary aim of this research was to study the following aspects:

1) To study the inflow and outflow of compacted saturated bentonites under applied hydraulic gradients to gain a better understanding of the limitations of hydraulic conductivity tests.

2) To investigate the influence of hydraulic gradient and dry density on the hydraulic conductivity of compacted saturated bentonite. A range of compaction dry densities will be considered. The hydraulic gradient applied to the specimens will be increased and decreased in a step-wise manner.

3) To determine the hydraulic conductivity for compacted saturated sand-bentonite mixtures at increasing compaction dry densities. The hydraulic conductivity tests will

be carried out under identical applied hydraulic gradients to those considered for tests on compacted bentonite. The proportion of sand to bentonite and the compaction dry densities will correspond to that proposed for backfilling material in deep geological repositories.

4) To quantify the expulsion of exchangeable cations from the compacted bentonite specimens during hydraulic conductivity tests. The hydraulic conductivity of compacted bentonite is reported to be influenced by the cation exchange capacity of the material. An expulsion of exchangeable cations from the bentonite-water system may result in an increase in the measured hydraulic conductivity, which is undesirable in the context of containment of waste materials.

5) To determine the gas permeability of air-dry compacted bentonite at low water contents and to assess whether the gas permeability of compacted bentonites can be used to determine the hydraulic conductivity. Compacted bentonites placed at low water contents can be used in geo-liners to form the capping layer of landfills, which can generate gases due to waste degradation.

6) To use existing models to establish the hydraulic conductivity in compacted saturated bentonites and to propose a new model for assessing the saturated hydraulic conductivity of compacted bentonites.

Detailed experimental studies on the unsaturated hydraulic conductivity of compacted bentonites, the effect of temperature on the saturated hydraulic conductivity of compacted bentonite, the influence of other permeants, the percentage of sand contained in the

compacted sand-bentonite specimen and the expulsion of anions during hydraulic conductivity tests was beyond the scope of this research.

1.3 Thesis outline

The thesis is divided into nine consecutive chapters.

Chapter 1 presents the background to the research, the main objectives of the research and the outline of the thesis.

Chapter 2 presents a review of literature relevant to this study. The structure of montmorillonite and the microstructure of compacted bentonites are presented. The mechanisms controlling the swelling of expansive clays are stated.

The initial and testing conditions of hydraulic conductivity tests reported in the literature are reviewed. The hydraulic gradients applied during testing are justified. The factors affecting the saturated hydraulic conductivity are brought out and discussed. The hydraulic conductivity of compacted sand-bentonite and crushed rock-bentonite specimens is reviewed. The determination of the gas permeability of compacted bentonites is presented. The models available for assessing the hydraulic conductivity of compacted saturated bentonites are discussed.

The bentonite used in the research was MX80 bentonite. Compacted MX80 bentonite has been proposed as a suitable material in high level toxic waste disposal repositories

(Pusch, 1982; Bucher and Muller-Vonmoos, 1989; Madsen, 1998; Montes-Hernandez et al., 2003; Pusch and Yong, 2006; Tang and Cui, 2008). The properties of the MX80 bentonite used are presented in **Chapter 3**. The physical and chemical properties are provided. The suction-water content soil-water characteristic curve determined from osmotic technique and vapour equilibrium technique is presented.

The rigid-walled fixed ring hydraulic conductivity cell used to determine the hydraulic conductivity of compacted bentonite and sand-bentonite specimens is presented. The experimental set-up for determining saturated hydraulic conductivity is shown. The compressibility of compacted bentonite and sand-bentonite specimens using standard oedometers is presented. The determination of gas permeability of compacted bentonite is described.

Compliance of the hydraulic conductivity experimental set-up is presented in **Chapter 4**. The expansion of the inflow system to the hydraulic conductivity cell was determined under instantaneous and step-wise pressure changes. The correction of inflow due to system expansion is discussed.

Chapter 5 presents the hydraulic conductivity test results of compacted bentonite specimens. The inflow and outflow behaviour is presented for the hydraulic gradients considered. The inflow and outflow rates at the end of hydraulic conductivity tests are determined. The hydraulic conductivity of each specimen is determined from the inflow and outflow rates.

The compressibility behaviour of saturated compacted bentonite specimens is presented. The coefficient of compressibility is calculated from Taylor's and Casagrande's methods. The hydraulic conductivity is calculated from the coefficient of compressibility. The percentage of exchangeable cations expelled from the compacted bentonite specimen during the hydraulic conductivity tests is determined.

The hydraulic conductivity of compacted sand-bentonite specimens is presented in **Chapter 6.** The inflow and outflow behaviour during hydraulic conductivity tests is presented. The hydraulic conductivity of the compacted sand-bentonite specimens is determined from the inflow and outflow rates. The compressibility behaviour of compacted saturated sand-bentonite is presented. The coefficient of compressibility is calculated from Taylor's and Casagrande's methods.

The gas permeability of air-dry compacted MX80 bentonite at low water contents is presented in **Chapter 7**. An existing device used for determining the gas permeability was utilised. The flow of nitrogen (N_2) gas through the specimens is measured. The gas permeability of the compacted specimens is calculated from Darcy's law. The appropriateness of determining the hydraulic conductivity of compacted bentonites from the measured gas permeability is discussed.

The hydraulic conductivities of compacted saturated bentonite are calculated from existing models in **Chapter 8**. The hydraulic conductivity of compacted saturated bentonites is calculated from the Kozeny-Carman model and the model described by Komine (2004). A model for determining the saturated hydraulic conductivity of compacted bentonite is proposed based on parallel plate flow. The hydraulic conductivities calculated from the

models considered are compared, and are also compared with the experimental results determined in this study.

The main conclusions drawn from this research are presented in **Chapter 9**.

CHAPTER 2

LITERATURE REVIEW

2.1 Introduction

Compacted bentonites and compacted sand-bentonite mixtures have attracted considerable attention as suitable materials for geoengineered barriers. Compacted bentonites have been proposed as barrier and backfilling material in high level radioactive waste disposal (Thomas et al., 1998). The deep geological repository will store the radioactive waste at depths of at least 500 m below the ground surface (Pusch, 1982). The waste material will be stored in a multi-barrier system comprising of a stainless steel canister and compacted bentonite blocks. The canisters will be placed in deposition holes throughout the underground

tunnel network. The excavated tunnels and shafts will then be sealed using a backfilling material. Compacted bentonite surrounding the waste canister will form a barrier between the canister and the host rock. Fluid will percolate from the host rock and will saturate the compacted bentonite. Once saturated, the flow of water through the compacted bentonite barrier will depend on a number of physical and physico-chemical aspects.

Geoengineered barriers such as geosynthetic clay liners are widely used in municipal solid waste disposal. Geosynthetic clay liners are a composite material, created from compacted bentonite and either geotextiles or a geomembrane (Bouazza and Vangpaisal, 2003). Geosynthetic clay liners can be used as part of the cover or lining of waste disposal facilities. The landfill liner is required to prevent leachate from the landfill entering groundwater (Environment Agency, 2011). Landfill liners will become saturated during operation due to the availability of fluid from the waste material. The rate of flow through the saturated liner is required to assess the effect of leachate on the groundwater and the wider geoenvironment.

This chapter presents a detailed literature review of the physico-chemical aspects and the physical process that may occur in compacted bentonites during saturation and hydraulic flow. The structure of montmorillonite and the microstructure of compacted bentonites are presented. The mechanisms governing the swelling of clays are discussed. The devices and procedures used to determine the saturated hydraulic conductivity of compacted bentonites are reviewed. The factors influencing the saturated hydraulic conductivity of compacted bentonites are discussed. The hydraulic conductivity of compacted sand-bentonite mixtures is reviewed. The mechanisms controlling the transport of ions in compacted bentonites are presented. The gas permeability of compacted bentonites is considered. Finally, available

models for assessing the hydraulic conductivity of compacted bentonites are presented. A summary of the chapter is provided.

2.2 Structure of montmorillonite

Clay minerals are predominantly composed of silicon-oxygen tetrahedral and aluminium- or magnesium-oxygen-hydroxyl octahedral layers and are classified depending upon the structural arrangement of mineral sheets (van Olphen, 1963; Grim, 1968). Pyrophyllite is a neutral 2:1 layer mineral, composed of two silica tetrahedral sheets, separated by an alumina octahedral sheet. The montmorillonite mineral is a derivative of pyrophyllite through substitution of atoms (van Olphen, 1963). The montmorillonite mineral is shown in Figure 2.1.

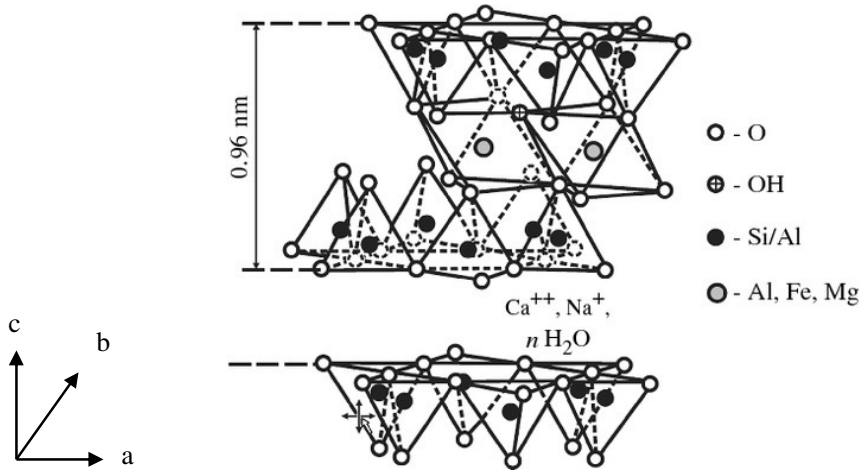

Figure 2.1 - Schematic diagram of the montmorillonite mineral (adapted from Mitchell and Soga, 2005)

The exchange of atoms within the crystalline structure is referred to as isomorphous substitution (van Olphen, 1963). The theoretical formula of montmorillonite is $(OH)_4Si_8Al_4.nH_2O$(interlayer), but the montmorillonite mineral always differs from this theoretical formula (Grim, 1968). Within the silica tetrahedral sheet, partial substitution of silicon by aluminium can occur. Each substitution that occurs will result in a deficit of positive charge (van Olphen, 1963). The charge deficiency per unit cell that results from these substitutions is between 0.5 and 1.2, although it is usually 0.66 per unit cell (Mitchell and Soga, 2005). Broken ionic and covalent bonds at the platelet edges are also thought to contribute up to 20% towards the charge deficit (Mitchell and Soga, 2005).

The charge deficit resulting from isomorphous substitution is compensated by the attraction of exchangeable cations (Na^+, Ca^{2+}, K^+, Mg^{2+} etc.) to the mineral surface. These cations can be exchanged with other cations when they are available in solution (van Olphen, 1963). The exchangeable cations can be replaced by cations of another species, dependant on the relative abundance of size of cations (Mitchell and Soga, 2005). The typical replaceability of cations is given as:

$$Na^+ < Li^+ < K^+ < Rb^+ < Cs^+ < Mg^{2+} < Ca^{2+} < Ba^{2+} < Cu^{2+} < Al^{3+} < Fe^{3+} < Th^{4+}$$

However, Mitchell and Soga (2005) reported that it is possible for a lower power cation to displace a higher power cation by mass action, if the concentration of the replacing power is high, relative to that of the ion which is to be replaced.

The montmorillonite platelet is continuous in both the *a* and *b* directions, but has a finite thickness of around 0.96 nm (van Olphen, 1963; Grim, 1968; Mitchell and Soga, 2005).

Weak bonds exist between neighbouring, due to charge repulsion between the adjacent, negative octahedral layers (Grim, 1968). These can become separated when water is allowed to permeate (Mering, 1946).

2.3 Structure of compacted bentonite

Bentonite was initially used in 1898 by W.C. Knight to describe a highly plastic clay from Wyoming. Bentonites are primarily composed of the montmorillonite mineral (Ross and Shannon, 1926). The montmorillonite mineral unit layers stack in the *c* dimension to form individual particles (Saiyouri et al., 1998). The number of unit layers in each particle is dependent on the main type of exchangeable cation, and the water content of the bentonite (Saiyouri et al., 2004).

Clay aggregates are composed of a number of particles. The schematic microstructure of powdered, air-dry bentonite, obtained through Scanning Electron Microscopy (SEM) by Pusch (1982), is shown in Figure 2.2.

Multiple pore types exist within the bentonite microstructure. Macro-pores are pores which exist between aggregates. Micro-pores are pores which are contained within aggregates (Delage et al., 2006), either between particles or between unit layers. The spaces between unit layers can be referred to as interlayer pores (Pusch, 1982; Kozaki et al., 2001; Montes-Hernandez et al., 2003; Likos, 2004; Montes-Hernandez et al., 2006). Bradbury and Baeyens (2003) stated that the porosity can be subdivided into three distinct pore regions; interlayer pores (0.2 - 1 nm), micro-pores (< 5 nm) and macro-pores (5 - 20 nm). Mercury

Intrusion Porosimetry (MIP) is commonly used to determine the pore size distribution for clay specimens (Dixon et al., 1999; Montes-Hernandez et al., 2003; Delage, 2006; Montez-Hernandez et al., 2006). Compacted bentonites can be described as 'dual porosity' due to the contribution of micro- and macro-porosity to the pore size distribution (Laird, 2006; Samper et al., 2008).

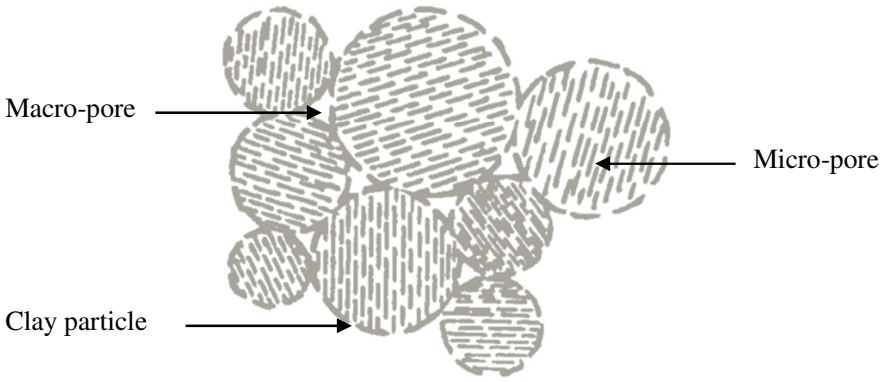

Figure 2.2 - Schematic microstructure of air-dry MX80 bentonite powder (from Pusch, 1982)

Thomas et al. (2003) and Lloret et al. (2004) stated that the expansion of the microstructure due to increases in water content reduces the macro-porosity of the compacted bentonite. Dixon et al. (1999) stated that the macro-porosity of compacted bentonites depended on the energy used during compaction. Delage et al. (2006) noted that at the same water content the changes in porosity observed were due to changes in the large pores. Bourg et al. (2006) proposed empirical derivations of the volume of pore space associated with micro- and macro-pores in compacted bentonite as a function of the compaction dry density. Pusch (2001) stated that changes in swelling pressure and hydraulic conductivity are observed due to microstructural changes.

2.4 Swelling mechanisms in bentonite

When in contact with water or electrolyte solution, bentonites will exhibit swelling. In unrestrained conditions, the volume of the bentonite will increase. When allowed to saturate under controlled volume conditions, a swelling pressure will develop. The swelling of bentonite occurs due to two distinct mechanisms; crystalline swelling and osmotic swelling.

The initial hydration of the bentonite microstructure will result in the hydration of exchangeable cations and the mineral surfaces (van Olphen, 1963; Push, 1982; Alther, 2004). Water is able to permeate between unit layers, resulting in changes in the *c* axis spacing. From a dry state, the water molecules entering between unit layers sequentially form distinct layers of water molecules (known as hydrate layers) between the surfaces of adjacent unit layers. This process is referred to as crystalline (Type I) swelling (Grim, 1968; Saiyouri et al., 2000; Likos, 2004; Saiyouri et al., 2004). Laird (2006) suggested that the potential energies of crystalline swelling are balanced by Columbic, van der Waals and Born's repulsion forces.

The *c* axis spacings can be determined through X-ray diffraction, with the reported *c* axis spacings increasing from 0.96 nm in a dry state, to 1.26, 1.56 and 1.86 nm for 1, 2 and 3 hydrate layers respectively (Saiyouri et al., 2000; Likos, 2004). Saiyouri et al. (2000) also report the presence of a fourth hydrate layer, with the corresponding *c* axis spacing reported to be 2.16 nm.

The hydration by distinct water layers is accompanied by a large amount of energy being released, due to hydration of both exchangeable cations and also the platelet surface (van Olphen, 1963; Pusch, 1982). Hydration of exchangeable cations on the platelet surface is

due to alignment of temporary negative dipoles within the water molecule towards the positive cation (Alther, 2004). The hydrated radii of cations are significantly greater than that of the unhydrated radii, as shown in Table 2.1 (Alther, 2004).

Table 2.1 - Radii sizes for unhydrated and hydrated cations (after Alther, 2004)

Cation	*Unhydrated radius (nm)*	*Hydrated radius (nm)*
Ca^{2+}	0.099	0.960
K+	0.133	0.530
Mg^{2+}	0.066	1.800[a]
Na^{+}	0.097	0.790

[a] *from Mitchell and Soga (2005)*

During osmotic (Type II) swelling, electrical diffuse double layers are formed between unit layers. Upon contact with water, cations on the platelet surface diffuse away from the mineral surface to equalise the cation concentration through the fluid. This is countered by an electrostatic attraction between the mineral surface and the cations, as a charge deficit is still present within the mineral (Mitchell and Soga, 2005). The distribution of ions adjacent to the clay surface is shown in Figure 2.3.

The Gouy-Chapman diffuse double layer theory can be used to determine the swelling pressure of bentonites (Bolt, 1956; van Olphen, 1977; Tripathy et al., 2004, Schanz et al., 2013). Shainberg and Kemper (1965) observed good agreement between the diffuse double layer theory and experimental data when the platelet surfaces were at distances large enough for diffuse double layers to form. However, at low separations, the clay platelets demonstrate significantly greater resistance than expected (Swartzen-Allen and Matijevic, 1973), which has been attributed to additional repulsive forces (van Olphen, 1963; Tripathy et al., 2006).

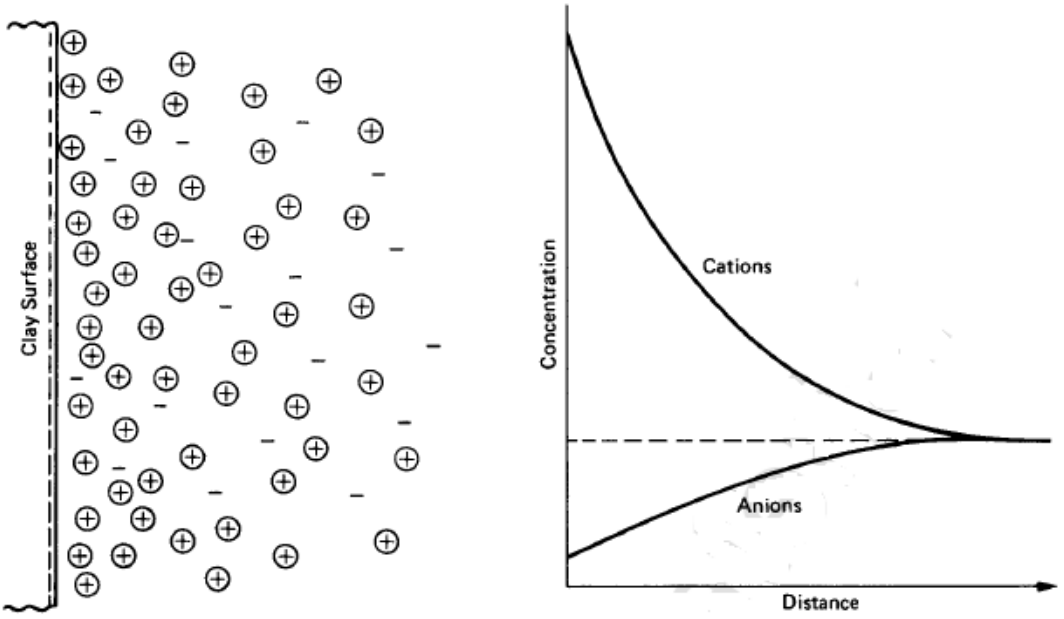

Figure 2.3 - Distribution of ions adjacent to a clay surface according to the concept of the diffuse double layer (from Mitchell and Soga, 2005)

2.5 Compressibility behaviour of bentonite

In deep geological repositories, compacted bentonites may experience high overburden pressures, subject to placement conditions. The compressibility behaviour of bentonites has been reported previously by several researchers, covering a wide range of void ratios (Bolt, 1956; Mesri and Olsen, 1971; Low, 1980; Al-Mukhtar et al., 1999; Fleureau et al., 2002; Marcial et al., 2002; Tripathy and Schanz, 2007; Baille et al., 2010). In the majority of cases, the compressibility behaviour of bentonites has been assessed from initially saturated clays with water contents greater than the liquid limit.

A range of applied pressures has been considered. Sridharan et al. (1986) applied pressures between 6.25 and 300 kPa to homo-ionised bentonites. Olsen and Mesri (1971) studied the compressibility behaviour of sodium and calcium bentonites up to a maximum pressure of 4000 kPa. Tripathy and Schanz (2007) showed that the Gouy-Chapman diffuse double layer theory, along with the compressibility behaviour of bentonite at small applied pressures, could be used to predict the compressibility behaviour of bentonites at large applied pressures.

Baille et al. (2010) studied the compressibility of bentonites at large applied pressures (up to 25 MPa). The bentonite specimens were compacted prior to testing being undertaken, and were allowed to swell upon saturation. The compaction paths of compacted saturated specimen remained below that of the compression path for the initially slurried specimen. The compressibility behaviour of the compacted bentonite specimens was used by Baille et al. (2010) to determine the hydraulic conductivity of the bentonite for void rations between 0.5 and 2, through determination of the coefficient of compressibility. The hydraulic conductivity was found to increase from approx. 5×10^{-13} m/s for a void ratio of 0.5 to around 6×10^{-12} m/s for a void ratio of 2.

2.6 Determination of saturated hydraulic conductivity in clays

The low hydraulic conductivity of compacted bentonites is one of the primary reasons for their selection in geoengineered barriers. In deep geological repositories, the bentonite barrier material will become saturated by the host rock (Alonso et al., 2008). The flow of

water to the canister will be dependent on the hydraulic conductivity of the bentonite, coupled with thermal and mechanical effects (Thomas et al., 1998).

Due to the low permeability of compacted bentonites, the apparatus and testing procedure adopted is critical in reducing and avoiding experimental errors. Darcy's law is commonly used to calculate the hydraulic conductivity of soils. The hydraulic conductivity cell used should suitably confine the specimen, and should avoid applying additional pressure. The chosen method of applying the hydraulic gradient to the specimen will dictate the experimental procedure to be followed.

Few researchers have explicitly stated the equilibrated inflow and outflow rates, and from which the hydraulic conductivity was determined. Chapius (2012) noted that measuring only one of the flow rates (either the inflow or outflow rate) is not advisable, as this may lead to significant errors when determining the hydraulic conductivity, particularly in fine grained soils. Dixon et al. (1999) presented the inflow and outflow rates measured during hydraulic conductivity tests. Some variation between the inflow and outflow of water was observed. It was observed by Dixon et al. (1999) that approximately 1% of fluid was lost from the specimen during the hydraulic conductivity tests.

To fully inform the experimental procedure to be adopted during this study, this section briefly reviews the use of Darcy's law in determining the hydraulic conductivity of bentonites, the types of cells reported in the literature for measuring hydraulic conductivity of bentonites, and the reported testing procedures adopted.

2.6.1 The use of Darcy's law in determining the hydraulic conductivity of bentonite

The hydraulic conductivity of soils is typically determined from Darcy's law (Darcy, 1856). Darcy's law states that a proportional relationship exists between hydraulic flux and hydraulic gradient. Darcy's law is stated as;

$$v = ki \tag{2.1}$$

where v is the hydraulic flux (m/s), k is the hydraulic conductivity (m/s) and i is the hydraulic gradient (m/m).

From Equation (2.1), the coefficient of proportionality, the hydraulic conductivity of the soil, can be determined from a linear relationship between hydraulic flux and hydraulic gradient, where the hydraulic conductivity is the gradient of the 'best fit' line. It follows from Equation (2.1) that the intercept for such a line would pass through the origin, as no flow would be expected in the absence of a hydraulic gradient on the soil.

In the literature, the use of Darcy's law for the determination of the hydraulic conductivity of bentonite has been widely used. However, the existence of 'threshold' gradients has been reported by several authors (Lutz and Kemper, 1959; Miller and Low, 1963; Pusch, 1982; Dixon et al., 1999). These 'threshold' gradients are hydraulic gradients under which no flow will take place through the bentonite. Dixon et al. (1999) state that for low hydraulic gradients (less than 30), the relationship between hydraulic gradient and hydraulic flux indicates that two zones of 'Darcian' flow exist where the relationship between flux and gradient are linear. These two zones are disjointed, with neither of the linear trend

lines passing through the origin, as is required for Darcian flow. Due to the low hydraulic gradients used, it is possible that the flow conditions observed are more significantly affected by experimental errors.

The vast majority of authors have not reported the existence of 'threshold' gradients for bentonites (Olsen, 1969; Miller et al., 1969; Chan and Kenney, 1973). Lloret et al. (2004) observed that the applied hydraulic gradient did not significantly influence the hydraulic conductivity of the bentonite specimens. Villar and Gomez-Espina (2009) also observed no clear trend between the applied hydraulic gradient and the hydraulic conductivities measured for the range of applied hydraulic gradients considered.

It is therefore considered for this study that it is appropriate to use Darcy's law to determine the hydraulic conductivity of bentonites, and that 'threshold gradients' within the bentonite are not present.

2.6.2 Cells used to measure the hydraulic conductivity of compacted bentonites

The cells used to determine the hydraulic conductivity of clays can be broadly described as two types; rigid- and flexible-walled permeameters. A brief description of each cell type is presented here, and the comparison between the measured hydraulic conductivity from the two cell types is discussed.

Rigid-walled permeameters have been widely used to determine the hydraulic conductivity of clays (Boynton and Daniel, 1984; Benson and Daniel, 1990; Chapius, 1990; Shackelford and Javed, 1991; Kenney et al., 1992, Dixon et al., 1999). The hydraulic

conductivity tests are conducted under constant-volume conditions i.e. the specimen is not permitted to swell during the test. Sidewall flow may occur in rigid-walled permeameters. Daniel (1994) stated that sidewall leakage does not occur in compressible soils that have been subjected to compressive stresses of at least 50 kPa. Dixon et al. (1999) reported that sidewall flow was overcome during the testing procedure by statically compacting specimens directly into the hydraulic conductivity cell. The expansive nature of compacted bentonites also stated prevented sidewall flow (Dixon et al., 1999).

Flexible-walled permeameters have been used to determine the hydraulic conductivity of clays (Boynton and Daniel, 1984; Mundell and Bailey, 1985; Chapius, 1990; Zimmie et al., 1992, Petrov et al., 1997; Shackelford et al., 2000). The test specimens are vertically confined within the permeameter, but a latex membrane around the specimen allows for volume change to occur. The cell is filled with water and pressurised. This ensures contact between the test specimen and the latex membrane, reducing sidewall flow in the permeameter.

The advantages and disadvantages of rigid- and flexible-walled permeameters were discussed by Daniel (1994). The main advantages of a rigid-walled permeameter are its simplicity to construct and the wide range of materials that can be tested, as the flexible-walled permeameter requires a more complicated testing procedure. Sidewall flow is minimised in flexible-walled permeameters, but can be significant in rigid-walled permeameters.

Daniel (1994) compared the hydraulic conductivities of bentonites determined from rigid- and flexible-walled permeameters, reported previously in the literature. The specimens

were saturated with distilled water in all cases. No significant difference was observed in the hydraulic conductivity determined from rigid- and flexible-walled permeameters. It is therefore considered that either a rigid- or flexible-walled permeameter would be suitable for determining the hydraulic conductivity of compacted bentonite.

2.6.3 Application of hydraulic gradient to determine the hydraulic conductivity in clays

The application of a hydraulic gradient is imperative for determination of the hydraulic conductivity of compacted bentonite. Several approaches have been used to apply a hydraulic gradient to bentonite specimens. The constant-head test maintains a constant water level in the inflow reservoir. In a variable-head test, the water levels in the influent and effluent reservoir will change during the hydraulic conductivity tests. The most common variable-head test is the falling-head test, where the water level of the inflow reservoir decreases through the hydraulic conductivity test. Constant flow and constant volume tests may also be used, with the influent and effluent reservoir heads adjusted to maintain these conditions.

For hydraulic conductivity tests on compacted bentonites, differing approaches have been considered. Dixon et al. (1999) applied constant-head test conditions during testing. Large water reservoirs were used, such that the change in water levels during the hydraulic conductivity test was negligible. Villar and Gomez-Espina (2009) conducted hydraulic conductivity tests on FEBEX bentonite using a constant-head approach. The water head was applied using a pressure-volume controller that maintained a constant inflow pressure.

Jo et al. (2005) and Ahn and Jo (2009) tested the long-term hydraulic conductivity of geosynthetic clay liners using the falling-head approach. The inflow water head decreased with the outflow head remaining constant. Lee and Shackelford (2005) also tested specimens of two geosynthetic clay liners using the falling-head method.

Petrov et al. (1997) conducted hydraulic conductivity tests in a fixed-ring permeameter using the constant-flow approach. The fluid was pressurised to flow through the specimen at a constant rate, and the induced pressure head was measured by an in-line transducer. Siemens and Blatz (2007) discussed the development of a new hydraulic conductivity apparatus. The cell described was used to determine the hydraulic conductivities under constant-volume conditions. The inflow and outflow were measured during the tests.

The three approaches for the application of a hydraulic gradient during hydraulic conductivity tests have been used successfully for compacted bentonites. However, constant flow and constant volume tests are considered more difficult to maintain, particularly for long test durations. It is also considered that the variable-head approach may introduce experimental errors in the determination of the hydraulic gradient, in particular with the potential for evaporation, and monitoring the rate at which the head changes. It is therefore concluded that the constant-head method will be used in the current study.

2.6.4 Typical hydraulic gradients applied during hydraulic conductivity tests

A range of applied hydraulic gradients have been considered in the literature for determining the saturated hydraulic conductivity of compacted bentonites. ASTM D 5084 states that for materials with low hydraulic conductivity a maximum hydraulic gradient of 30

should be applied. However, due to experimental practicalities, in particular testing time, significantly higher hydraulic gradients have been considered. In the case of compacted bentonites, assuming a hydraulic conductivity of 10^{-13} m/s and a specimen diameter of 100mm, an applied hydraulic gradient of 30 will lead to a volumetric flow rate of 2ml per day.

Benson and Daniel (1990) determined the hydraulic conductivity of compacted clays under applied hydraulic gradients between 10 and 100. Cho et al. (1999) conducted hydraulic conductivity tests on compacted bentonite specimens with dry densities up to 1.8 Mg/m^3. Hydraulic gradients of 20600 were applied to the densest specimens. Lloret et al. (2004) applied gradient up to 30000 to determine the hydraulic conductivity of highly compacted bentonite specimens.

Although it is recommended that low hydraulic gradients are applied when determining hydraulic conductivity, the low permeability nature of bentonite will lead to small flow volumes, which may introduce error and lead to longer test durations. It has been reported within the literature that hydraulic gradients up to 30000 have been used for determining the hydraulic conductivity of bentonite, and so it is considered in this study that larger hydraulic gradients can be applied.

2.7 Factors affecting the saturated hydraulic conductivity of clays

An appreciation of the factors which influence the hydraulic conductivity of bentonites is essential, in order to place the experimental results determined in the context of

that reported by others. Previous studies on the saturated hydraulic conductivity of clays have attempted to assess the influence of a number of physical and chemical properties. The main findings of these studies are presented in this section.

2.7.1 Influence of dry density on saturated hydraulic conductivity of compacted bentonites

The hydraulic conductivity of bentonite is widely reported to be influenced by the compaction dry density (Pusch, 1982; Cho et al., 1999; Dixon et al., 1999; Villar, 2008; Baille et al., 2010). The available porosity within the specimen, through which the flow occurs, reduces as the dry density increases. This results in a reduction in the measured hydraulic conductivity.

Cho et al. (1999) produced a number of water-saturated calcium bentonite specimens with dry densities of 1.4, 1.6 and 1.8 Mg/m^3. The reported hydraulic conductivities were shown to reduce from about 10^{-12} m/s to about 10^{-14} m/s when the compaction dry density was increased from 1.4 to 1.8 Mg/m^3.

Dixon et al. (1999) determined the hydraulic conductivities of compacted bentonite specimens under an applied hydraulic gradient between 1 and 1000. The diameter chosen for the specimen was dependant on the applied hydraulic gradient, as the observed flow was greater for larger diameters. Compacted specimens with dry densities between 0.5 Mg/m^3 and 1.5 Mg/m^3 were tested. The hydraulic conductivity reduced from 10^{-11} m/s to 10^{-13} m/s over the range of compaction dry densities considered.

2.7.2 Influence of montmorillonite content on saturated hydraulic conductivity of compacted bentonites

As discussed previously, the montmorillonite minerals are responsible for swelling within the bentonite microstructure during saturation. The development of diffuse double layers between platelet stacks leads to an overall increase in the inter-layer porosity, with an accompanying reduction in the available macro-porosity (Saiyouri et al., 2000).

Flow through the compacted bentonite has been reported to occur through the macro-pores (Pusch, 1999; Bourg et al., 2006). As the available macro-porosity reduces due to osmotic swelling, it is expected that the hydraulic conductivity of the bentonite would reduce. Several authors have investigated the effect of montmorillonite content on the hydraulic conductivity.

Lee and Shackelford (2005) determined the saturated hydraulic conductivity of two bentonites. The high quality bentonite was found to have a greater montmorillonite content (86%) than the low quality bentonite (77%). The water hydraulic conductivity of the high quality bentonite was significantly lower than the low quality bentonite.

Dananaj et al. (2005) increased the montmorillonite content of two bentonites from 68% to 92%. The measured hydraulic conductivity was found to be greater for the bentonites with 68% montmorillonite content than for those with 92% montmorillonite content.

2.7.3 Influence of microstructure on saturated hydraulic conductivity

The microstructure of compacted bentonite is significant in understanding the available flow channels through which flow will be able to take place. In geosynthetic clay liners, and as buffer and barrier material for deep geological repositories, the compacted bentonites will be artificially prepared to the dry density required by the design.

The effect of microstructure on the hydraulic conductivity of bentonite has been reported in the literature. Benson and Daniel (1990) investigated the influence of clod size on the saturated hydraulic conductivity of compacted clay. Low hydraulic conductivities were measured in specimens where the large inter-clod voids had been eliminated during specimen compaction, corresponding to a reduction in the available flow paths within the microstructure.

Pusch and Schomburg (1999) considered the hydraulic conductivity of in-situ and artificially prepared specimens of Friedland clay. Artificially prepared specimens were prepared by oven-drying, grinding and compacting Friedland clay. The hydraulic conductivity of artificially prepared specimens was found to be slightly higher than that of the undisturbed specimens. The hydraulic conductivity differences were attributed to microstructural homogenisation in the undisturbed specimen.

Pusch (1999) stated that as the bentonite hydrates, the platelets stacks expand and exfoliate. This exfoliation of platelets from the platelet stacks produces a low permeability gel between platelet stacks. High voltage transmission electron microscopy was used to investigate the hydration process. The density and permeability of the gel was found to vary.

2.7.4 Influence of exchangeable cation type on saturated hydraulic conductivity

The swelling of bentonite during hydration is a function of a number of factors, including the montmorillonite content, which has been discussed previously in Subsection 2.7.2. The inter-layer spacing due to the formation of diffuse double layers can be calculated from the Gouy-Chapman diffuse double layer theory (Tripathy et al., 2004). The separation of platelets (the inter-platelet distance, *d*) is a function of the valency of the bentonite. As the inter-platelet distance increases, the overall swelling of the platelet stack increases, reducing the available flow channels through the bentonite microstructure.

Rao and Mathew (1995) prepared homo-ionic clays by displacing the exchangeable cations with a leachate, and then treating the clay with a metal chloride. Mono-, di- and tri-valent cations were considered. It was reported that as the valency of the exchangeable cation increased, the hydraulic conductivity of the clay increased. The hydraulic conductivity determined for aluminium-exchanged clay was found to be an order of magnitude greater than that of sodium-exchanged clay for pressures between 25 and 800 kPa. For cations of the same valency, the hydraulic conductivity was also found to decrease as the hydrated ion radius increased.

Dananaj et al. (2005) determined the hydraulic conductivity of a calcium and sodium bentonite. The sodium bentonite was found to have a lower hydraulic conductivity than that of the calcium bentonite, for the smectite contents considered. Ahn and Jo (2009) also considered the difference in measured hydraulic conductivity in calcium and sodium bentonite. As the fraction of sodium (Na^+) ions within the bentonite increased, the hydraulic

conductivity decreased. This effect was observed to be more significant at higher sodium fractions.

2.7.5 Influence of permeant on saturated hydraulic conductivity

The hydraulic conductivity of compacted saturated bentonites permeated with an ionised solution has attracted considerable attention in literature. In deep geological repositories, the compacted bentonite may be saturated by saline water from the host rock, depending on the proximity to seawater. Geosynthetic clay liners may be required to retard the flow of other ionic solutions other than water (Shackelford et al, 2000). As with montmorillonite content and predominant type of exchangeable cation, the swelling of the bentonite is a function of the ionic concentration of the bulk fluid. The thickness of the diffuse double layer reduces as the concentration increases, with a lower degree of swelling observed of the platelet stacks.

Dixon et al. (2002) studied the influence of the permeant salinity on the saturated hydraulic conductivity of bentonites. Sodium chloride (NaCl) solutions were prepared with concentrations increasing from 10 g/l to 350 g/l. The hydraulic conductivity of bentonite was found to increase as the electrolyte concentration increased. Significant differences were observed in the measured hydraulic conductivities when the NaCl concentration was increased from 10 g/l to 350 g/l, with greater concentrations of NaCl leading to larger hydraulic conductivities.

Shackelford et al. (2000) determined the hydraulic conductivity of geosynthetic clay liners when permeated with zinc chloride ($ZnCl_2$) solutions from 0.01 M to 0.1M. Increases

in electrolyte concentration were reported to result in an increase in the saturated hydraulic conductivity.

Jo et al. (2005) measured the long term hydraulic conductivity of sodium bentonite permeated with salt solutions. Three salt solutions, sodium chloride (NaCl), potassium chloride (KCl) and calcium chloride ($CaCl_2$) were considered. The hydraulic conductivity determined using NaCl and KCl solutions was found to be twice that determined using distilled water. The hydraulic conductivity of bentonite when permeated with $CaCl_2$ was found to be greater than that which was obtained using NaCl and KCl solutions.

2.7.6 Influence of temperature on saturated hydraulic conductivity

The physical properties of water, including density and viscosity, are temperature dependant (Handbook of Physics and Chemistry, 2006). Olsen and Daniel (1981) stated that a 1 ºC temperature change can result in a 3% change in hydraulic conductivity. To minimise experimental error due to temperature fluctuations, a temperature controlled environment should be considered during testing.

Cho et al. (1999) measured the saturated hydraulic conductivity of calcium bentonite between 20 ºC and 80 ºC. Multiple specimens were prepared at three compaction dry densities. Tests were conducted at 10 ºC pressure increments. The hydraulic conductivities determined were found to increase with an increase in temperature. The increase of hydraulic conductivity with temperature was observed to be more pronounced at lower compaction dry densities.

The hydraulic conductivity-temperature relationship determined by Villar and Gomez-Espina (2009) also showed that the hydraulic conductivity of FEBEX bentonite increased as the temperature increased from 25 ºC to 80 ºC. It was also observed that the influence of temperature was more significant for the specimens with dry densities of 1.5 Mg/m^3 than that for specimens with dry density of 1.7 Mg/m^3.

2.8 Hydraulic conductivity of sand-bentonite and crushed rock-bentonite mixtures

Sand-bentonite and crushed rock-bentonite mixtures have been proposed as suitable backfilling materials for high level radioactive waste disposal in deep geological repositories. The backfilling material is required to have a similar hydraulic conductivity to that of the host rock, to have a high resistance to erosion, be mechanically and chemically stable, and to limit the expansion of the contacting buffer material (Pusch, 1978; Villar, 2005). Sand-bentonite and crushed rock-bentonite mixtures possess higher thermal conductivity and stiffness, and are more economical than pure bentonite (Tien et al., 2004).

The hydraulic conductivity of compacted bentonite mixtures has been widely reported in literature. Similarly to that reported for bentonite, the hydraulic conductivity of bentonite mixtures has been found to decrease as the compaction dry density increased (Kenney, 1992; Dixon et al., 1999; Sivapullaiah et al., 2000). Constant-head, variable head and constant flow hydraulic conductivity tests have all been reported within the literature.

Hydraulic conductivity tests have been conducted for a range of bentonite to sand or crushed rock percentages. Chapius (1989) determined the hydraulic conductivity of sand-

bentonite specimens containing up to 33% bentonite. Kenney et al. (1992) reported the hydraulic conductivity of sand-bentonite mixtures with a bentonite content increasing to 30%. Studds et al. (1998) determined the hydraulic conductivity of 10 and 20% bentonite contents in sand-bentonite mixtures. Sivapullaiah et al. (2000) and Prikryl et al. (2003) tested a range of sand-bentonite mixtures, where the bentonite content increased from 0-100%. Komine (2010) considered the hydraulic conductivity of sand-bentonite mixtures with 10, 20, 30 and 50% bentonite by mass.

Several authors have reported the hydraulic conductivity behaviour of several ratios of sand to bentonite to assess the influence of the extent of the bentonite matrix on the conductivities observed. Kenny et al. (1992) conducted a series of tests on compacted sand-bentonite specimens. Specimens were tested under a hydraulic gradient of 15. The hydraulic conductivity of the sand-bentonite mixture was found to decrease as the percentage of bentonite within the mixture increased. It was concluded that low hydraulic conductivity in sand-bentonite mixture required continuity of the bentonite matrix within the specimen.

The hydraulic conductivity behaviour determined by Sivapullaiah et al. (2000) supported the findings of Kenney et al. (1992). It was found that the size of the sand particles in the sand-bentonite mixtures controlled the hydraulic conductivity of the mixture at low bentonite contents and that when then bentonite content in the sand-bentonite mixture was greater than the voids present within the sand, the hydraulic conductivity was controlled by the clay content.

Numerous authors have determined the swelling and hydraulic conductivity behaviour of crushed rock-bentonite and sand-bentonite mixtures at 30:70 (Sivapullaiah et al., 2000;

Borgesson et al., 2003; Prikryl et al., 2003; Komine, 2004; Villar, 2005; Sun et al., 2008; Cui et al., 2008; Komine, 2010). This percentage of bentonite to sand or crushed rock has been proposed as suitable for deep geological disposal (Gunnerson et al., 2004; Nirex, 2005).

Borgesson et al. (2003) considered the effect of heterogeneity on the hydraulic conductivity of crushed rock-bentonite mixtures. Crushed granite was used in the mixture. The measured hydraulic conductivity was compared with the expected values, assuming a homogeneous distribution of crushed rock and bentonite throughout the mixture. A heterogeneous distribution of the clay matrix was observed. It was concluded that the heterogeneities within the mixture increased with decreasing bentonite content. It was also observed that the hydraulic conductivity increased with increased heterogeneities.

A review of literature pertaining to the measurement of the hydraulic conductivity of compacted sand-bentonite and crushed rock-bentonite mixtures have highlighted several points requiring consideration during this study. Firstly, the application of hydraulic gradient using the constant-head method has been reported within the literature, and is therefore considered appropriate for sand-bentonite and crushed rock-bentonite mixtures. The behaviour of the mixtures has been reported to be largely controlled by the sand content at higher sand contents, and by the bentonite at higher bentonite contents.

The continuity of the bentonite matrix is required for low hydraulic conductivities. Lastly, a homogeneous mixture is desirable to ensure an accurate representation of the hydraulic conductivity is determined. At low bentonite contents, the effect of heterogeneities within the matrix has been reported to be more pronounced, leading to more permeable channels within the microstructure, leading to an increased hydraulic conductivity.

2.9 Gas permeability of compacted bentonite

The gas permeability of compacted bentonites is an important consideration in both municipal and high level radioactive waste facilities. Gas emissions from landfills are predominantly carbon dioxide and methane. The migration of methane from landfills to the surrounding area should be prevented, due to the explosive nature of the gas.

The gas permeability of geosynthetic clay liners with nitrogen gas has been studied previously. Didier et al. (2000) carried out a series of gas permeability tests on a partially saturated geosynthetic clay liner with nitrogen gas. The influence of volumetric water content, hydration process and overburden pressure was studied. It was found that an increase of overburden pressure lead to a reduction in the determined gas permeability. The gas permeability was also found to decrease from 10^{-16} to 10^{-18} m^2 as the volumetric water content increased from 46 to 79%.

Bouazza and Vangpaisal (2003) carried out a series of tests to determine the relationship between gas permeability and volumetric water content for geosynthetic clay liners. The tests were carried out under constant gas pressure differentials using nitrogen gas as the permeant. The extended Darcy's law, to account for flow volumes, was used to calculate the gas permeability. The range of gas permeabilities determined was found to decrease from 10^{-13} m^2 when the volumetric water content was 10% to 10^{-18} m^2 at 60% water content.

Vangpaisal and Bouazza (2004) investigated the effect on the gas permeability of different geosynthetic clay liners. Needle punched and stitched bonding liners were

considered, produced with both granular and powdered bentonite. The gas permeability of the granular bentonite clay liner was found to be higher than that of the powdered bentonite liner. Similar to previous studies, the gas permeability decreased as the volumetric water content increased. Similar trends were observed to those reported by Bouazza and Vangpaisal (2003). The volumetric water contents considered ranged from 20% to 120%.

Determining the gas permeability of compacted bentonites using nitrogen gas has been reported previously. The gas permeability has been calculated from the flow through the specimen and the pressure differential applied. However, the determination of the gas permeability for bentonites with low water contents (<20%) is limited within the literature.

Iversen et al. (2001) reported that the determination of gas permeability was a more time-efficient method of characterising non-clayey soils, and could be used to determine the hydraulic conductivity of the soil, using the viscosity and density of water and the permeating gas. The hydraulic conductivity of predominately sandy soils has been reported from the gas permeability (Riley and Ekeberg, 1989; Loll et al., 1999). However for clays, the structure of the clay is dependent on the degree of saturation (Mitchell and Soga, 2005).

2.10 Models available to assess the hydraulic conductivity of compacted bentonites

The hydraulic conductivity is an important parameter for assessing flow in compacted saturated bentonites. Historically, a number of models have been proposed to determine the hydraulic conductivity in compacted saturated bentonite. Hazen (1892) developed an empirical formula for predicting the hydraulic conductivity of sands, based on the particle

size of which 10% of the soils is finer, and an empirical coefficient (C_H) that is usually assumed to be around 100, but stated to range between 1 and 1,000 (Carrier III, 2003).

Continuing improvements and developments in the analytical determination of hydraulic conductivity have been proposed. The following sections describe a number of these models.

2.10.1 Kozeny-Carman model for saturated hydraulic conductivity

The Kozeny-Carman model is derived from Poiseuille's law of flow through a series of capillary tubes (Mitchell and Soga, 2005). The model was proposed by Kozeny (1927), and was modified by Carman (1937, 1956). The Kozeny-Carman model is expressed as

$$k_h = \left(\frac{\gamma_p}{\mu_p}\right)\frac{1}{k_0 T^2 S_0^2}\left(\frac{e^3}{1+e}\right) \tag{2.2}$$

where k_h is the hydraulic conductivity, γ_p is the unit weight of the permeant, μ_p is the viscosity of the permeant, S_0 is the wetted surface area per unit volume of particles, T is the tortuosity factor, k_0 is the pore shape factor and e is the void ratio. k_0 is typically assumed to be 2.5, with T taken as $\sqrt{2}$ (Mitchell and Soga, 2005).

Carrier III (2003) stated a number of limitations of the Kozeny-Carman model. The physico-chemical forces present within bentonite are not considered in the model. It is also assumed that the soil particles are compact and regular; in compacted bentonites, the total porosity is comprised of a macro- and micro-porosity. The model is also stated not to be appropriate if a large fine fraction is observed from the particle size distribution of the soil.

The empirical parameters assumed within the model, namely k_0 and T, have not been reported for differing soil types.

Chapius and Aubertin (2003) presented a review of hydraulic conductivity determined using the Kozeny-Carman model. For homogenised soil specimens, the hydraulic conductivity determined from the Kozeny-Carman model was observed to fall within a range of 1/3 to 3 times that measured in hydraulic conductivity tests. Chapius and Aubertin (2003) stated that observed differences between the predicted hydraulic conductivity from the Kozeny-Carman model and test results may be due to incorrect estimates of specific surface area, testing procedures and theoretical limitations.

Singh and Wallender (2008) modified the Kozeny-Carman model to take into account the influence of adsorbed water layers to the clay platelet surfaces. The volumes of water associated with increasing numbers of hydrate layers (0, 1, 2 and 3) were calculated from the specific surface area of the bentonite. The effective porosity was calculated, assuming this to be the previous porosity of the bentonite with the proportion of available pore space occupied by the fixed hydrate layers removed. The effective porosity was then used in place of the 'true' porosity in the Kozeny-Carman model. The effective porosity with three hydrate layers was report a reasonable approach to the evaluation of the hydraulic conductivity.

2.10.2 Cluster model for saturated hydraulic conductivity

The Cluster model was proposed by Olsen (1962) to account for the different porosities within saturated clays. Olsen (1962) reported discrepancies between the hydraulic conductivity determined in tests with that which was predicted by the Kozeny-Carman

model. The Cluster model considers the void ratio of the clay as two distinct components; the intra-cluster (micro-pore) void ratio e_c and the inter-cluster (macro-pore) void ratio e_p. The total void ratio was stated as

$$e_T = e_c + e_p \tag{2.3}$$

where e_T is the total void ratio, e_c is the intra-cluster void ratio and e_p is the inter-cluster void ratio. Olsen (1962) assumed that the flow occurred through the inter-cluster pores within the clay and that the clusters were spherical. The hydraulic conductivity of the clay was calculated from the Cluster model as

$$\frac{k_{CM}}{k_{KC}} = N^{\frac{2}{3}} \frac{\left(1-\frac{e_c}{e_T}\right)^3}{(1+e_c)^{\frac{4}{3}}} \tag{2.4}$$

where k_{CM} is the hydraulic conductivity determined from the Cluster model, k_{KC} is the hydraulic conductivity calculated from the Kozeny-Carman model and N is the average number of clay particles per cluster.

Achari et al. (1999) used the Cluster model and Gouy-Chapman diffuse double layer theory to calculate the hydraulic conductivity of clays. The intra-cluster void ratio was determined from the equation of true effective stress in saturated clay (Lambe and Whitman, 1969), stated as

$$\sigma^* = (\sigma - u_w) - (R - A) \tag{2.5}$$

where σ^* is the true effective stress, σ is the total stress, u_w is the pore-water pressure, R is the repulsive stress and A is the attractive stress.

The repulsive stress was determined from the Langmuir equation, stated in Equation (2.4) (Verwey and Overbeek, 1948). The attractive stress was determined from van der Waal's attractive stress, stated in Equation (2.7) (Sridharan and Jayadeva, 1982).

$$R = 2nk'T(\cosh u - 1) \tag{2.6}$$

$$A = \frac{B}{48\pi}\left[\frac{1}{d^3} + \frac{1}{(d+\delta)^3} - \frac{2}{(d+0.5\delta)^3}\right] \tag{2.7}$$

where n is the concentration of ions in solution, k' is the Boltzmann constant, T is the absolute temperature, u is the dimensionless electric potential midway between two interacting double layers, B is a constant, d is the half separation distance between the clay platelets, and δ is the thickness of the unit layers of the clay platelet.

Achari et al. (1999) determined the hydraulic conductivity from the Cluster model for sodium and calcium bentonites. Equations (2.5) - (2.7) were used to determine the intra-cluster and inter-cluster void ratios, and the resultant total void ratio. The Kozeny-Carman model was then used to determine the hydraulic conductivity from the Cluster Model, using Equation (2.4). The number of platelets per cluster, N, was not known, and was assumed from an empirical relationship. The calculated values were compared with the hydraulic conductivities determined by Mesri (1969). A reasonable agreement was noted between the theoretical and experimental data. However, the age of the experimental data and subsequent

developments in the experimental determination of the hydraulic conductivity of bentonites was not included in the assessment.

2.10.3 Komine (2004)'s model for saturated hydraulic conductivity

Komine and Ogata (1999) proposed a model for saturated hydraulic conductivity based on the swelling potential of compacted specimen under a constant applied vertical pressure. The model was modified by Komine (2004) to include the effect of exchangeable cations on the predicted hydraulic conductivity. The swelling strain of montmorillonite, ε_{sv}* was stated as

$$\varepsilon_{sv}^{*} = \frac{V_v + V_{sw}}{V_m} \tag{2.8}$$

where V_v is the volume of voids within the bentonite, V_{sw} is the swelling deformation under constant vertical pressure and V_m is the volume of montmorillonite within the bentonite. It is assumed that the swelling of the bentonite is due to the hydration of the montmorillonite.

Komine (2004) calculated the swelling strain of montmorillonite (ε_{sv}*) from the increase in inter-platelet distance during swelling. The half distance between two montmorillonite platelets for each exchangeable cation species considered was determined.

$$d_i = \frac{\varepsilon_{sv}^{*}}{100}\{t + (R_{ion})_i\} + (R_{ion})_i \tag{2.9}$$

where d_i is the half distance between two platelets for exchangeable cation i (in m), t is the thickness of the montmorillonite platelet (in m) and R_{ion} is the non-hydrated radius of the

exchangeable cation (in m). The hydraulic conductivity was determined for each cation type considered. Equation (2.10) was used to calculate the individual hydraulic conductivities. The weighted average hydraulic conductivity was calculated using Equation (2.11).

$$k_i = \frac{\gamma_{aw}}{12\mu_{aw}}(2d_i)^2 \quad (2.10)$$

$$k = \frac{1}{B}\sum_i [B_i k_i] \quad (2.11)$$

where k_i is the hydraulic conductivity determined for each exchangeable cation species (in m/s), γ_{aw} is the density of adsorbed water within the montmorillonite platelets (in Pa/m), μ_{aw} is the viscosity of adsorbed water within the montmorillonite platelets (in Pa.s), B is the cation exchange capacity (in meq/100g) and B_i is the individual exchange capacities for the exchangeable cation species considered (in meq/100g).

The properties of the interlayer water are unknown. Komine and Ogata (1999) stated that the ratio between density (γ_{aw}) and viscosity (μ_{aw}) of adsorbed water was calculated as

$$\frac{\gamma_{aw}}{\mu_{aw}} = \frac{1}{R}\frac{\gamma_{fw}}{\mu_{fw}} \quad (2.12)$$

where R is an empirical factor, γ_{fw} is the density of free water (in Pa/m) and μ_{aw} is the viscosity of free water (in Pa.s). The values of R have not been determined within the literature. Sato (1971) reported that the empirical value of R as 79 for bentonite clay and 14 for silty clay (Sato, 1971). Komine (2004) has considered both values when using the proposed model.

Komine and Ogata (1999) experimentally determined the hydraulic conductivity of compacted bentonite specimens. The results were compared with the predicted hydraulic conductivity determined through the proposed model. It was observed that the predicted hydraulic conductivity when R was assumed to be 79 was a good approximation of the experimental behaviour. This corresponded to that reported by Sato (1971).

2.11 Summary

A detailed literature review of the hydraulic behaviour of compacted bentonites was presented in this chapter, relating to its use as a barrier and backfilling material in engineered barriers. The structure of the montmorillonite mineral and the microstructure of compacted bentonites were stated. The swelling mechanisms of compacted bentonites were discussed.

A brief review of the methods of determining the hydraulic conductivity of compacted saturated bentonites was presented. The factors affecting the hydraulic conductivity of clays were considered. The hydraulic conductivity of compacted sand-bentonite and crushed rock-bentonite mixtures was reviewed. The determination of the gas permeability of compacted bentonites was presented. The theoretical models used to assess hydraulic conductivity of compacted saturated bentonite were briefly discussed.

A review of literature pertaining to the hydraulic conductivity of compacted bentonites has highlighted a number of areas that require further investigation;

1. It has been reported by Chapius (2012) that the determination of hydraulic conductivity should not be calculated from either inflow or outflow. However, the studies reported in the literature have only used the inflow or outflow rate when calculating hydraulic conductivity. The compatibility between flow rates is required to assess whether it is appropriate to only consider inflow or outflow.

2. Darcy's law is widely reported to be valid for compacted bentonites, although the existence of 'threshold' gradients has been noted. A linear relationship between hydraulic flux and hydraulic gradient will indicate whether Darcy's law is valid.

3. The gas permeabilities of compacted bentonites have been determined for a range of volumetric water contents between 20 and 120%. However, limited data exists for bentonites with low water contents (<20%). In the case of landfill covers, the bentonite will be initially placed in unsaturated conditions and, subject to environmental conditions, may become air-dry. An understanding of the gas permeability at low moisture contents is required to assess the potential flow of gases through the cover.

4. Several models exist for the determination of the hydraulic conductivity of bentonites. A review of the current literature has indicated limitations in each of the models, primarily in relation to assumptions of certain parameters. Assessment of these models is required using the experimental hydraulic conductivity data derived in this study.

CHAPTER 3

MATERIALS AND METHODS

3.1 Introduction

This chapter presents the physical and chemical properties of the materials used in this research. The experimental procedures used in subsequent chapters are also described. The properties determined for the materials used in this study are presented in Subsections 3.3 and 3.4. The bentonite properties were compared with corresponding results in literature. The bentonite suction-water content soil-water characteristic curve is presented in Subsection 3.5.

Three testing procedures are described in Subsection 3.6. The preparation of compacted specimens for each procedure is presented. The experimental set-up and testing procedure for determining the hydraulic conductivities of compacted specimens is provided. The step-wise consolidation of compacted specimens is described. The procedure to determine the gas permeabilities of compacted bentonite using a gas permeability cell is presented. Concluding remarks on material properties and experimental methods are made.

3.2 Material used in the current study

The main material considered in this study is commercially available MX80 bentonite. It is provided as a fine, granular powder, predominately grey in colour. The bentonite was stored at room temperature prior to testing in a sealed, airtight environment. MX80 has been considered previously in reference to barrier and backfill materials for deep geological disposal (Pusch, 1982; Pusch and Yong, 2006; Delage et al., 2006). Leighton Buzzard sand, a commercially available silica sand (250 - 600 μm) supplied from Sibelco Ltd has also been used in the experimental programme, due to its relative availability.

3.3 Properties of the bentonite studied

The mineralogy of MX80 bentonite was determined using x-ray diffraction. The use of x-ray diffraction allows for determination of specific minerals through measurement of the intercept angle and the *c* axis spacing. Figure 3.1 shows the x-ray diffraction chart for MX80 bentonite. The minerals were assigned to the corresponding peaks, and through semi-

quantative analysis, it was determined that MX80 bentonite consisted of 76% montmorillonite, 14% cristobailite and 10% quartz.

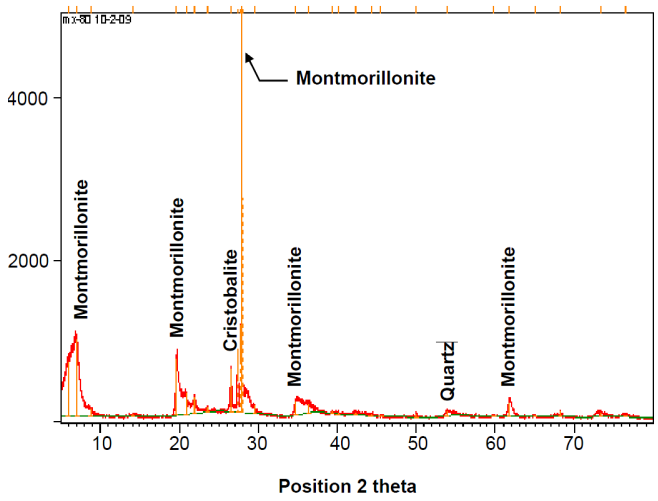

Figure 3.1 - X-ray diffraction chart for MX80 bentonite

The grain size distribution of the bentonite was determined using particle size distribution and hydrometer analysis, as described in the British Standards (BS 1377:2:1990). The results obtained are presented in Figure 3.2.

The percentage of grains passing 2 µm was 84%. The grain size distribution obtained during this study was compared with that reported by Singh (2007) and was found to be in good agreement. Cerato and Lutenegger (2002) reported that the percentage passing 2 µm was 60%. Masden (1998) reported the percentage passing 2 µm was 77.6%, while Villar (2007) has reported the percentage between 76 and 90%. The liquid limit and plastic limit were determined following the procedure detailed in British Standards (BS1377:2:1990) and were found to be 396% and 45% respectively. The shrinkage limit was determined by wax method (ASTM D 4930:08:2008) and was found to be 16%.

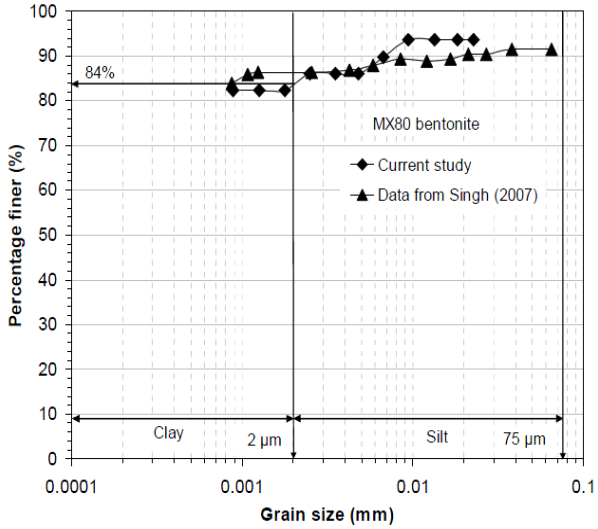

Figure 3.2 - Grain size distribution of MX80 bentonite, compared with that obtained by Singh (2007)

The percentage of grains passing 2 µm was 84%. The grain size distribution obtained during this study was compared with that reported by Singh (2007) and was found to be in good agreement. Cerato and Lutenegger (2002) reported that the percentage passing 2 µm was 60%. Masden (1998) reported the percentage passing 2 µm was 77.6%, while Villar (2007) has reported the percentage between 76 and 90%. The liquid limit and plastic limit were determined following the procedure detailed in British Standards (BS1377:2:1990) and were found to be 396% and 45% respectively. The shrinkage limit was determined by wax method (ASTM D 4930:08:2008) and was found to be 16%.

The cation exchange capacity describes the amount and type of cations present on the clay platelet surface that can be easily exchanged by other cations when available in solution (van Olphen, 1977). The cation exchange capacity of MX80 bentonite was determined using the ammonium acetate technique at pH 7 (Grim, 1968, Thomas 1982). The individual cation

exchange capacities for Na^+, K^+, Ca^{2+} and Mg^{2+} were found to be 45.7, 1.6, 31.9, and 9.1 meq/100g respectively. The total cation exchange capacity was determined to be 88.3 meq/100g. The weighted average valency (Tripathy et al., 2004) of the exchangeable cations was calculated to be 1.46.

The specific gravity of MX80 bentonite was determined following the procedure detailed in the British Standards (BS 1377:3:1990). The specific gravity of solids was determined with kerosene as the dispersing fluid. The specific gravity was determined to be 2.76.

The total surface area of a clay specimen is determined from the ethylene glycol mono-ethyl ether (EGME) method (Heilman et al., 1965). The total surface area of MX80 bentonite was found to be 640 m^2/g.

The properties of the MX80 bentonite are presented in Table 3.1 and are compared with those reported in literature. Some differences were observed between the properties determined in this study and those reported. The liquid limit determined was found to be lower than that reported elsewhere. This difference was primarily attributed to a lower montmorillonite content. The Atterberg limits and specific gravity of bentonite solids were found to be comparable to those determined by other authors.

3.4 Properties of the sand studied

The air-dry water content and the particle size distribution of the Leighton Buzzard sand were established following the procedure given in British Standards (BS 1377:2:1990). The air-dry water content of the sand was found to be 3%. Figure 3.3 shows the particle size distribution for Leighton Buzzard sand. Figure 3.3 shows that Leighton Buzzard sand is poorly graded with a 93% of particles having a diameter between 300 and 600 μm.

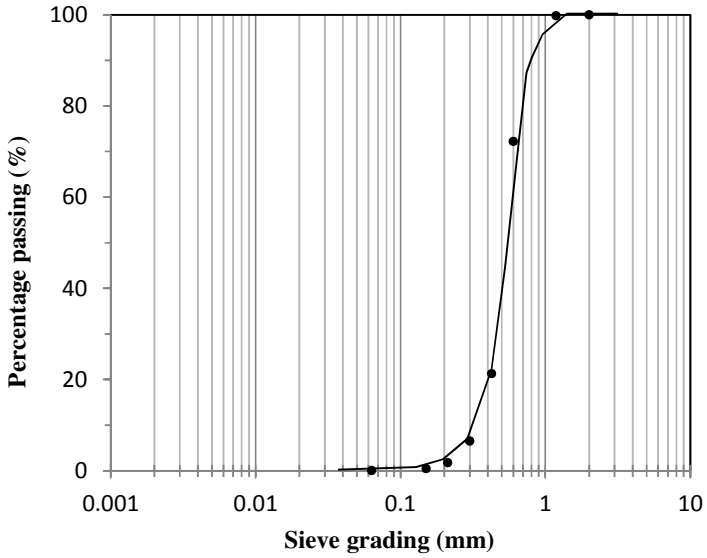

Figure 3.3 - Particle size distribution for Leighton Buzzard sand.

Table 3.1 - Selected properties of MX80 bentonite

Author	*This study*	*Pusch (1982)*	*Müller-Vonmoos and Kahr (1987)*	*Saiyouri et al. (1998)*	*Sauzeat et al. (2001)*	*Cerato and Lutenegger (2002)*	*Mata et al. (2002)*	*Villar (2007)*	*Tadza (2011)*
Liquid limit (%)	396	-	411 ± 10	-	520	519	-	526	437
Plastic limit (%)	45	-	47	-	46	35	-	46	163
Shrinkage limit (%)	16	-	14	-	-	-	-	-	12.2
Specific gravity	2.76	-	-	-	2.65	-	2.76	2.82	2.8
Total surface area (m^2/g)	640	700	562	522	-	637	-	-	676
Cation exchange capacity (meq/100g)	88.3	-	-	82.3	70	76.4	-	75 - 82	90.3
Montmorillonite content (%)	76	80-90	-	-	82	80	-	-	75

3.5 Soil-water characteristic curve

The soil-water characteristic curve provides the relationship between suction and water content in soils (Fredlund and Rahardjo, 1993). Two techniques were used to establish the suction-water content soil-water characteristic curve. For lower suction ranges, the osmotic technique was used. Higher suction values were determined through vapour equilibrium technique. The results obtained were compared with those reported by Bag (2011).

3.5.1 Osmotic technique

Bentonite-water mixtures were prepared by mixing MX80 bentonite powder with distilled, de-aired water. The distilled water was held under a vacuum overnight, using a vacuum pump, to minimise the volume of dissolved air within the water. The initial water content targeted was 1.15 times the liquid limit of the MX80 bentonite. The bentonite-water mixtures were stored in an airtight container in a temperature controlled room for seven days to allow for water equilibrium to take place. The mixtures were mixed intermittently during this period.

The osmotic technique uses solutions of polyethylene glycol (PEGs) to control and apply suction to soils. In the current study, solutions of PEG and water were prepared by dissolving a predetermined mass of PEG-6000 into 500 ml of distilled, de-aired water. The mass of PEG-6000 to be added was calculated from the empirical relationship between suction and PEG concentration stated by Delage et al. (1998). Three suctions values were

targeted; 0.2, 0.5 and 1 MPa. Samples of the bentonite-water mixture were inserted into a previously-wetted semi-permeable membrane that was sealed at either end.

The initial water content of the bentonite-water mixture was determined prior to testing following the procedure in the British Standard (BS1377-2:1990). The mass of the membrane and sealing attachments were recorded prior to the tests commencing. The specimen and membrane was then submerged into the PEG solution, which was magnetically stirred. The total mass of the bentonite-water specimen, the membrane and attachments was monitored until the mass became constant (i.e. suction equilibrium was reached). The final water content of the bentonite-water specimen was then determined.

3.5.2 Vapour equilibrium technique

The wetting suction-water content soil-water characteristic curve of the MX80 bentonite was established using vapour equilibrium technique. Tests were conducted within closed-lid desiccators using saturated salt solutions (ASTM E 104-85, 1998). Six saturated salt solutions were considered, which generated relative humidities corresponding to suctions between 3.3 and 294.8 MPa. Details of the salts used are presented in Table 3.2.

Table 3.2 - Details of the saturated salt solutions used

Salt	*Relative humidity (%) at 20˚C*	*Suction (MPa)*
Potassium Sulphate (K_2SO_4)	97.6 ± 0.5	3.3
Potassium Nitrate (KNO_3)	94.6 ± 0.7	7.5
Potassium Chloride (KCl)	85.1 ± 0.3	21.8
Sodium Chloride (NaCl)	75.5 ± 0.1	38.0
Potassium Carbonate (K_2CO_3)	43.2 ± 0.3	113.3
Lithium Chloride (LiCl)	11.3 ± 0.3	294.8

Specimens were prepared by statically compacting MX80 bentonite powder at the air-dry water content into thick-walled stainless steel specimen rings, following the procedure subsequently detailed in Subsection 3.6.1.1. The specimens prepared were 45 mm in diameter and 8 mm in height. Specimens were produced to 1.2, 1.3 and 1.4 Mg/m^3 targeted dry densities. The compacted MX80 bentonite specimens were then equilibrated at the six relative humidities in the closed-lid desiccators until the measured masses of the specimens became constant (i.e. suction equilibrium had been reached). Specimens of MX80 bentonite powder were also equilibrated.

3.5.3 Soil- water characteristic curve

The suction-water content soil-water characteristic curve obtained for MX80 bentonite is shown in Figure 3.4. For the vapour equilibrium technique, the data points relating to the powder samples are presented in Figure 3.4. The equilibrated water contents of the powder and compacted specimens were observed to be similar (Bennett et al., 2012). Although the initial conditions of the specimens prior to testing differed (slurried saturated bentonite for osmotic technique, and air-dry powder bentonite for vapour equilibrium technique), good agreement is noted at suctions at the overlap between osmotic and vapour equilibrium techniques (between 1 and 5 MPa).

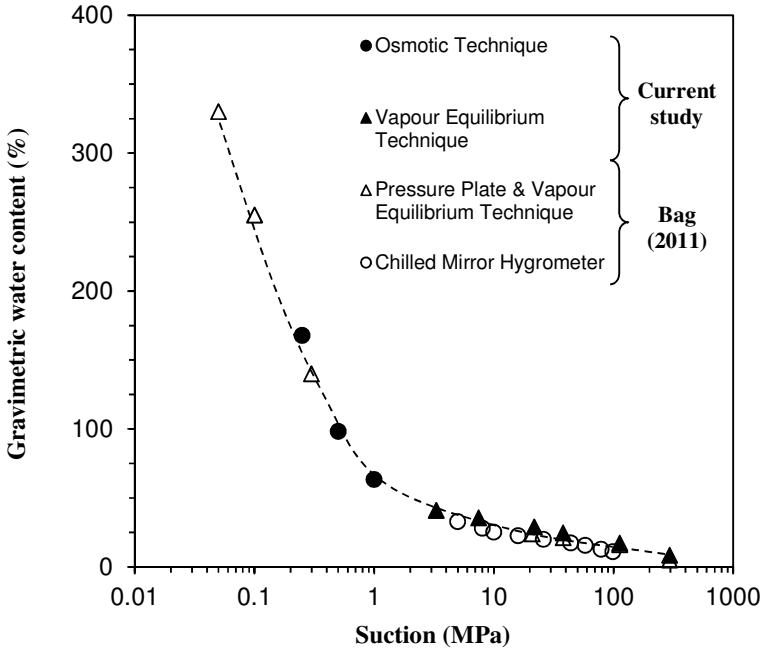

Figure 3.4 - Suction-water content soil-water characteristic curve for MX80 bentonite

Figure 3.4 also shows the suction-water content soil-water characteristic curve obtained by Bag (2011). Tang and Cui (2010) also presented the suction-water content soil-

water characteristic curve for MX80 bentonite. The suction-water content soil-water characteristic curve obtained in this study shows good agreement with that determined by Tang and Cui (2010) and Bag (2011).

3.6 Experimental programme

The experimental programme for this study consists of three types of tests (i) saturated hydraulic conductivity tests (ii) consolidation tests and (iii) gas permeability tests. Saturated hydraulic conductivity tests were conducted using a modified swelling pressure cell connected to two pressure-volume controllers. The compressibility behaviour of compacted specimens was carried out using conventional one dimensional oedometers. The gas permeability of compacted MX80 bentonite specimens was established using an existing device for determining gas permeability in cast concrete. The following subsections present details of the preparation of specimens and the experimental procedures adopted to carry out the laboratory tests.

3.6.1 Saturated hydraulic conductivity tests

The saturated hydraulic conductivities of compacted MX80 bentonite and sand-bentonite mixtures were considered in this study. A modified swelling pressure cell was used in conjunction with two pressure-volume controllers. A software package, GDSlab, was used to control the inflow and outflow pressures of the pressure-volume controllers, and to record the flow volumes. The preparation of compacted specimens, details of the experimental apparatus assembly and testing procedure are detailed here.

3.6.1.1 Specimen preparation

Specimens were produced by static compaction. The diameter and height of the specimens produced were 45 mm and 8 mm respectively. The compaction device consists of five main components; (a) a base, (b) a specimen ring, (c) a collar, (d) a locking ring and (e) a compaction piston. The specimen ring fitted in to a recess in the base of the compaction mould. The collar was placed onto the specimen ring. The locking ring was placed onto the collar, securing the collar to the base of the mould. The locking ring is fastened to the base using three 10 mm bolts. The components of this compaction mould are shown in Figure 3.5.

Figure 3.6 shows the assembled compaction mould. Prior to the specimen being compacted, the inner surface of the collar was lubricated using silicon grease, to minimise the friction between the collar and piston. The specimen ring was not lubricated, due to the possibility of contamination of the specimen with silicon grease. The travel direction of the piston would result in vertical travel of the silicon grease on the piston surface through the final stages of the compaction process.

The assembled compaction mould was transferred to a high capacity, static compaction machine. Load was applied until the piston rim and the collar made contact. The load was maintained for five minutes to minimise elastic rebound within the specimen once the compaction pressure had been removed. The height and diameter of the specimen were re-measured, and the achieved dry density was calculated.

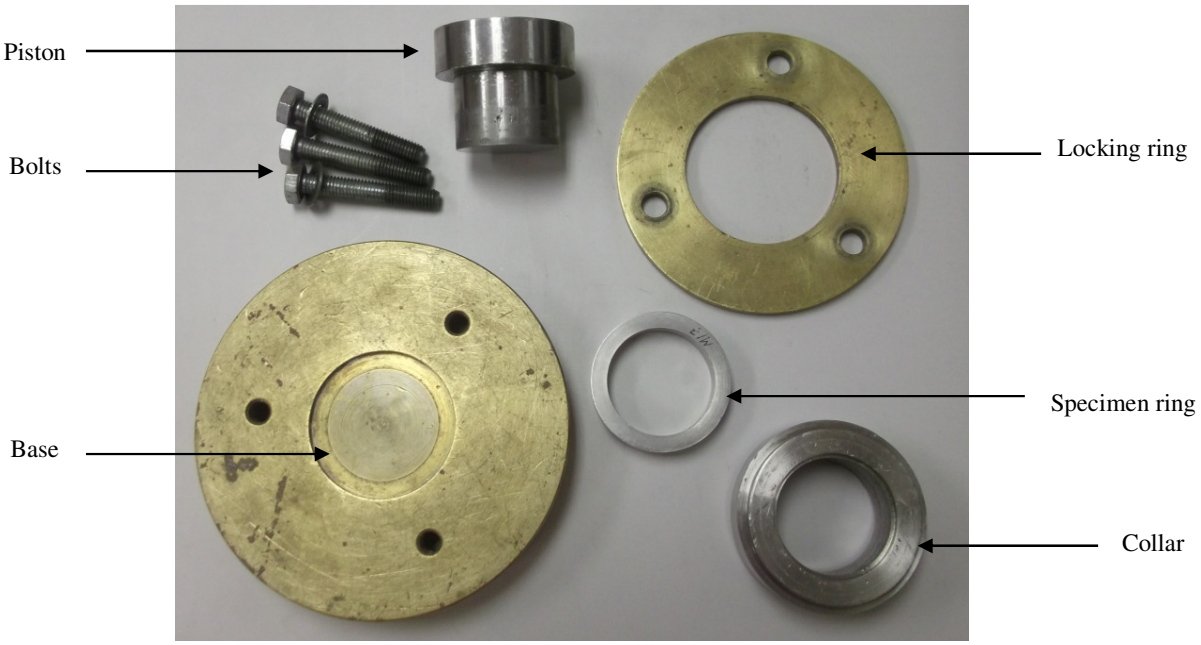

Figure 3.5 - The constituent components of the compaction mould

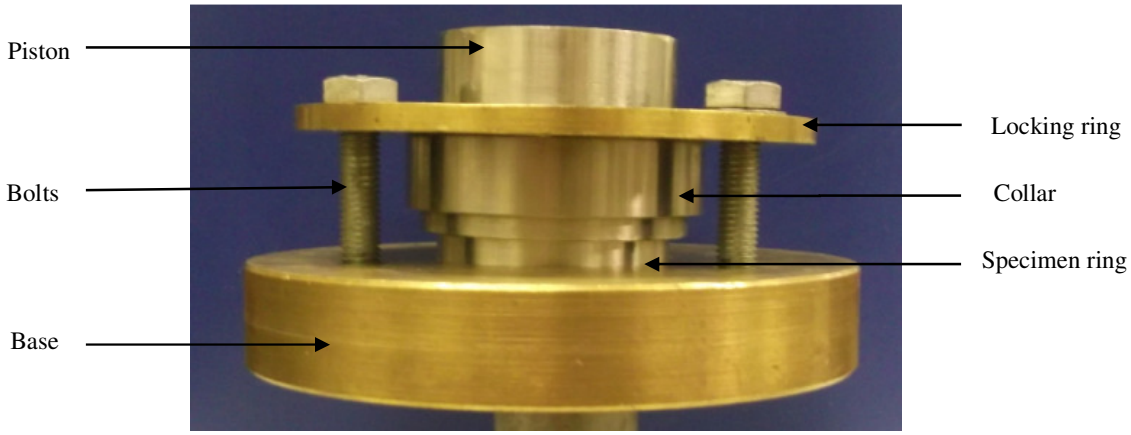

Figure 3.6 – The assembled compaction mould for preparing compacted specimens

3.6.1.2 Testing procedure

The hydraulic conductivity cell used in this study was modified from a swelling pressure device that was previously used for swelling pressure determination (Tadza, 2011).

The cell consists of five components; (a) a base, (b) a compaction ring, (c) a collar, (d) a locking ring and (e) a piston. Six 10 mm bolts were used to secure the locking ring to the base. The components of the hydraulic conductivity cell are shown in Figure 3.7. The assembled cell is shown in Figure 3.8.

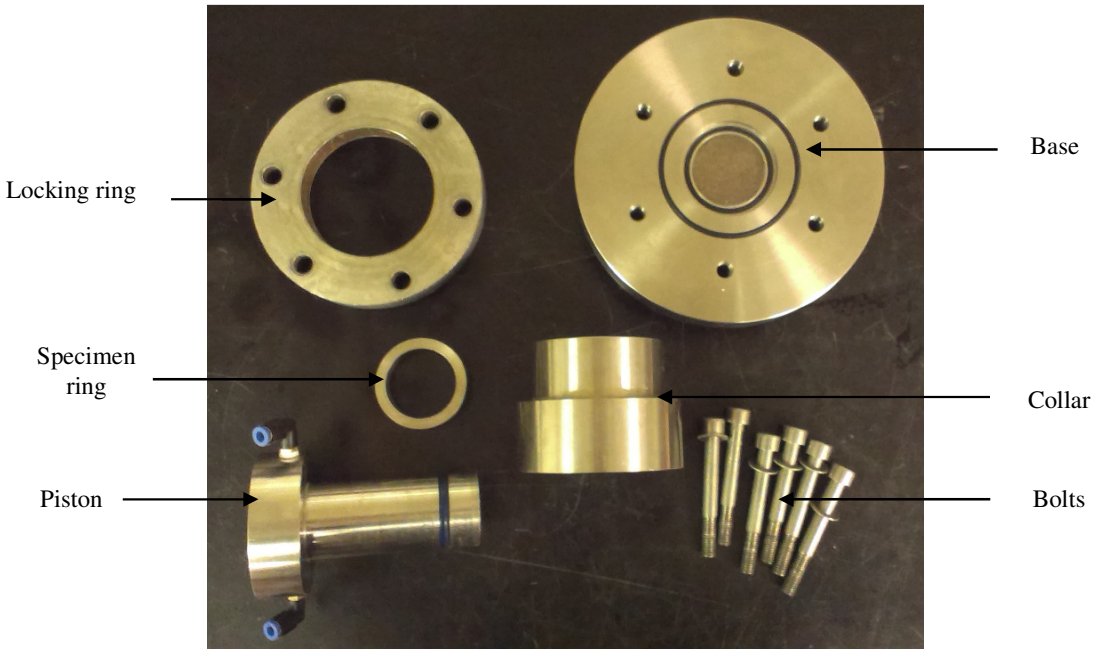

Figure 3.7 - The constituent components of the hydraulic conductivity cell

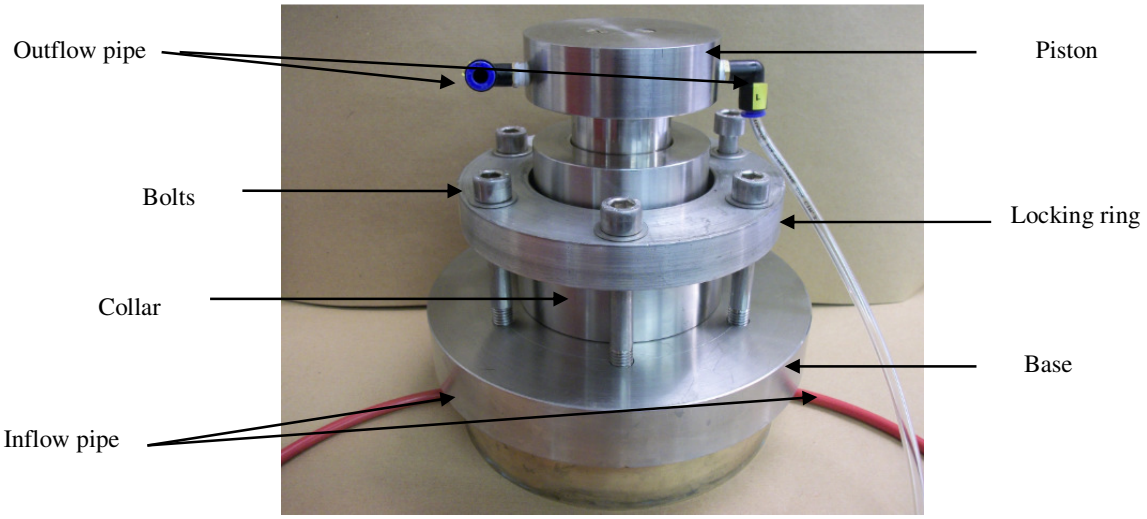

Figure 3.8 - Assembled arrangement of the hydraulic conductivity cell

Figure 3.9 shows the cross-sectional arrangement of the components of the hydraulic conductivity cell. Figure 3.10 shows the exploded arrangement of the hydraulic conductivity cell, showing the assembly to the individual components. The specimen ring, containing the compacted specimen, was placed into a circular recess in the base. The specimen rested on the porous stone. The collar was positioned onto the specimen ring, and was held in position by the locking ring. The locking ring was bolted to the base. The piston is then inserted into the collar onto the top surface of the compacted specimen. Three seals in the cell reduced leakage from the system. Two O-rings rest within groves in the base, one between the specimen ring and the base, and a second between the collar and the base. A vertical seal is positioned around the piston.

The pressure-volume controllers used in this experimental programme were supplied from GDS Instruments, model V2 New Style 200cc/4MPa (STANDARD). The pressure-volume controllers contained an internal water reservoir of 200,000 mm^3 and pressurised water to 4 MPa. The resolution of pressure and volume of the controllers was 1 kPa and 1 mm^3 respectively. The accuracy of pressure and volume recorded by the controller was 0.15% of maximum pressure, and 0.25% of the measured volume ± 30 mm^3. Figure 3.11 shows the pressure-volume controller used.

Distilled de-aired water was provided to the top and bottom of the cell by two pressure-volume controllers. The pipe from each pressure-volume controller was split into two smaller pipes that were connected to the hydraulic conductivity cell. Fluorinated ethylene propylene pipes were used. A tap was incorporated into both inflow and outflow pipe loops to allow for entrapped air to be flushed from the system. Figure 3.12 shows a schematic of the pipe systems connecting the hydraulic conductivity cell to the pressure-volume controllers.

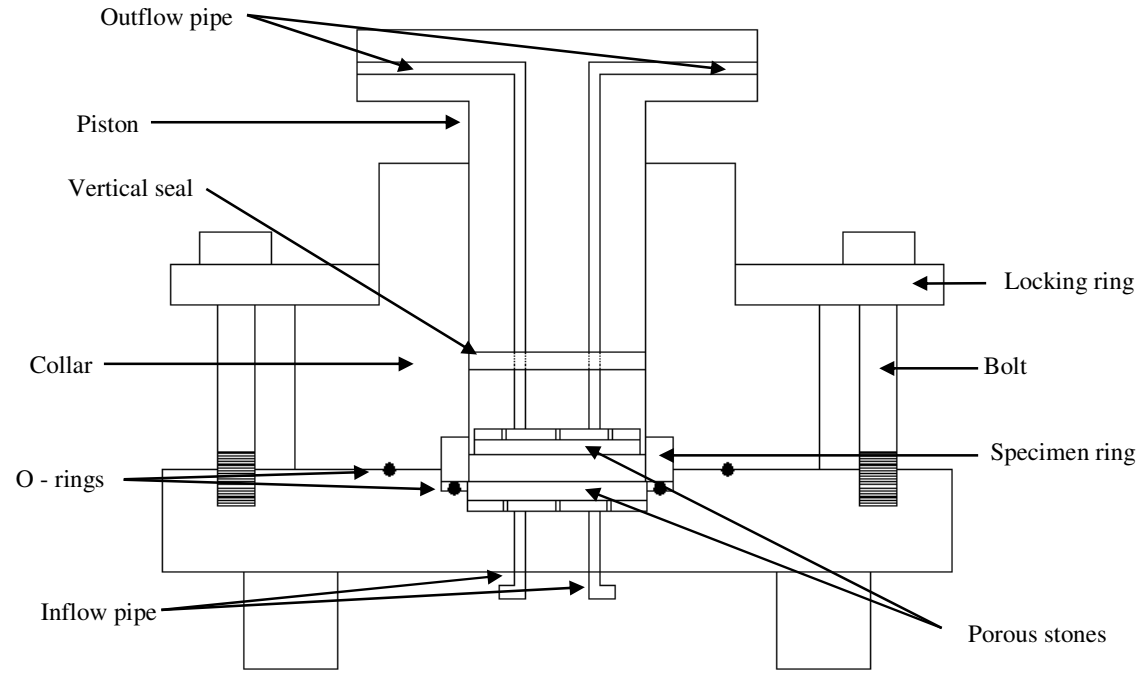

Figure 3.9 - Cross-sectional arrangement of the hydraulic conductivity cell

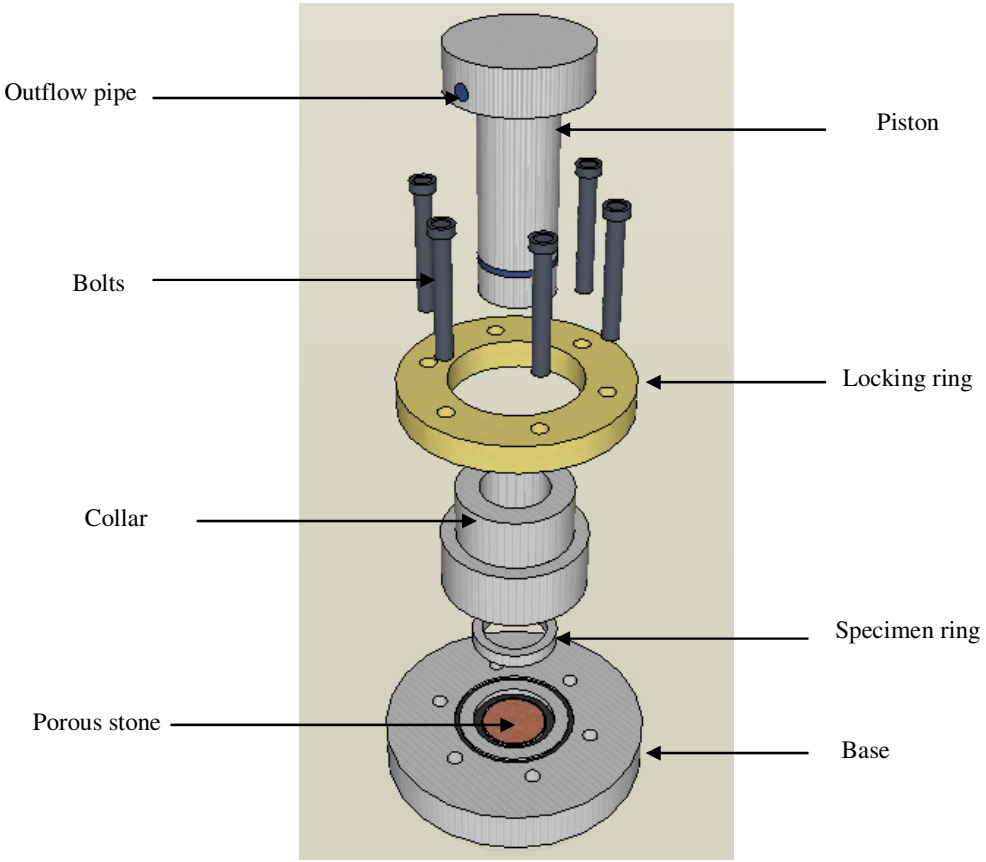

Figure 3.10 - Exploded view of the hydraulic conductivity cell

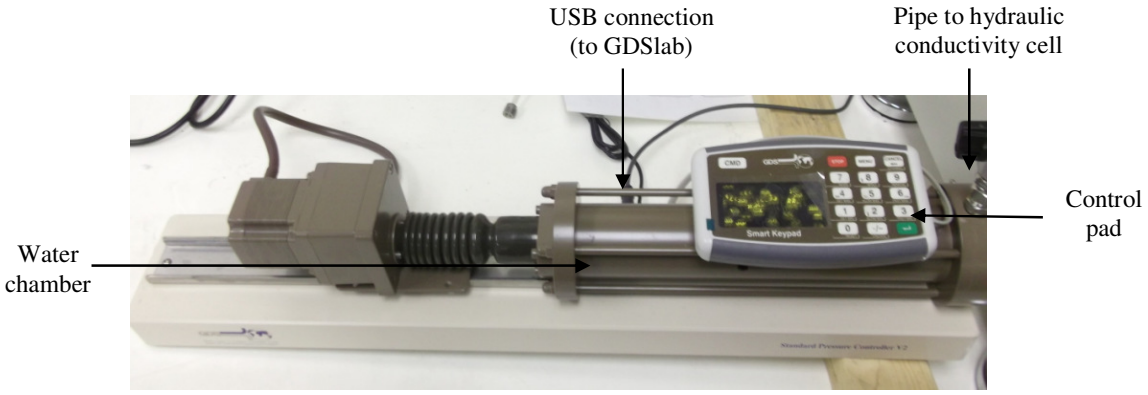

Figure 3.11 - The pressure-volume controller used in this study

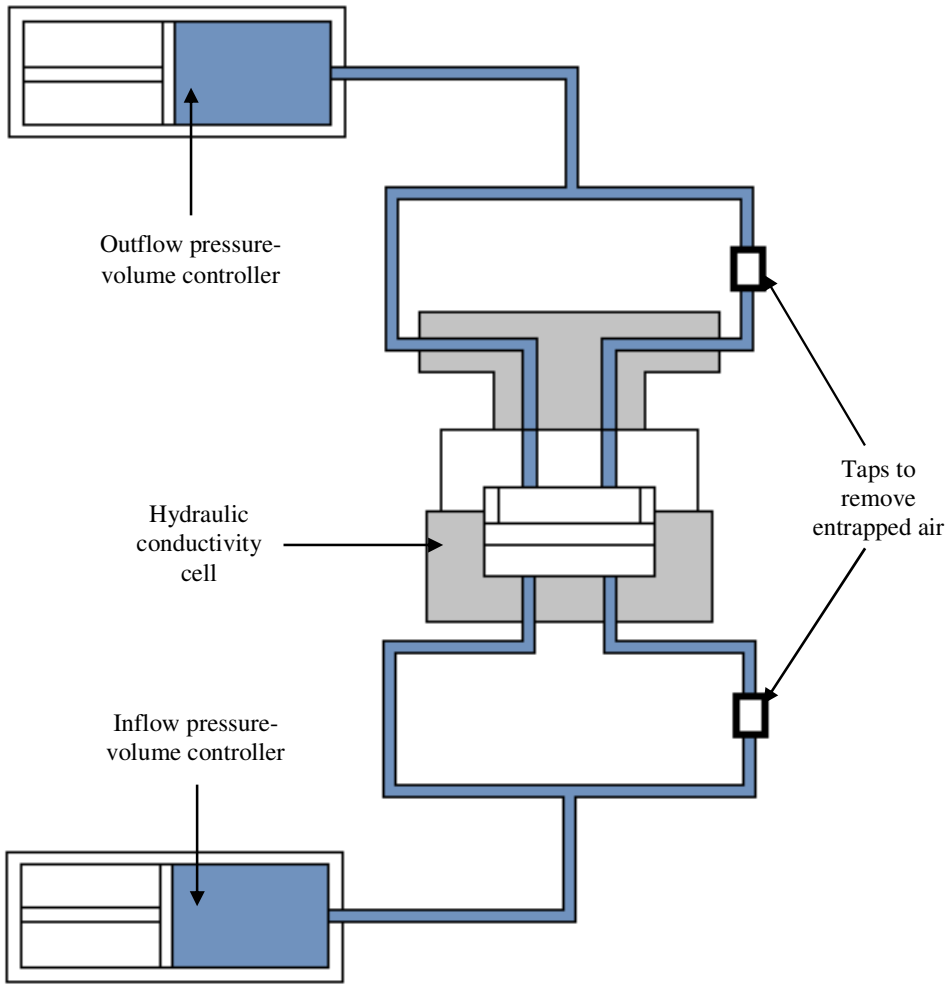

Figure 3.12 - Schematic arrangement of pipes connecting the hydraulic conductivity cell to the pressure volume controllers

The experimental set-up is shown in Figure 3.13. The assembled cell was positioned in the load frame. The load cell was placed on the hydraulic conductivity cell, and the base of the load frame was then raised until contact was made between the load frame and the load cell. The load frame was held in position to allow for constant volume tests to be carried out. The saturation of compacted bentonite specimens, and subsequent hydraulic conductivity tests were carried out under constant volume conditions. The pressure-volume controllers were connected to GDSlab so that the inflow and outflow pressures could be maintained electronically. The load cell was also connected to GDSlab.

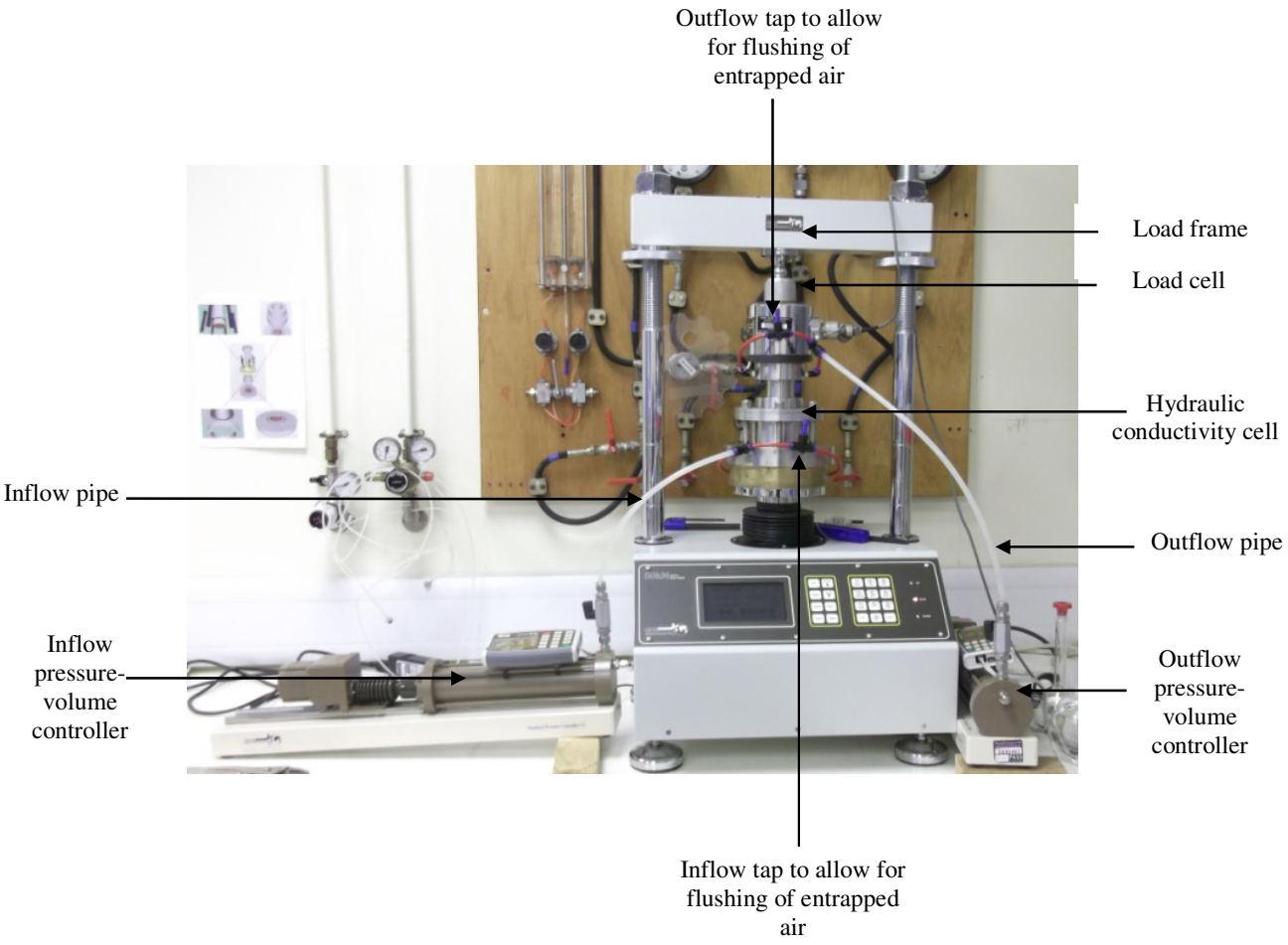

Figure 3.13 - Saturated hydraulic conductivity test set up

The compacted specimens were saturated under a nominal inflow and outflow pressure of 20 kPa. Once the swelling pressure had stabilised, the saturated hydraulic conductivity tests were carried out. The inflow pressure was increased to the required value. The pressure was maintained at this level for 60 seconds prior to the test commencing. The outflow pressure was maintained at 20 kPa throughout the testing programme. Logging intervals were set to 150 seconds for compacted MX80 bentonite specimens, and to 60 seconds for compacted sand-bentonite specimens.

Each hydraulic conductivity test was terminated when the inflow and outflow rates were constant for a specified time period, as detailed in subsequent chapters. After each test, fluid samples were taken from the inflow and outflow reservoirs. The experimental set-up was then prepared for the next hydraulic conductivity test.

The saturated hydraulic conductivity of compacted MX80 bentonite specimens and the analysis of the fluid samples are presented in Chapter 5. The saturated hydraulic conductivity of compacted sand-bentonite specimens is presented in Chapter 6.

3.6.2 Consolidation tests

A series of consolidation tests were carried out on compacted bentonite and sand-bentonite specimens. The specimens were prepared and were allowed to swell under an applied vertical pressure. Once saturated, the specimens were step-wise consolidated under increasing applied pressures. The preparation of specimens and the testing procedure is detailed.

3.6.2.1 Specimen preparation for consolidation tests

The compacted specimens were statically compacted at the air-dry water content with diameter and height of 70 mm and 6 mm respectively. The specimens were compacted directly into the oedometer ring, and then transferred to the oedometer cell. The height of the oedometer ring was 19 mm, and so an initial specimen height after compaction was chosen to ensure the swelling of the specimen during saturation would be maintained with the oedometer ring. The components of the compaction device are shown in Figure 3.14. Figure 3.15 shows the assembled compaction mould.

The compaction device consists of five main components; (a) a base, (b) an oedometer cutting ring, (c) a collar, (d) a locking ring and (e) a compaction piston.. The oedometer ring was placed in a prefabricated grove in the base of the compaction mould. The collar was placed onto the oedometer ring, and secured with the locking. The inner surface of the collar was lubricated using silicon grease, to minimise the friction between the collar and piston.

The specimen was compacted using a high capacity static compaction machine. Load was applied to the specimen until the desired height had been reached. The load was maintained for an additional five minutes to minimise elastic rebound from the specimen. The achieved dry density of the specimen was then calculated by re-measuring the height and diameter of the compacted specimen.

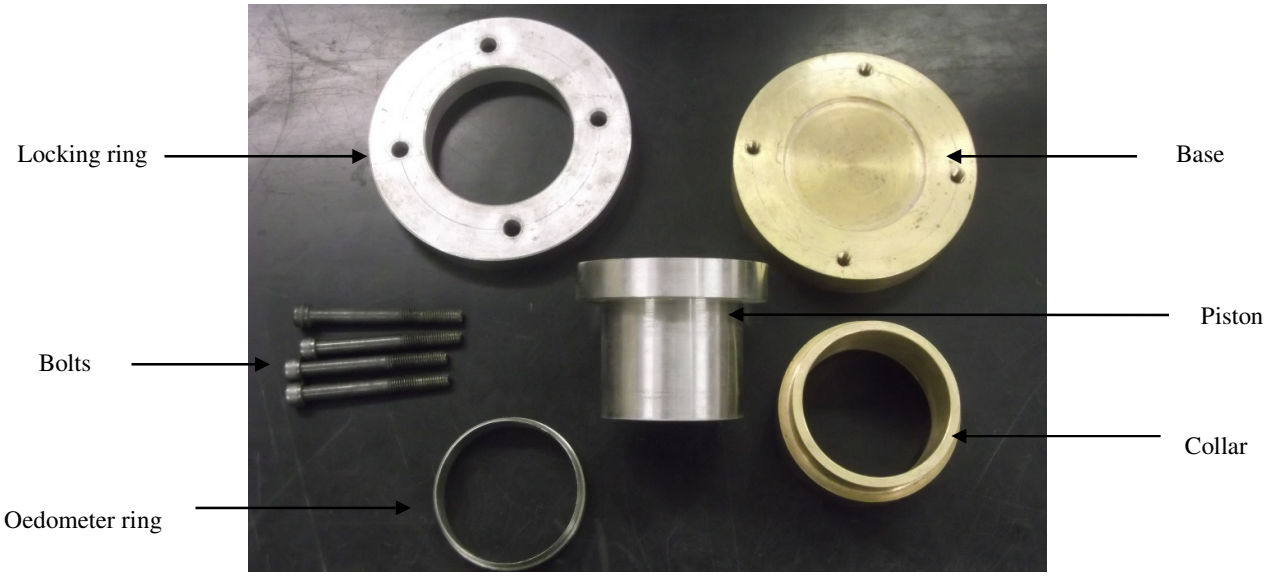

Figure 3.14 - The constituent components of the compaction mould

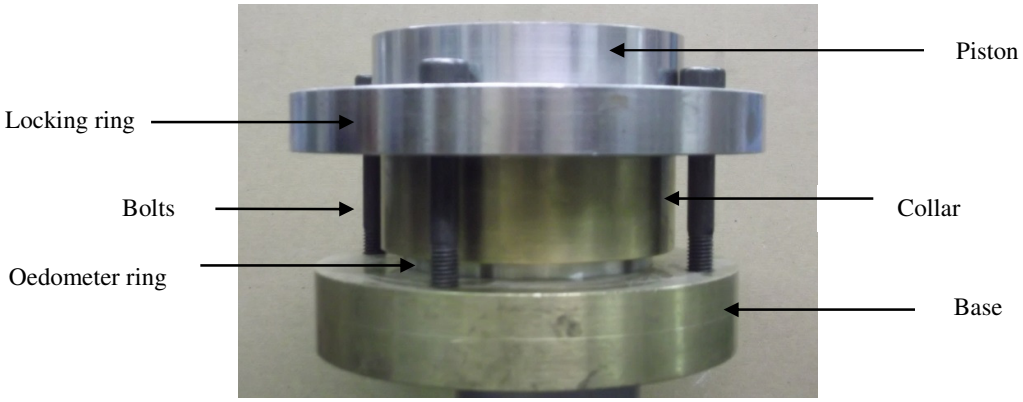

Figure 3.15 - The assembled compaction mould for consolidation testing

3.6.2.2 Consolidation testing procedure

One dimensional conventional oedometers were used to establish the consolidation behaviour of compacted specimens. The applied vertical pressure was increased in a step-wise manner to 800 kPa. The lever arm used during testing was 1:10. The 70 mm diameter oedometer cell was used during this study. Compacted specimens were saturated with distilled water at vertical applied pressures of 50 or 100 kPa. The specimens exhibited

swelling upon inundation with distilled water. Once the swelling had stabilised, the specimen was step-wise loaded.

The consolidation behaviour of compacted MX80 bentonite specimens is presented in Chapter 5. The consolidation behaviour of compacted sand-bentonite specimens is presented in Chapter 6.

3.6.3 Gas permeability tests

In deep geological repositories, the anaerobic corrosion of the waste disposal canisters can produce hydrogen. The flow of gas in compacted saturated bentonites has been studied by other researchers (Harrington and Horseman, 1997; Romero et al., 2003; Olivella and Alonso, 2008). The gas permeabilities of compacted bentonite with increased water contents have been measured in the context of geosynthetic clay liners (Didier et al., 2000; Bouazza, 2002; Vangpaisal and Bouazza, 2003). In this study, the gas permeability of compacted bentonite specimens was determined using an existing gas permeability cell.

3.6.3.1 Specimen preparation for gas permeability tests

Compacted MX80 bentonite specimens were prepared at the air-dry water content (8%). An existing concrete casting mould was modified to prepare compacted specimens. The height and diameter of the specimens were 100 mm in both cases. The components of the compaction mould are shown in Figure 3.16. The mould consists of five main components; (a) a base, (b) two connecting sleeves, (c) base connection pieces, (d) a piston and (e) four bolts. The assembled compaction mould is shown in Figure 3.17.

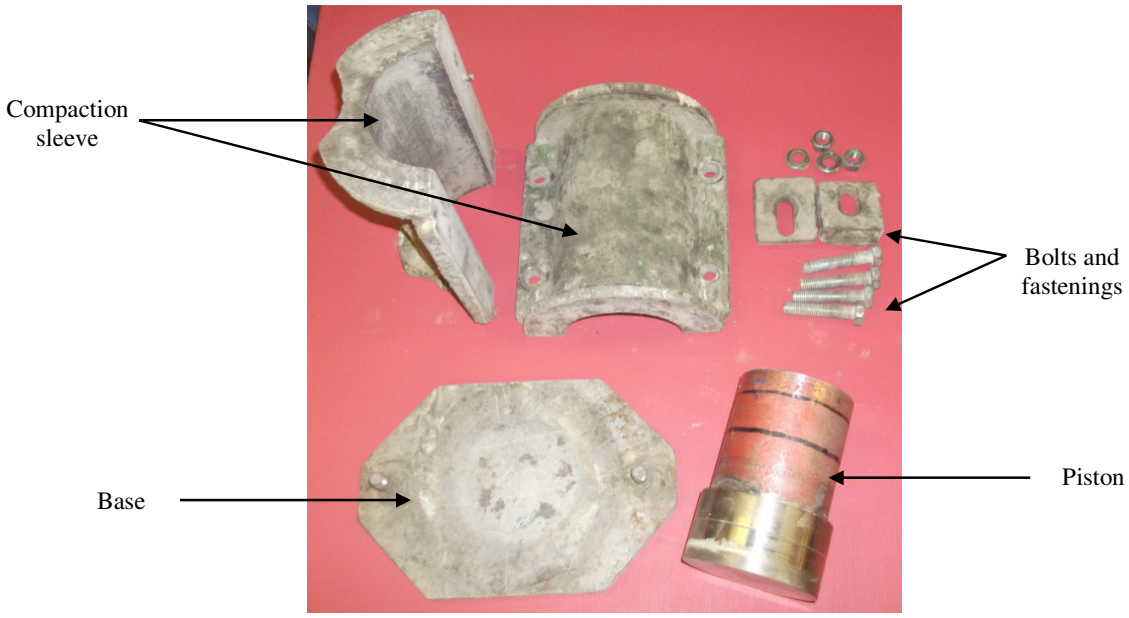

Figure 3.16 - The constituent components of the compaction mould

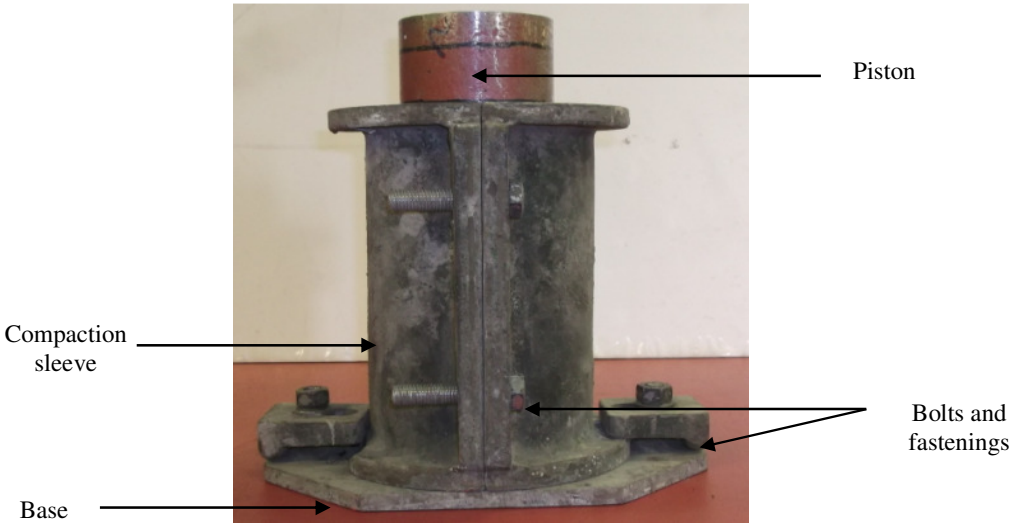

Figure 3.17 - Compaction mould for producing specimens for gas permeability testing

The two halves of the sleeve were positioned together, and held in position using the four bolts. The sleeve was then positioned on the base and fastened. The compaction mould was transferred to a high capacity static compaction machine. The specimen was then

compacted to the required height. The compaction load was maintained on the specimen for an additional five minutes to reduce elastic rebound in the specimen.

After compaction, the specimen was prepared for testing. A 7.5 mm hole was drilled centrally through the length of the specimen. An augered drill bit was used, with the drilled material being removed in stages to reduce the internal stresses within the specimen. The hole was drilled from either end to the centre of the specimen to prevent break-out.

3.7.3.2 Gas permeability testing procedure

The gas permeability of compacted MX80 bentonite specimens was determined in a device developed by Martin (1986) and modified by Lydon (1993). The device had previously been used for testing the gas permeability of cast concrete specimens. Figure 3.18 shows the gas permeability cell used in this study.

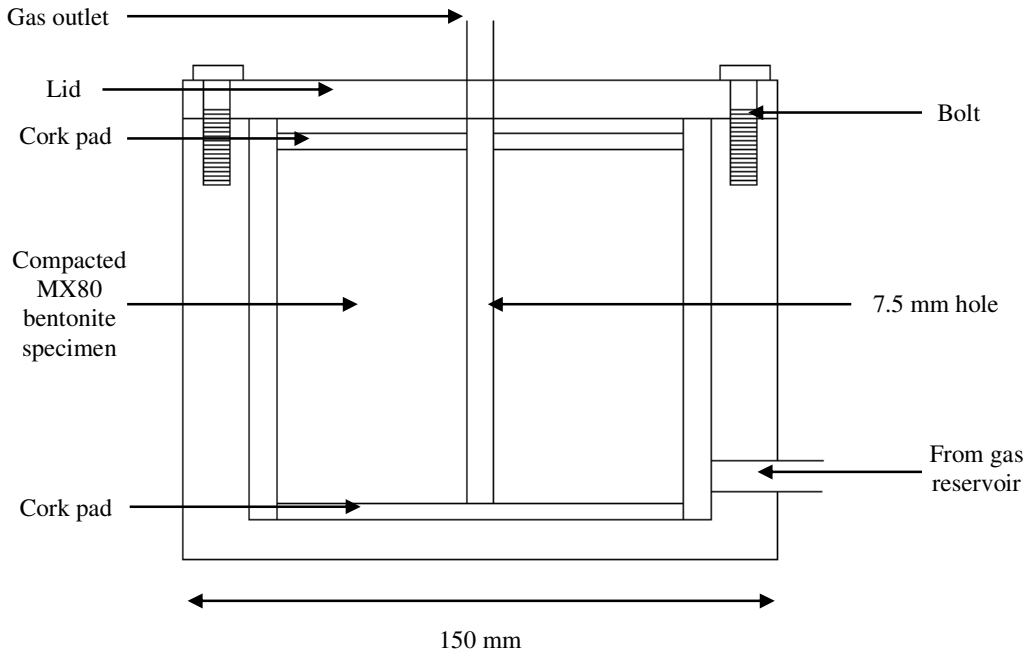

Figure 3.18 - Schematic of the gas permeability cell

The specimen was sealed on the top and base faces with petroleum jelly. Cork pads, 100 mm diameter and 3 mm thickness, were placed on the top and bottom surfaces of the specimen, in contact with the petroleum jelly. The cork pad at the top of the specimen contained a prefabricated hole in the centre. The specimen and the attached cork pads were placed into the gas permeability cell. Additional cork pads were placed at the top of the specimen to ensure an airtight seal. The lid of the gas permeability cell was secured with twelve bolts with 10 mm diameter.

The experimental set-up is shown in Figure 3.19. The gas permeability cell was separated from the gas reservoir by an isolation valve, Valve B. The gas reservoir was connected to the pressurised N_2 gas cylinder. Valve A separated the pressurised gas cylinder from the gas reservoir. The pressure within the gas reservoir was logged using a pressure gauge.

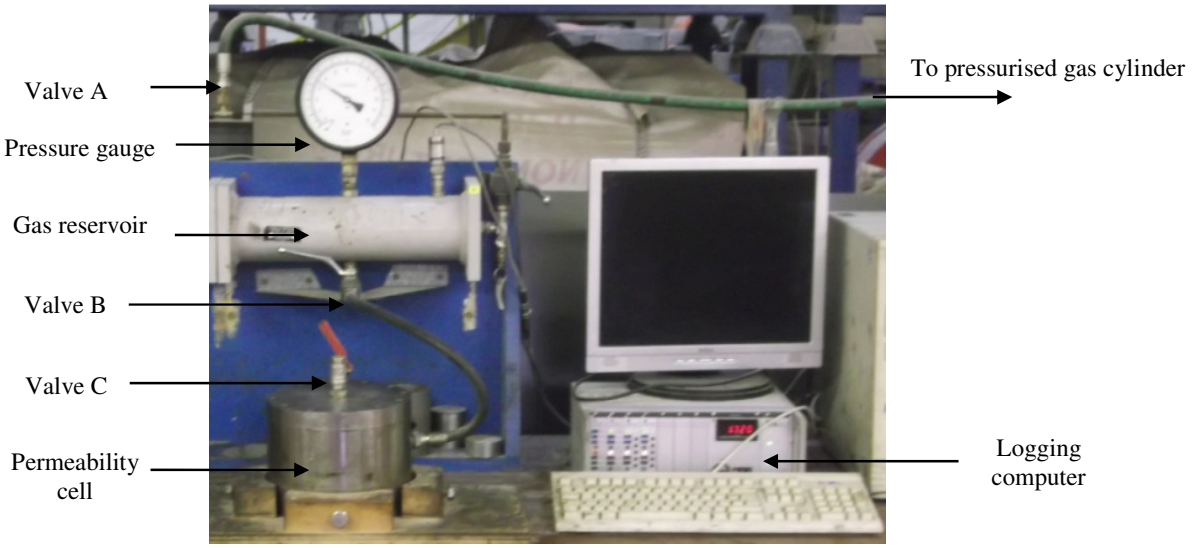

Figure 3.19 - Experimental set-up for determining gas permeability

The outlet valve on the cell, Valve C, was closed. Valve B was also closed. Valve A was opened, and the pressure within the gas reservoir was increased to the required pressure for the test. Valve A was then closed. Valve B was opened, so that the pressure in the reservoir and the cell were equal, after which, Valve B was then closed. This reduced the pressure in the gas reservoir. The pressure in the gas reservoir was increased to the required pressure value by opening Valve A once again. Valve A was then closed, and Valve B opened, increasing the pressure in the air permeability cell. The process of opening Valve A, and then Valve B, in turn was continued until the pressure in the gas permeability cell and the gas reservoir was that required for the test.

The pressure in the gas reservoir (and the gas permeability cell) was logged every 0.1 seconds. Prior to testing, Valves A and C were closed, and Valve B was open. The test was started and Valve C was opened. The reduction of gas pressure within the gas permeability cell was logged. The test was terminated once the pressure had equilibrated. The lid was removed from the permeability cell, and the specimen was inspected for pressure cracks. If required, the assembly was then prepared for another test.

The gas permeability of compacted MX80 bentonite determined under gas flow is presented in Chapter 7.

3.7 Concluding remarks

The properties of MX80 bentonite and Leighton Buzzard sand used in the study were presented in this chapter. The physical properties determined included the liquid, plastic and

shrinkage limits, the mineralogical composition and the particle size distribution. The chemical properties determined included the cation exchange capacity and average cation valence. Some differences were observed, which were attributed to a lower montmorillonite content and lower specific surface area determined for the MX80 bentonite to that reported in the literature. The suction-water content soil-water characteristic curve of MX80 bentonite was also presented, and was compared with literature.

The experimental procedures for determining the saturated hydraulic conductivity, consolidation behaviour and gas permeability of compacted bentonite specimens were presented. The results obtained from the procedures detailed in this chapter are presented in Chapters 5, 6 and 7.

CHAPTER 4

COMPLIANCE OF THE HYDRAULIC CONDUCTIVITY EXPERIMENTAL SET-UP

4.1 Introduction

In Chapter 3, the experimental set-up for determining the saturated hydraulic conductivity of compacted specimens was presented. The procedure for conducting constant-head tests was described. The hydraulic gradient was applied to the specimen by a pressure differential between the inflow and outflow pressure-volume controllers. The experimental set-up was newly assembled for the current study.

Experimental factors affecting the determination of saturated hydraulic conductivity have been reported in literature. Benson and Daniel (1990) reported that discrepancies between field and laboratory measurement may be due to differences in clod size. Dixon et al. (1999) stated a number of factors that can affect saturated hydraulic conductivity determination, including bacterial action in test cells and changes in soil structure.

Temperature changes have been reported to affect the saturated hydraulic conductivity of bentonite (Cho et al., 1999). The applied hydraulic gradient may also lead to the development of coupled processes that can influence the hydraulic behaviour observed (Mitchell and Soga, 2005). Chapius (2012) stated that the losses in the pipes, valves and porous stones are often ignored during hydraulic conductivity tests.

Additional factors may affect the determination of saturated hydraulic conductivity. Temperature fluctuations can cause expansion or contraction of the experimental set-up. Internal pressure changes can also result in expansion or contraction of the system. Air may become dissolved into the water if the system is not entirely saturated. Fluid can be lost from the system through leakage, particularly at the connections between the pipes and the hydraulic conductivity cell.

The experimental procedure adopted in this study mitigated some of the experimental issues. Distilled de-aired water was used to minimise dissolved air within the fluid during the hydraulic conductivity tests. The compacted bentonite specimens were saturated under constant volume conditions, and saturation of the specimen was assumed to have occurred once the swelling pressure had stabilised (i.e. no further swelling was occurring). The hydraulic conductivity tests were carried out in a temperature controlled environment.

However, the effect of system expansion and contraction due to pressure changes is expected to be significant in this study.

In this chapter, the expansion of the inflow system due to changes in pressure is determined. The total expansion of the inflow system is established for step-wise and instantaneous pressure changes. The expansion is considered with and without a dummy specimen. The secondary expansion of the inflow system is discussed. The relationship between inflow pressure and secondary inflow system expansion is shown. An empirical equation is stated to account for secondary expansion in the inflow system due to the applied water pressure.

4.2 Total system expansion due to changes in inflow system pressure

4.2.1 Experimental procedure

During saturated hydraulic conductivity tests, a constant outflow water pressure of 20 kPa was maintained. The inflow water pressure was varied to apply the pressure differential required for each applied hydraulic gradient. The inflow pipe system expanded due to changes in the applied pressure. No pressure-induced expansion occurred in the outflow pipe system.

The inflow pressure was applied through two testing procedures (i) step-wise pressure changes and (ii) instantaneous pressure changes. The initial inflow pressure was 20 kPa. The

first test was carried out at a pressure of 45 kPa. The expansion of the inflow pipe system was also determined at 100, 200, 400, 600, 800, 1000 and 1200 kPa.

For the step-wise procedure, the inflow pressure was increased from 45 kPa to 1200 kPa through each of the pressure values considered. Each pressure was applied for 360 minutes before being changed. Once the expansion at 1200 kPa was established, the inflow pressure was then reduced to each of the stated values in an identical step-wise manner to 20kPa.

Instantaneous changes in pressure were also considered. The expansion at each pressure value considered was measured for 360 minutes. The inflow pressure was reduced to 20 kPa for 360 minutes between testing stages. The inflow pressures were considered in increasing magnitude up to 1200 kPa. The expansion at each pressure was then repeated by decreasing the inflow pressure in sequential order.

To determine the total inflow system expansion, the hydraulic conductivity cell was assembled as described in Chapter 3. The pressurised system consisted of the pressure-volume controller, the inflow pipes and the hydraulic conductivity cell. It was not possible to isolate the outflow system entirely, as entrapped air needed to be able to be removed from the system. To minimise the effect of the inclusion of the outflow pipes, the outflow pipe length was reduced, with the connection to the outflow pressure-volume controller removed.

The volume of water contained within the pipes was 8.6×10^{-5} mm^3. The testing procedures were carried out with and without a stainless steel dummy specimen in place. The volume of water within the cell without the dummy specimen was 1.4×10^{-5} m^3. The volume

of water within the cell with the dummy specimen was 2 x 10^{-6} m^3. The volume of water within the pressure-volume controller initially was approximately 1.8 x 10^{-4} m^3. This volume reduced during the testing steps undertaken.

The cell was allowed to saturate for 24 hours prior to the start of the test. The expansion of the inflow pipe system was measured by the volume of fluid in the inflow pressure-volume controller.

4.2.2 Total inflow system expansion due to pressure changes

Figure 4.1 shows the total inflow system expansion due to step-wise pressure changes (a) with and (b) without the dummy specimen. Figure 4.2 shows the total inflow system expansion measured from the instantaneous pressure changes (a) without and (b) with the dummy specimen. The expansion of the inflow system was observed to be significantly lower with the inclusion of a dummy specimen for both testing procedures. This difference was attributed to the expansion of the hydraulic conductivity cell.

Figure 4.1(a) and Figure 4.2(a) show that the maximum expansion with the dummy specimen was not significantly affected by the method of applying inflow pressure. Similarly, Figure 4.1(b) and Figure 4.2(b) show that the expansion of the inflow system without the dummy specimen determined by the two testing procedures was similar. The application of inflow pressure in either a step-wise or instantaneous method was therefore concluded not to significantly affect the total inflow system expansion.

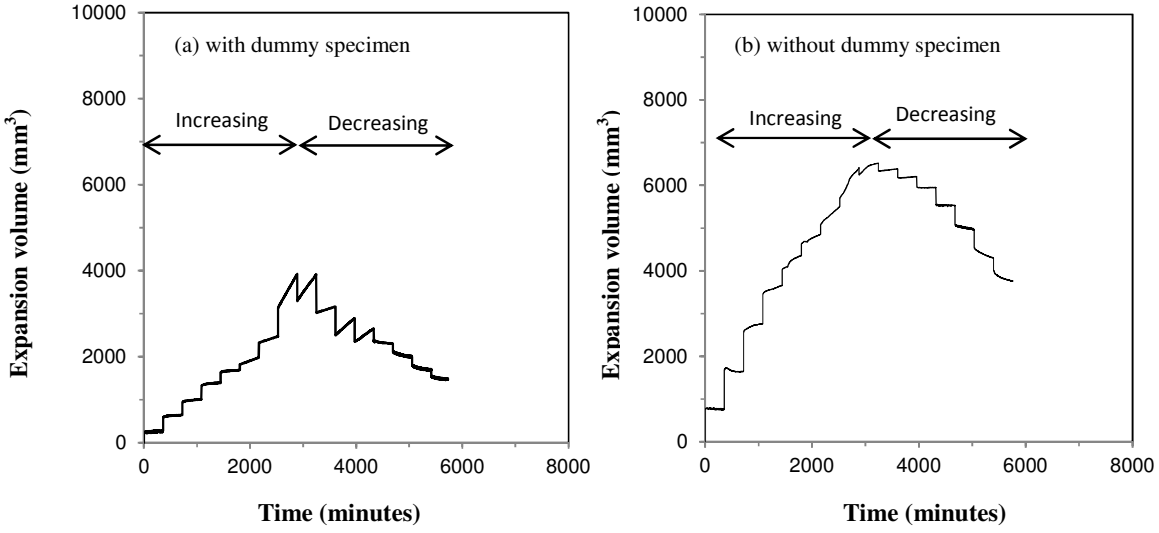

Figure 4.1 - Total expansion of the inflow system (a) with and (b) without a dummy specimen due to step-wise pressure changes (45, 100, 200, 400, 600, 800, 1000, 1200, 1000, 800, 600, 400, 200, 100, 45 and 20 kPa)

From Figure 4.1 and 4.2, it was observed that the expanded volume of the system did not recover to its original level at the end of the testing programmes. The difference between the initial and final volume of the system was found to be about 3000 mm^3 without the dummy specimen, and about 2000 mm^3 with the dummy specimen for both testing procedures.

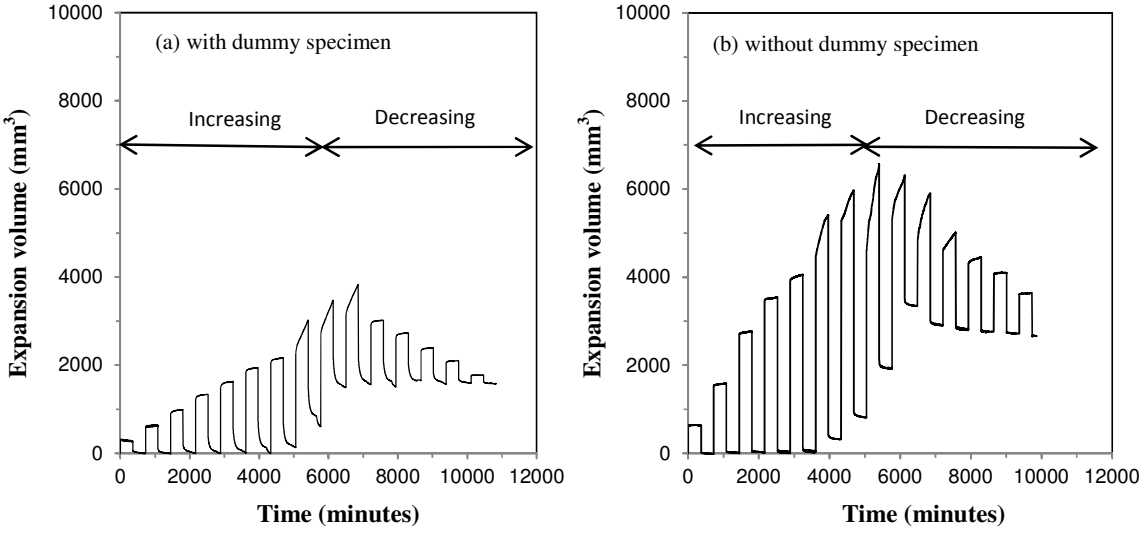

Figure 4.2 - Total expansion of the inflow system (a) with and (b) without a dummy specimen due to instantaneous pressure changes (45, 20, 100, 20, 200, 20, 400, 20, 600, 20, 800, 20, 1000, 20, 1200, 20, 1000, 20, 800, 20, 600, 20, 400, 20, 200, 20, 100, 20, 45, 20 kPa)

The compressibility of water was assessed for each inflow pressure applied to the system. Prior to testing commencing, the total volume of water contained within the cell was 1.4 x 10^{-5} m^3 without the dummy specimen in place, and approximately 2 x 10^{-6} m^3 with the dummy specimen. The volume of water contained within the pressure-volume controller ranged from 1.2 x 10^{-4} m^3 to 1.8 x 10^{-4} m^3. The volume of water contained within the pipes was 8.6 x 10^{-5} m^3.

The bulk modulus of water was assumed to be 2.2 x 10^9 Pa at 20ºC (Handbook of Chemistry and Physics, 1996). The reduction in volume contained within the hydraulic conductivity system due to compressibility of the water under the applied pressure was determined to be 3ml when the pressure was increased from 20 kPa to 45 kPa, increasing to 134 ml when the pressure was increased from 20 kPa to 1200 kPa. Given the volume of water

entering the system when the inflow pressure was increased, it is not considered the compressibility of water is a significant contributor.

The theoretical hoop stresses within the pipes were calculated (Young and Budynas, 2002). The pipes were assumed to be thin-walled. The elastic limit for fluorinated ethylene propylene pipes was stated as 620 ± 30 MPa (FEP Handbook, 2009). The hoop stresses calculated at each pressure value were within the elastic limit. The difference between initial and final expansion was therefore not due to plastic deformation of the pipes.

From the instantaneous pressure changes, it was seen that the system did not contract to its initial volume after the 1000 kPa test with the dummy specimen and 800 kPa without the dummy specimen (Figure 4.3). For testing stages after this, the measured expansion volume when the pressure was reduced to 20 kPa remained consistent. This suggests that a volume of fluid was lost from the system during the 1200 kPa test with the dummy specimen, and during the 1200 kPa and 1000 kPa tests without the dummy specimen. The connections between the pipes were stated to have a maximum working pressure of approximately 1000 kPa (SMC Pneumatics Tube and Fittings Information Sheet).

It was not possible to carry out repeats of the system expansion, due to time constraints. From the behaviour of the system under increasing pressures, it was concluded that the applied inflow pressure was to be limited to 1000 kPa, as larger inflow pressures caused leakage from the inflow pipe system.

4.3 Secondary system expansion

Saturated hydraulic conductivity tests on compacted saturated bentonite can be time consuming, due to its low hydraulic conductivity. In the current study, the long term response of the system is required to calibrate the inflow and outflow volumes determined during hydraulic conductivity tests.

From the expansion of the system determined in Subsection 4.2, the most significant inflow system expansion was observed to occur immediately after a change in pressure. After this, further expansion of the system was observed, but this secondary expansion was significantly less than the initial expansion.

For each hydraulic gradient applied during hydraulic conductivity tests, the required inflow pressure was applied for one minute prior to the start of the test. The majority of the expansion of the inflow system occurred during this time, immediately after the pressure was increased. The hydraulic conductivity tests were started after the initial expansion had occurred. Secondary expansion was therefore continuing to occur during the hydraulic conductivity tests. The quantification of this secondary expansion was required to correct the inflow behaviour observed during the hydraulic conductivity tests.

The total inflow system expansion shown in Subsection 4.2 was used to determine the secondary expansion. The expansion with the dummy specimen was considered, as the response was more representative of the inflow system during the hydraulic conductivity tests. The secondary expansion was calculated up to and including the expansion due to 1000

kPa. The increases in inflow pressure, i.e. from 45 kPa to 100 kPa to 200 kPa etc, were considered only, due to the loss of fluid from the system at pressures larger than 1000 kPa.

The secondary expansion of the inflow system was determined once the initial expansion of the system had occurred. For the step-wise pressure changes, the secondary inflow system expansion was calculated from the previous to the current inflow pressure. The cumulative secondary inflow system expansion was calculated for the step-wise procedure. Figure 4.3 shows the secondary inflow system expansion of the system determined at the end of each testing step (after 360 minutes).

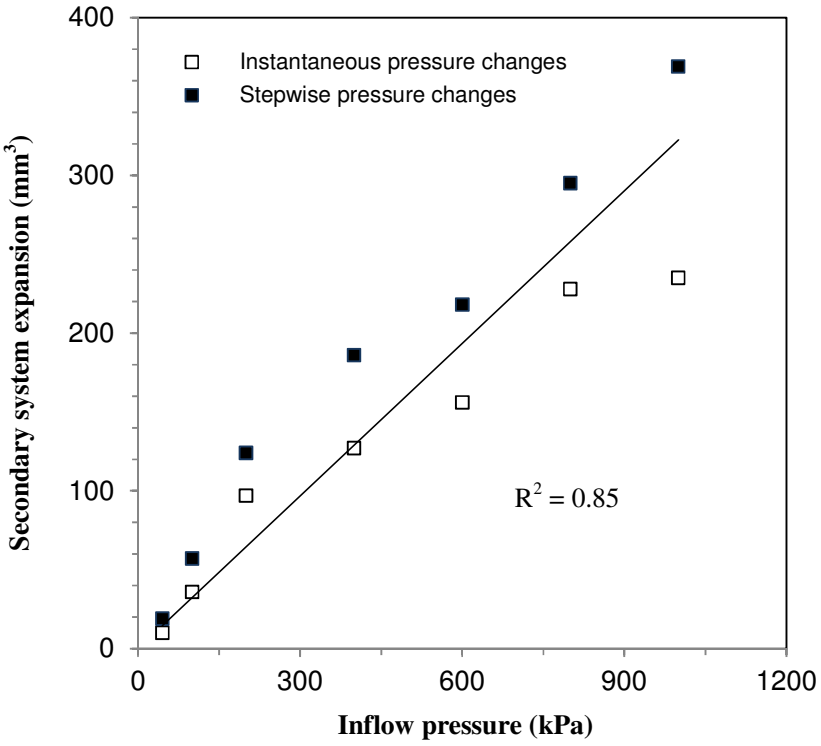

Figure 4.3 - Secondary system expansion due to inflow pressure with a dummy specimen

From Figure 4.3, an empirical relationship for the inflow pressure and the secondary expansion of the inflow system was proposed.

$$v = 0.323p \quad (4.1)$$

where v is the secondary inflow system expansion (in mm^3) and p is the inflow pressure (in kPa).

The empirical relationship stated in Equation (4.1) calculates the secondary system expansion of the inflow system due to the inflow pressure. The inflow measured during hydraulic conductivity tests presented in Chapter 5 and 6 was adjusted using this equation to better assess the compatibility between inflow and outflow.

4.4 Concluding remarks

A number of experimental factors can influence the determination of hydraulic conductivities. The head losses in the pipes, valves and porous stones are often ignored during hydraulic conductivity tests (Chapius, 2012). In the current study, the expansion of the experimental system was measured at different inflow pressures.

The total pipe expansion was presented for the system with and without a dummy specimen. The method of applying the inflow pressure, either step-wise or instantaneously was not shown to significantly affect the observed expansion. The total inflow system expansion without the dummy specimen was found to be greater than with the dummy specimen. This difference was due to the expansion of the hydraulic conductivity cell.

In all tests conducted, a volume of fluid entering the system was not recovered at the end of the testing procedure. It was determined that no plastic deformation of the pipes occurred, as the calculated hoop stresses were within the elastic limit. Significant fluid was lost when the applied inflow pressure was 1200 kPa. The maximum working pressure of the pipe connections was reported to be 1000 kPa. It was concluded that inflow pressures greater than 1000 kPa should not be applied to the inflow system during the hydraulic conductivity tests.

The secondary system expansion was determined by considering the additional expansion of the system one minute after the inflow pressure was changed. Consideration of the secondary pipe expansion was more appropriate due the length of the hydraulic conductivity tests, and the low flow volumes expected. An empirical relationship between secondary inflow system expansion and applied inflow pressure was determined. This equation was subsequently used to correct the inflow behaviour observed during hydraulic conductivity tests.

CHAPTER 5

SATURATED HYDRAULIC CONDUCTIVITY OF COMPACTED MX80 BENTONITE

5.1 Introduction

The saturated hydraulic conductivity of compacted bentonites is of particular importance in geoenvironmental applications. In deep geological repositories, bentonite powder or pellets will be compacted to high compaction dry densities to form the barrier and backfilling material (Pusch, 1982; Bucher and Muller-Vonmoos, 1989; Borgesson et al., 1996; Karnland et al., 2007). The bentonite barrier will be initially unsaturated, but will become hydrated due to available water percolating from the host rock. The flow of water

from the host rock to the canister is a key consideration to ensure the integrity of the high level radioactive waste is maintained.

Municipal solid waste disposal also requires understanding of the saturated hydraulic conductivity of compacted bentonites. The lining of landfills is required to mitigate the flow of leachate from the landfill to the surrounding groundwater (Environment Agency, 2011). The flow rate through the liner will dictate the flow of leachate from the landfill.

The saturated hydraulic conductivity of bentonite can be determined in a number of ways. A rigid- or flexible-walled permeameter can be used to test compacted bentonite specimens. Daniel (1994) reported that the hydraulic conductivity results obtained from rigid- and flexible-walled permeameters were comparable. The hydraulic gradient can be applied to the specimen through constant head conditions, falling head conditions and constant flow conditions.

A number of factors have been reported to affect the saturated hydraulic conductivity of compacted bentonites. These include compaction dry density (Pusch, 1982; Dixon et al., 1999; Baille et al., 2010), microstructure of the specimens (Benson and Daniel, 1990; Pusch, 1999), type of exchangeable cation in the bentonite (Rao and Mathew, 1995; Ahn and Jo, 2009), permeant type (Shackelford et al., 2000; Dixon et al., 2002), applied temperature (Olsen and Daniel, 1981; Cho et al., 1999) and applied hydraulic gradient (Pusch, 1982; Dixon et al., 1999).

An important issue to be considered during the hydraulic conductivity tests is the loss of ions from the bentonite-water system due to ion transport processes, including advection

and diffusion processes. In low permeability barriers, diffusion may become the dominant transport mechanism (Shackelford and Daniel, 1991). Coupled flows may also develop due to imposed hydraulic gradients (Mitchell and Soga, 2005).

The loss of ions from the compacted saturated bentonites can impact a number of parameters due to a reduction in the cation exchange capacity of the bentonites. The effects of ion loss can include a reduction in the swelling pressure and an increase in the hydraulic conductivity. Changes to the behaviour of the bentonite-water system may affect the integrity of the geological barrier.

The main objective of this chapter is to determine the saturated hydraulic conductivity of compacted MX80 bentonite at compaction dry densities from 1.1 to 1.7 Mg/m^3. The swelling pressures developed by the compacted specimens during saturation are presented. The inflow and outflow volumes measured during the hydraulic conductivity tests is presented and compared. The swelling pressure and flow behaviour throughout the hydraulic conductivity testing programme for each specimen is shown.

The saturated hydraulic conductivities of compacted MX80 bentonite are determined. The total loss of exchangeable cations as a percentage of the initial cations within the compacted bentonite specimen is studied. The compressibility behaviour of compacted saturated bentonite under increasing vertical loads is presented. The hydraulic conductivities are calculated from the compressibility behaviour of the specimens, and are compared with measured values.

5.2 Saturated hydraulic conductivity of compacted MX80 bentonite

5.2.1 Experimental programme

The saturated hydraulic conductivities were determined directly using the experimental set-up described in Subsection 3.6.1. Specimens were prepared at targeted dry densities of 1.1, 1.2, 1.3, 1.4, 1.5, 1.6 and 1.7 Mg/m^3. Tripathy and Schanz (2007) stated that for deep geological disposal of high level radioactive waste, bentonite barriers will be prepared at compaction dry densities between 1.3 and 2.0 Mg/m^3. Dixon et al. (1999) conducted hydraulic conductivity tests on compacted bentonite specimens for a range of dry densities between 0.5 and 1.5 Mg/m^3.

The actual dry density of each specimen was calculated after the compaction process, based on the final height of the specimen. Table 5.1 shows the targeted and actual dry densities of the compacted specimens. Bag (2011) reported that the extrusion and reinsertion of compacted specimens into the rings resulted in greater swelling pressures being exhibited by the specimen. In this study, the extrusion and reinsertion of specimens was not considered.

Table 5.1 - Targeted and actual dry densities of compacted MX80 bentonite specimens prepared for saturated hydraulic conductivity tests

Specimen	Targeted dry density (Mg/m^3)	Actual dry density (Mg/m^3)
1	1.100	1.088
2	1.200	1.191
3	1.300	1.283
4	1.400	1.379
5	1.500	1.478
6	1.600	1.582
7	1.700	1.684

ASTM D 5084 stated that a maximum hydraulic gradient of 30 should be applied when determining the saturated hydraulic conductivity of low permeability materials. Applied hydraulic gradients reported in literature have exceeded this (Benson and Daniel, 1990; Cho et al.. 1999; Dixon et al., 1999; Lloret et al., 2004). In the current study, the maximum applied water inflow pressure was determined previously to be about 1000 kPa, due to experimental limitations. The maximum applied hydraulic gradient under this pressure differential was therefore to 12500. The minimum hydraulic gradient that would result in water flow through the specimen was not known. A series of preliminary tests were conducted to establish the minimum hydraulic gradient.

The specimen prepared to a compaction dry density of 1.088 Mg/m^3 was chosen for the preliminary experimental programme. Four hydraulic gradients were applied to the specimen to assess the water inflow and outflow. Details of the preliminary experimental programme are shown in Table 5.2.

Table 5.2 - Preliminary experimental programme for saturated hydraulic conductivity tests

Test number	Inflow pressure (kPa)	Outflow pressure (kPa)	Pressure differential (kPa)	Hydraulic gradient (m/m)
A	45	20	25	311
B	70	20	50	623
C	95	20	75	934
D	120	20	100	1245

The water inflow and outflow during preliminary tests A-D is shown in Figure 5.1(a) - (d) respectively. For all tests, a difference was observed between the water volume entering and leaving the specimen. This difference was attributed partially to the internal swelling and shrinkage of the specimen upon application of a hydraulic gradient, and the ongoing secondary expansion within the system due to the applied water pressure. Volumes of water within the inflow and outflow pressure-volume controllers were zeroed prior to the test commencing. The water inflow and outflow rates were observed to become constant within 5000 minutes.

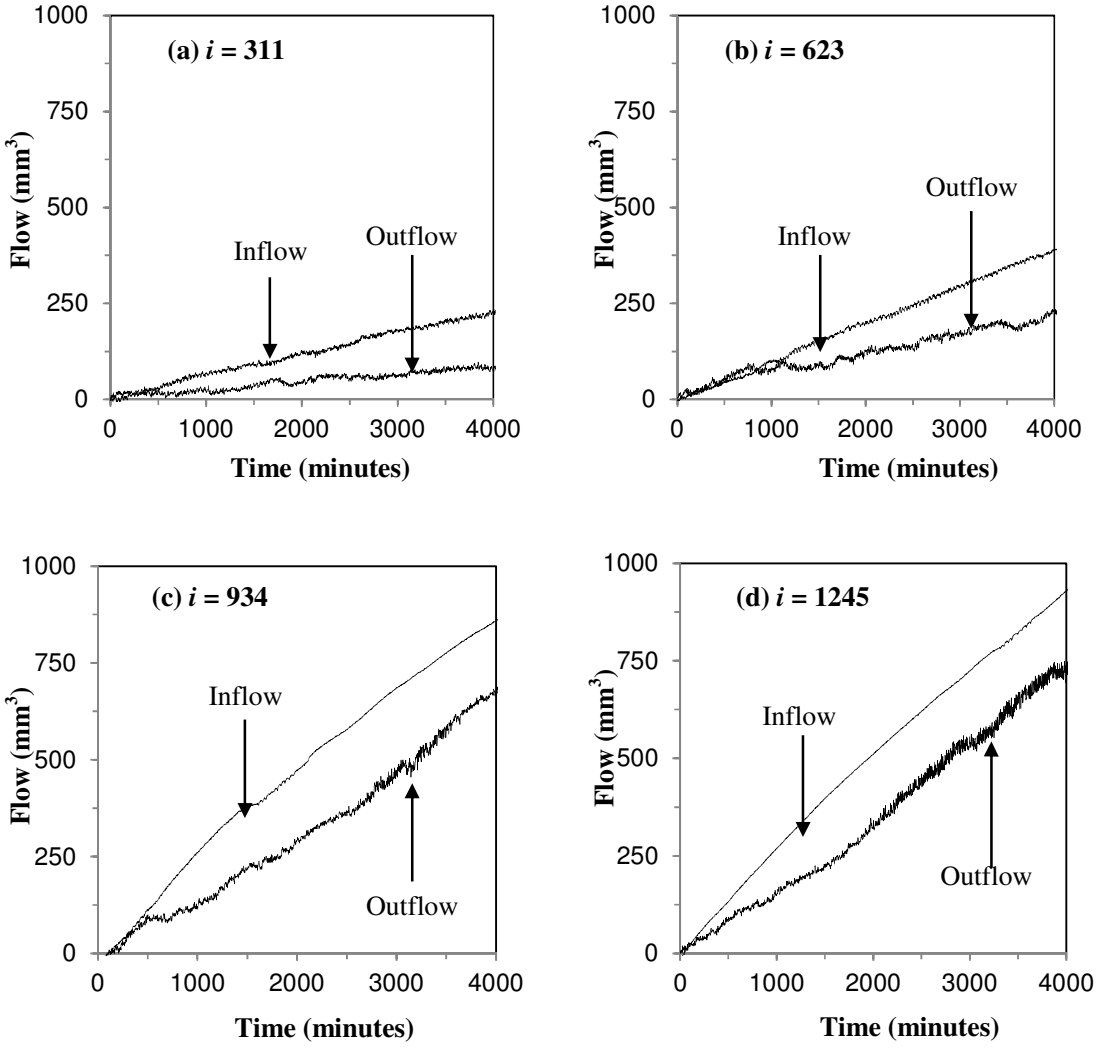

Figure 5.1 - Inflow and outflow during preliminary hydraulic conductivity tests for the 1.088 Mg/m^3 specimen

For tests (b)-(d), the water inflow and outflow rates calculated were found to be comparable. The time for equilibrium to be reached was observed to reduce as the hydraulic gradient increased. From the preliminary tests, it was decided that the minimum hydraulic gradient to be applied was that which corresponded to a 100 kPa water pressure differential. Lower applied hydraulic gradients were not considered due to time limitations.

During the main experimental programme, five hydraulic gradients were considered. The water pressure differentials between the inflow and outflow water pressures applied to the specimens were 100, 250, 500, 750 and 1000 kPa. These differentials corresponded to hydraulic gradients of approximately 1250, 3125, 6250, 9375 and 12500. The exact hydraulic gradients applied were calculated from the actual height of the specimens after compaction.

Nine hydraulic conductivity tests were conducted on each of the specimens. The five hydraulic gradients considered were applied to the specimen in order of increasing magnitude. Each hydraulic gradient was then retested as the water pressure differential applied to the specimens was reduced in a step-wise manner.

5.2.2 Saturation of compacted bentonite specimens under constant volume conditions

The compacted MX80 bentonite specimens were saturated using distilled de-aired water supplied to the inflow and outflow under an applied pressure of 20 kPa. The specimens were allowed to saturate until the measured swelling pressure had equilibrated. Figure 5.2 shows the equilibrated swelling pressures developed for the compacted MX80 bentonite specimens considered.

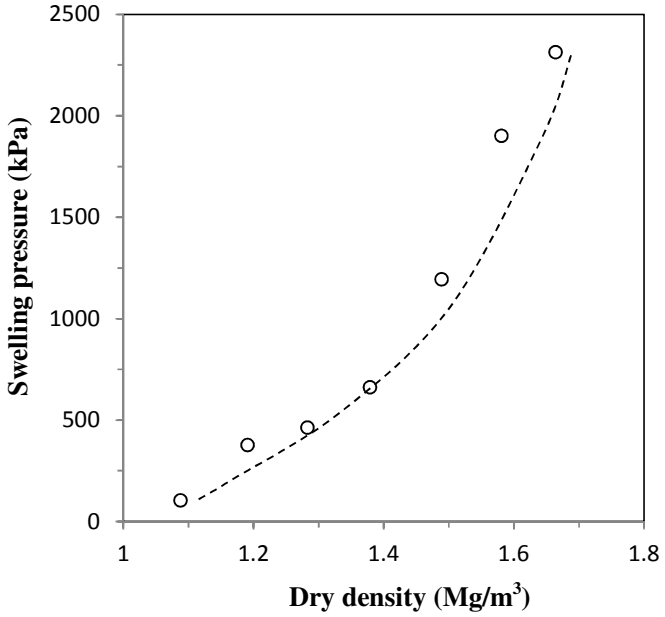

Figure 5.2 - Equilibrated swelling pressures of compacted bentonite developed during saturation

The results are plotted based on the initial dry density of the specimens. The measured swelling pressures are in reasonable agreement with those reported by Bucher and Muller-Vonmoos (1989) but are lower than those reported by Karnland et al. (2007). The differences in swelling pressure are attributed to the lower cation exchange capacity of the bentonite used in this study, compared with those reported in literature.

5.2.3 Evolution of swelling pressure during hydraulic conductivity tests

The swelling pressure exhibited by the compacted bentonite specimens was monitored throughout the hydraulic conductivity tests on each specimen. Figure 5.3 and Figure 5.4 shows the (a) swelling pressure evolution under a variable applied water pressure differential and (b) measured inflow and outflow volumes for the specimens with dry densities of 1.191 Mg/m^3 and 1.664 Mg/m^3 respectively.

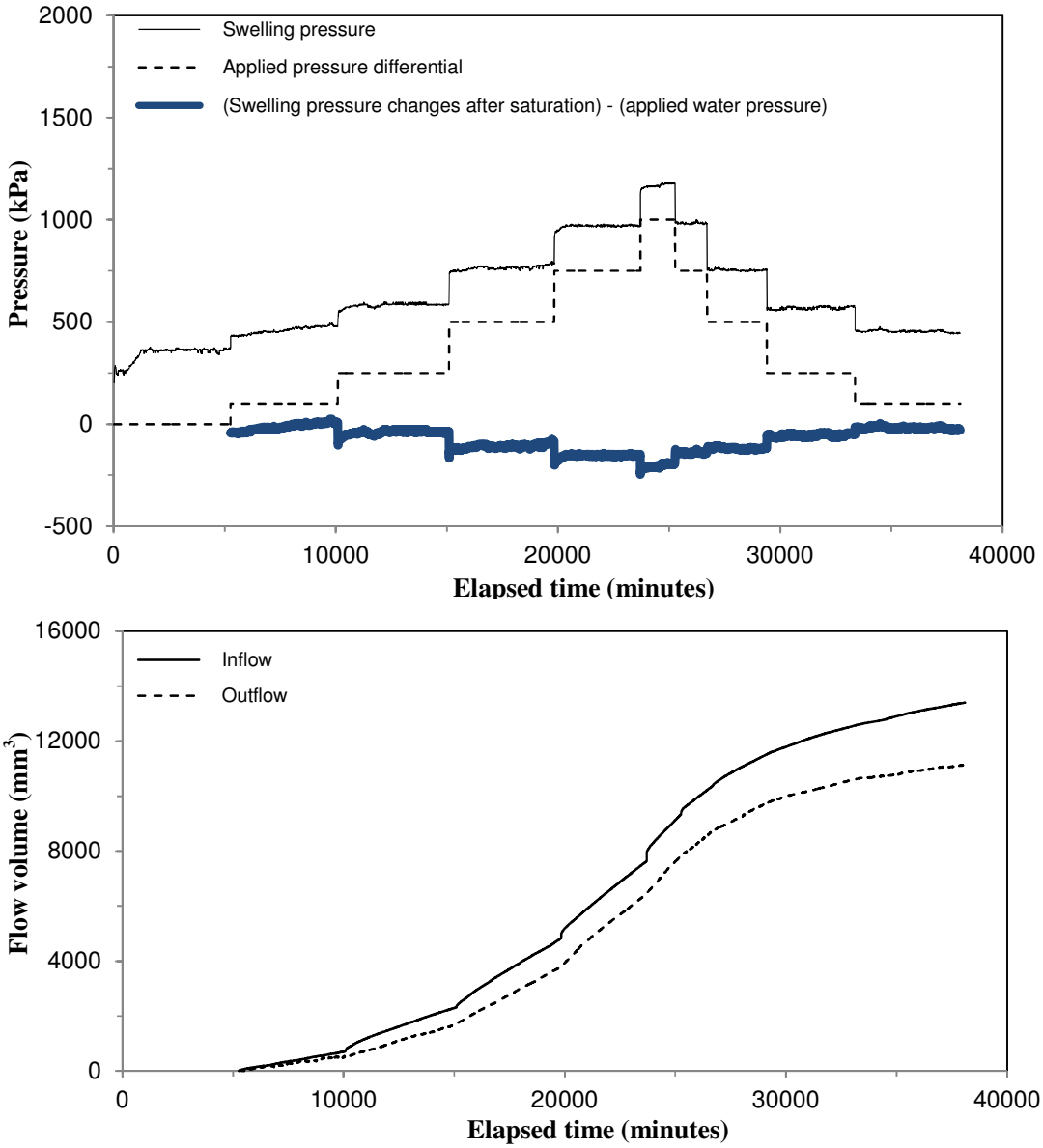

Figure 5.3 - (a) Swelling pressure changes and (b) measured flow during hydraulic conductivity tests for the specimen with dry density of 1.191 Mg/m^3

Figures 5.3(a) and 5.4(a) also show the calculated difference between the swelling pressure changes (after saturation has occurred) and the applied water pressure differential (applying the hydraulic gradient). In an ideal situation, no increase of swelling pressure would be observed, as fluid entering the system would pass through the specimen.

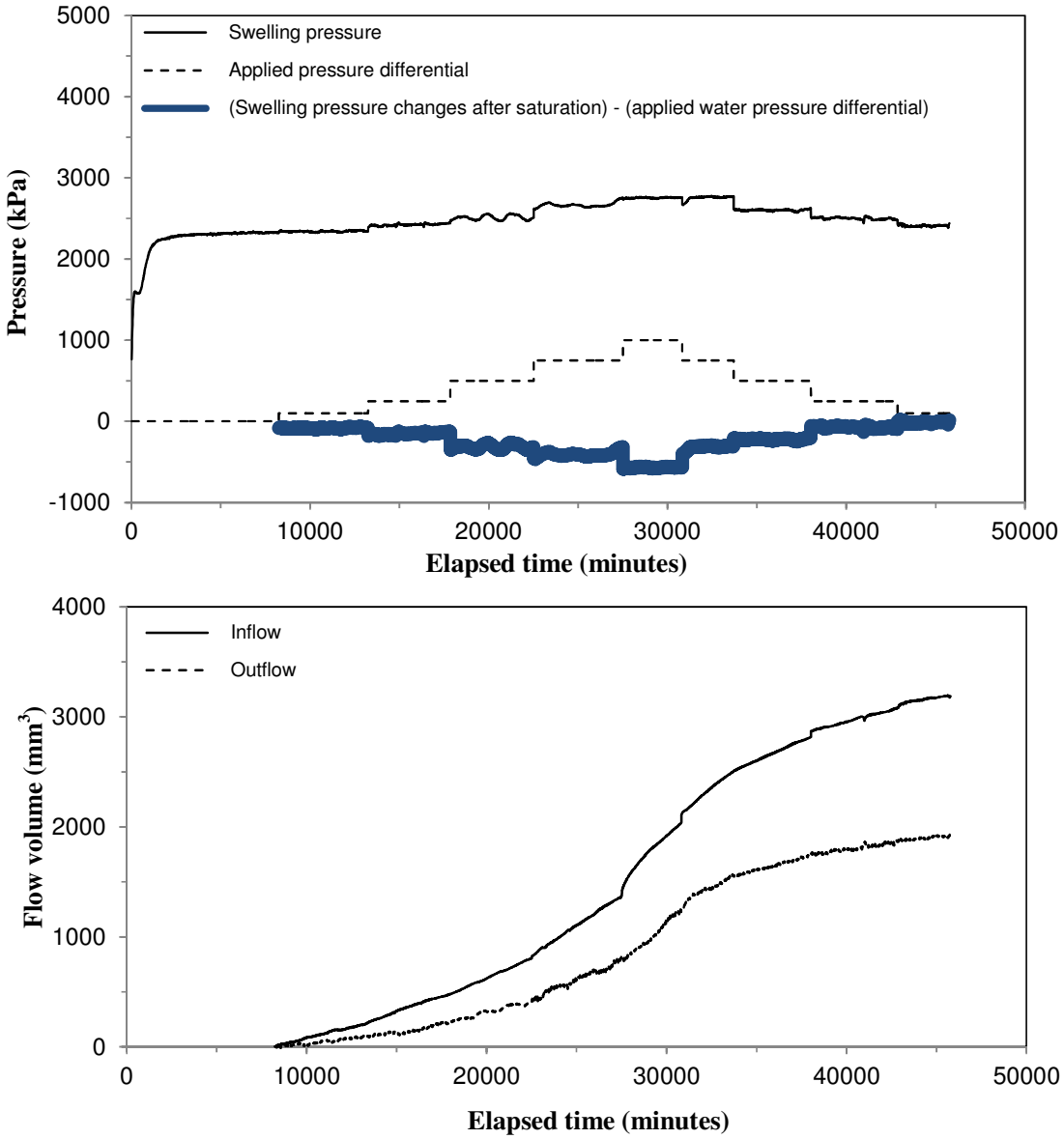

Figure 5.4 - (a) Swelling pressure changes and (b) measured flow during hydraulic conductivity tests for the specimen with dry density of 1.664 Mg/m^3

Conversely, if no flow was occurring, the applied inflow pressure would generate an identical response in the swelling pressure observed, as the fluid stagnated within the system. Figures 5.3(a) and 5.4(a) indicate that an increase of swelling pressure was observed during the hydraulic conductivity tests, suggesting that some stagnation of water within the system

has occurred. However, the increases in swelling pressure observed are less than the applied pressure differential, indicating that some flow through the specimen has occurred.

5.2.4 Measured inflow and outflow during saturated hydraulic conductivity tests

During the hydraulic conductivity tests, the water inflow and outflow volumes under each hydraulic gradient were monitored until the flow rates became constant. The hydraulic conductivity tests were terminated once constant flow conditions were observed. The system expansion was observed previously to be significant, and so the inflow was corrected to account for the secondary expansion of the system. Equation (4.1) was used to calculate the volume of secondary expansion of the inflow system due to the inflow pressure. The inflow behaviour observed during each tests was corrected by the secondary system expansion volume.

The inflow and outflow behaviour for each specimen during the nine hydraulic conductivity tests is presented here. Figures 5.5 - 5.11 show the water inflow and outflow volumes with elapsed time for the specimens with dry densities of 1.088, 1.191, 1.283, 1.379, 1.489, 1.581 and 1.664 Mg/m^3 respectively. The corrected inflow is also shown in each case.

In all cases, the water flow rates were observed to become constant within 5000 minutes. Specimens prepared at higher compaction dry densities were found to require an increased time for water flow rates to become constant. The corrected water inflow volumes were generally found to more closely equate to the outflows in the majority of cases. The inflow and outflow rates at the end of the hydraulic conductivity tests are presented in Table

5.3. The outflow rate, calculated as a percentage of the inflow rate, is also shown in Table 5.3 for each test conducted.

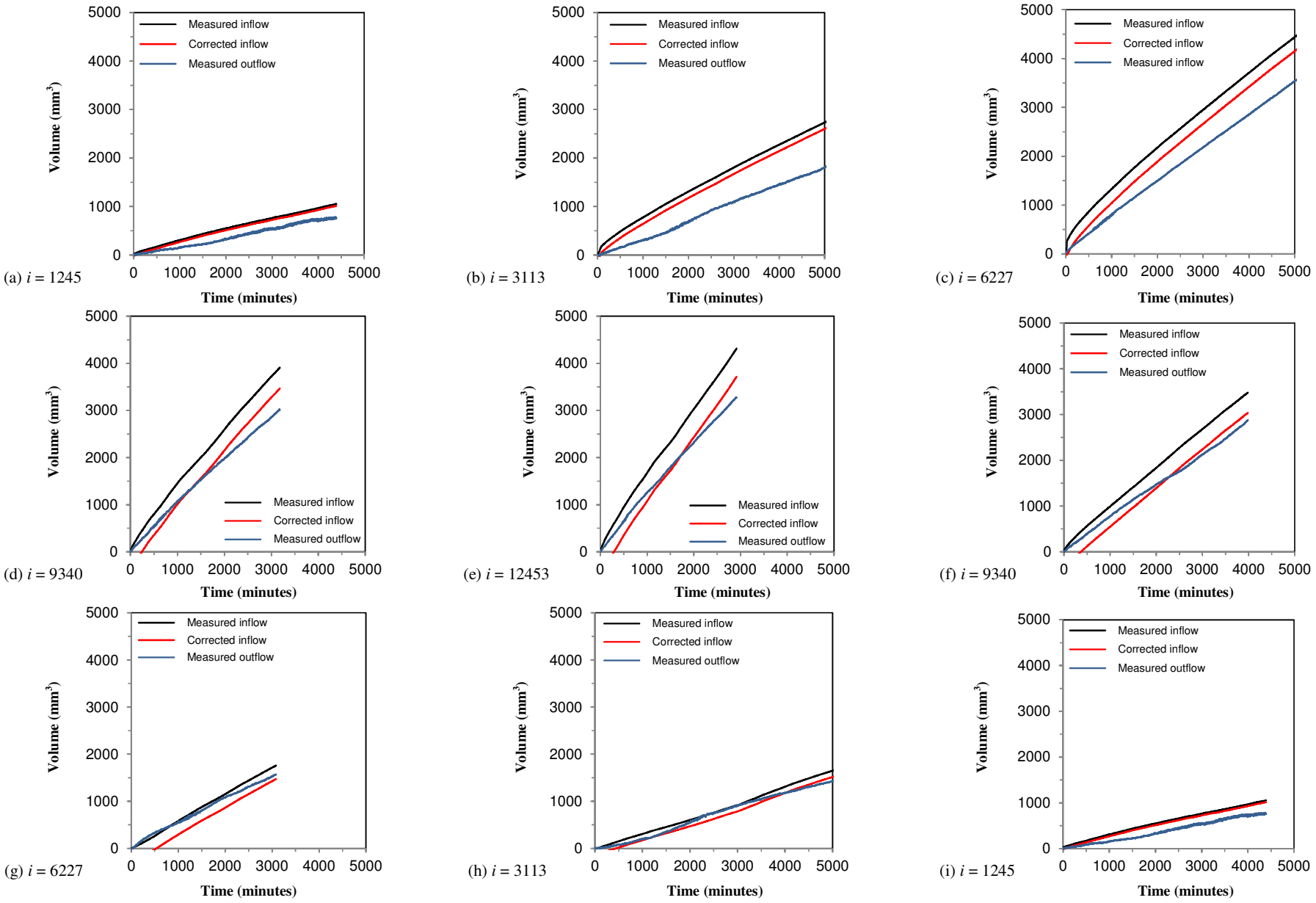

Figure 5.5 - Inflow and outflow behaviour determined for the 1.088 Mg/m³ specimen

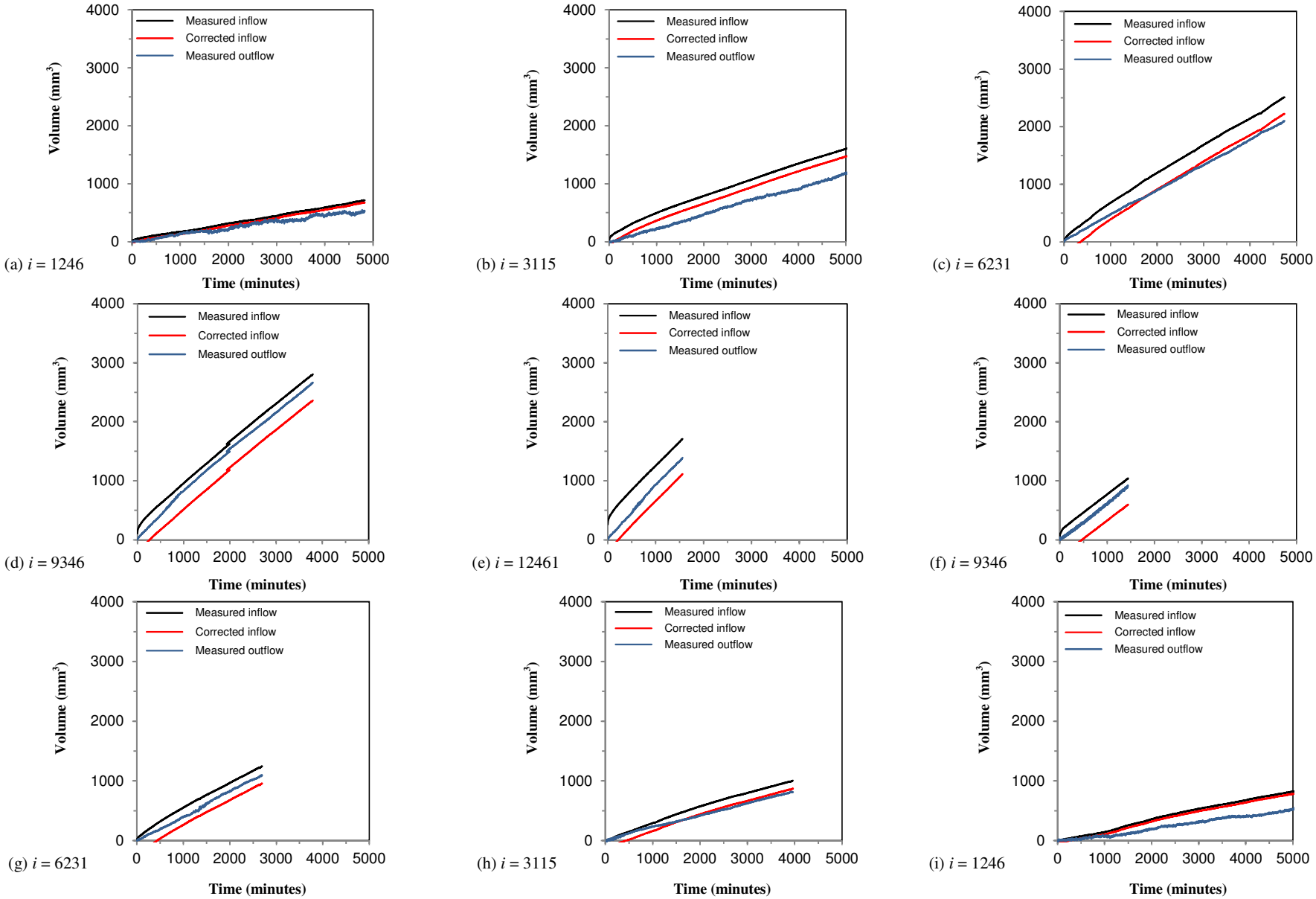

Figure 5.6 - Inflow and outflow behaviour determined for the 1.191 Mg/m^3 specimen

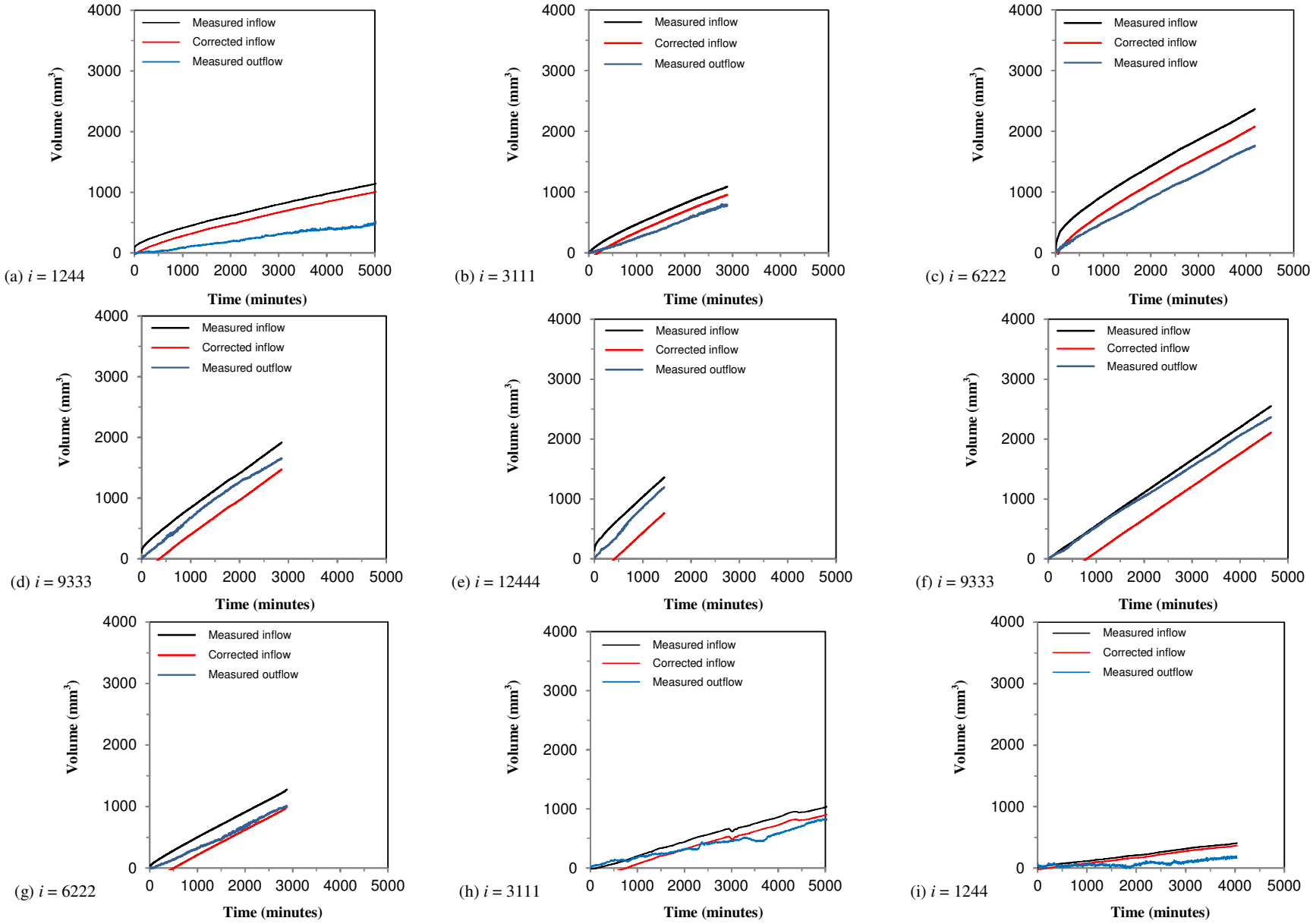

Figure 5.7 - Inflow and outflow behaviour determined for the 1.283 Mg/m^3 specimen

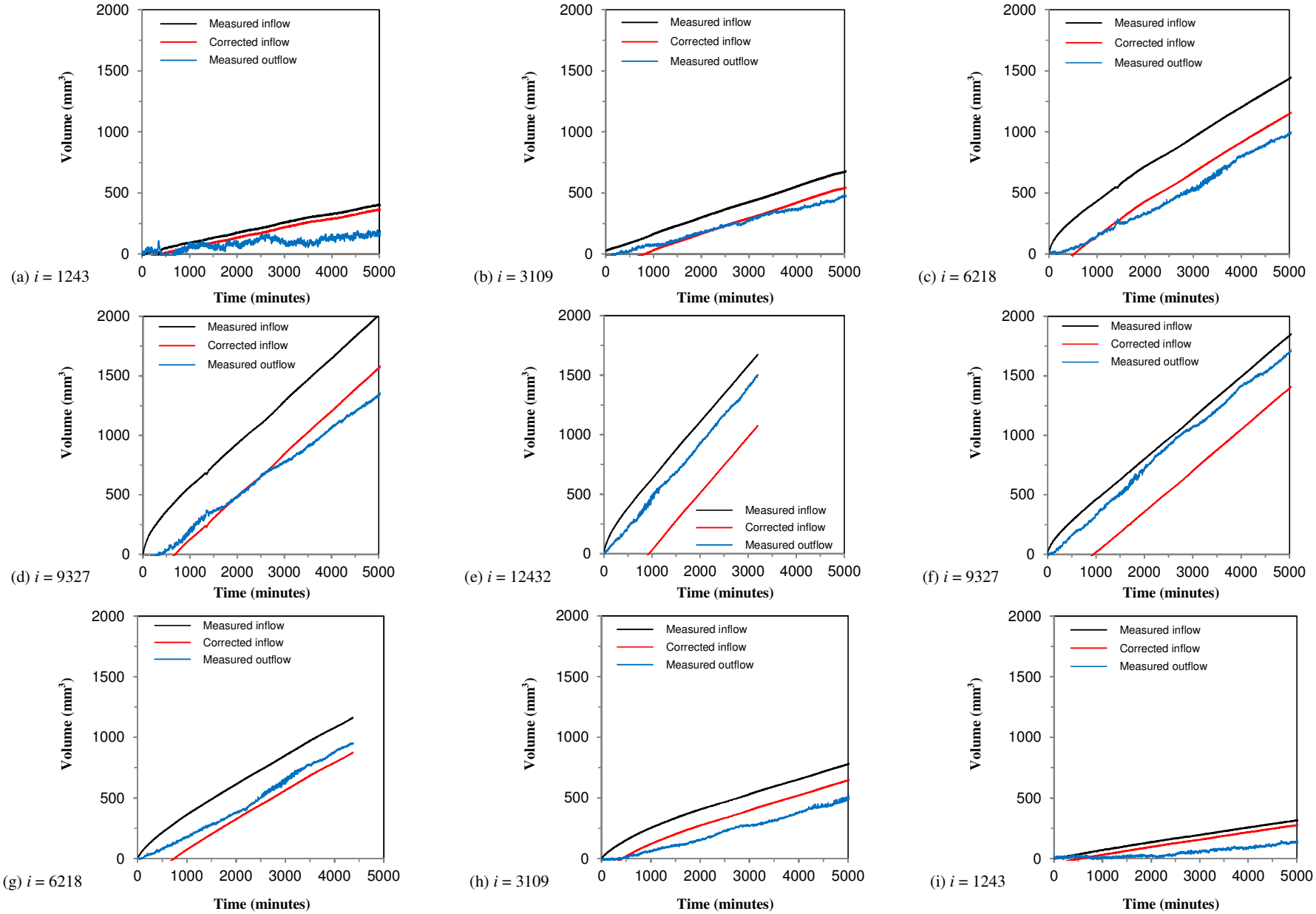

Figure 5.8 - Inflow and outflow behaviour determined for the 1.379 Mg/m^3 specimen

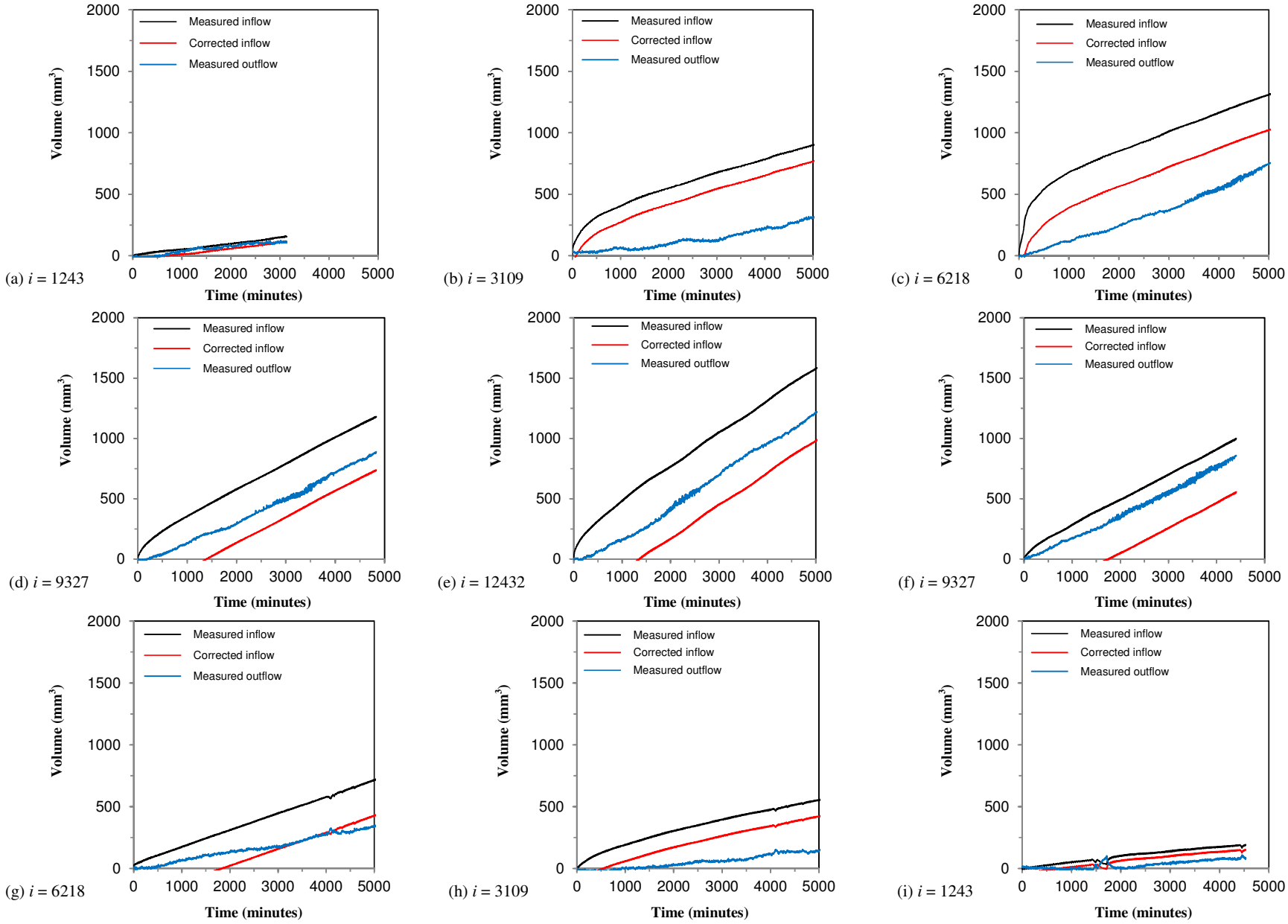

Figure 5.9 - Inflow and outflow behaviour determined for the 1.478 Mg/m³ specimen

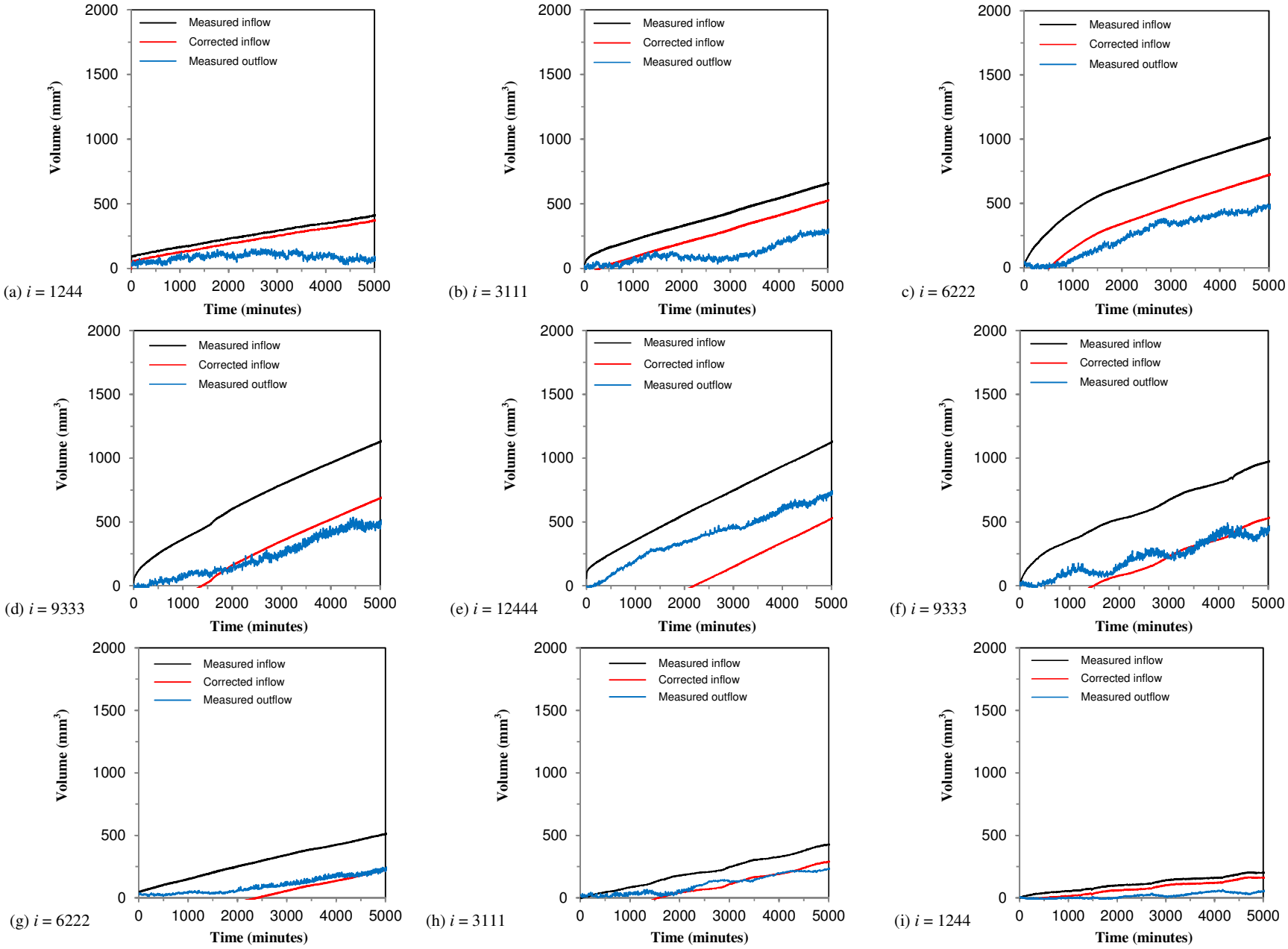

Figure 5.10 - Inflow and outflow behaviour determined for the 1.581 Mg/m^3 specimen

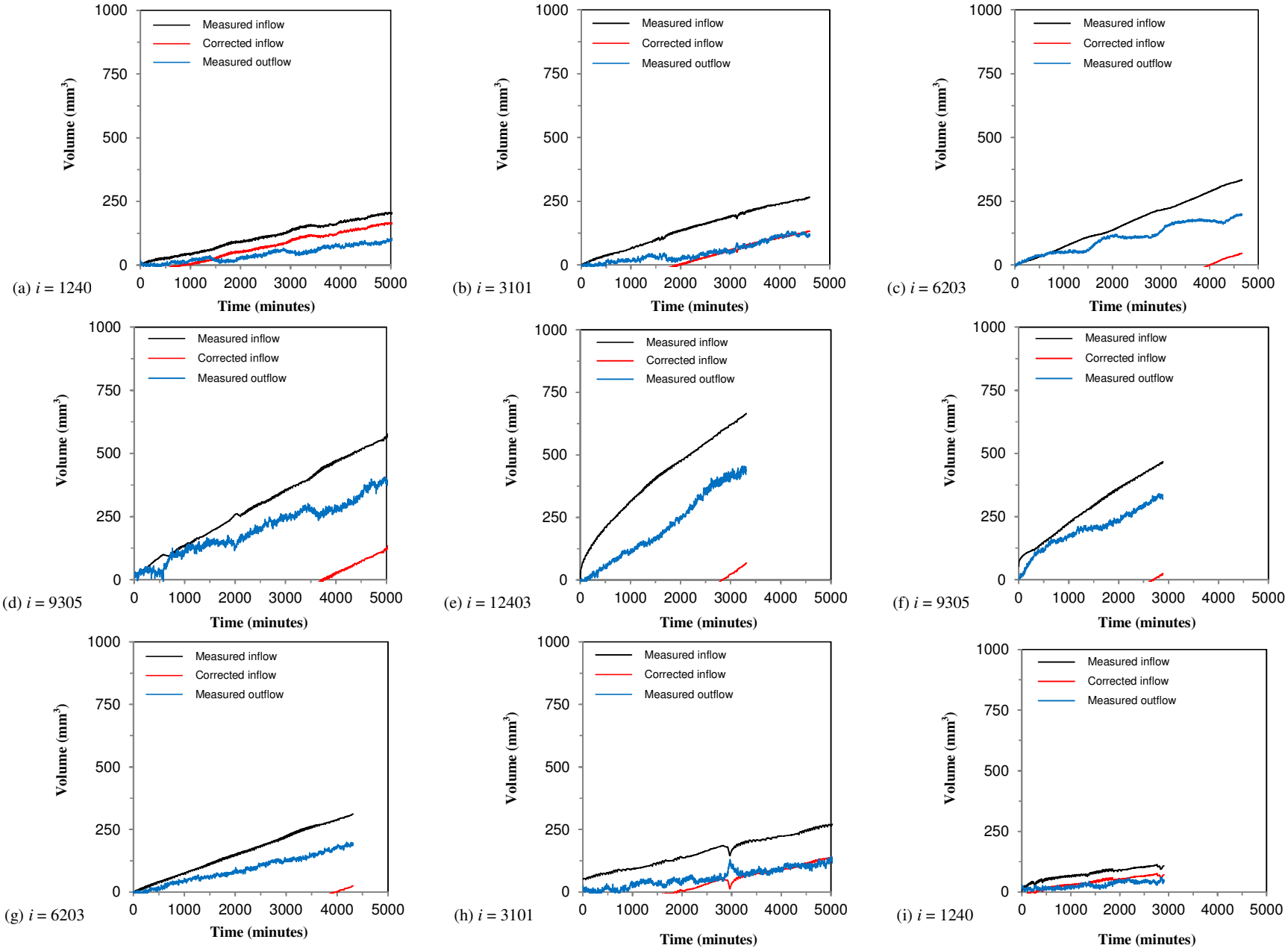

Figure 5.11 - Inflow and outflow behaviour determined for the 1.664 Mg/m³ specimen

Equilibrium inflow and outflow was calculated once the flow rates became constant for a minimum of 1440 minutes. The outflow rate was calculated to be between 95-100% of the inflow velocity in the majority of tests. Differences between the inflow and outflow rates were concluded to be due primarily to continuing secondary system expansion. The step-wise increasing and decreasing of hydraulic gradient was not observed to have any significant effect on the inflow and outflow rates.

Table 5.3 - Equilibrated inflow and outflow rates determined during this study

Specimen	Dry density (Mg/m^3)	Test step	Pressure differential (kPa)	Hydraulic gradient (m/m)	Inflow rate (mm^3/min)	Outflow rate (mm^3/min)	Outflow as percentage of inflow (%)
		a	100	1245	0.287	0.271	94.4
		b	250	3113	0.419	0.397	94.7
		c	500	6227	0.774	0.730	94.3
		d	750	9340	1.032	0.957	92.7
1	1.088	e	1000	12453	1.411	1.299	92.1
		f	750	9340	0.912	0.859	94.2
		g	500	6227	0.651	0.597	91.7
		h	250	3113	0.422	0.397	94.1
		i	100	1245	0.290	0.268	92.4
		a	100	1246	0.124	0.118	95.2
		b	250	3115	0.263	0.252	95.8
		c	500	6231	0.477	0.455	95.4
		d	750	9346	0.679	0.654	96.3
2	1.191	e	1000	12461	0.853	0.825	96.7
		f	750	9346	0.717	0.684	95.4
		g	500	6231	0.440	0.421	95.7
		h	250	3115	0.214	0.208	97.2
		i	100	1246	0.114	0.114	100.0
		a	100	1244	0.161	0.169	105.0
		b	250	3111	0.288	0.281	97.6
		c	500	6222	0.411	0.403	98.1
		d	750	9333	0.573	0.551	96.2
3	1.283	e	1000	12444	0.741	0.739	99.7
		f	750	9333	0.541	0.517	95.6
		g	500	6222	0.391	0.375	95.9
		h	250	3111	0.233	0.202	86.7
		i	100	1244	0.104	0.103	99.0

Table 5.3 - Equilibrated inflow and outflow rates determined during this study (continued)

Specimen	Dry density (Mg/m^3)	Test step	Pressure differential (kPa)	Hydraulic gradient (m/m)	Inflow rate (mm^3/min)	Outflow rate (mm^3/min)	Outflow as percentage of inflow (%)
4	1.379	a	100	1243	0.064	0.066	103.1
		b	250	3109	0.115	0.109	94.8
		c	500	6218	0.239	0.221	92.5
		d	750	9327	0.350	0.298	85.1
		e	1000	12432	0.396	0.388	98.0
		f	750	9327	0.344	0.342	99.4
		g	500	6218	0.251	0.251	100.0
		h	250	3109	0.130	0.129	99.2
		i	100	1243	0.059	0.057	96.6
5	1.478	a	100	1243	0.042	0.042	100.0
		b	250	3109	0.087	0.086	98.9
		c	500	6218	0.143	0.138	96.5
		d	750	9327	0.211	0.207	98.1
		e	1000	12436	0.243	0.235	96.7
		f	750	9327	0.213	0.204	95.8
		g	500	6218	0.125	0.118	94.4
		h	250	3109	0.072	0.068	94.4
		i	100	1243	0.033	0.032	97.0
6	1.581	a	100	1244	0.025	0.023	92.0
		b	250	3111	0.063	0.045	71.4
		c	500	6222	0.125	0.094	75.2
		d	750	9333	0.153	0.151	98.7
		e	1000	12444	0.190	0.185	97.4
		f	750	9333	0.150	0.147	98.0
		g	500	6222	0.091	0.088	96.7
		h	250	3111	0.075	0.065	86.7
		i	100	1244	0.027	0.026	96.3
7	1.664	a	100	1240	0.025	0.025	100.0
		b	250	3101	0.052	0.050	96.2
		c	500	6204	0.084	0.081	96.4
		d	750	9305	0.100	0.098	98.0
		e	1000	12407	0.144	0.137	95.1
		f	750	9305	0.123	0.115	93.5
		g	500	6204	0.067	0.064	95.5
		h	250	3101	0.039	0.033	84.6
		i	100	1240	0.028	0.027	96.4

5.2.3 Saturated hydraulic conductivity of compacted bentonite calculated from Darcy's law

The hydraulic conductivity of soils is commonly determined using Darcy's law (1856). Darcy's law states that the hydraulic flux is proportional to the hydraulic gradient applied to the soil. The validity of Darcy's law in saturated expansive clays has been discussed previously (Lutz and Kemper, 1959; Olsen, 1969; Miller et al., 1969; Chan and Kenney, 1973; Dixon et al., 1999). The existence of transitional or threshold hydraulic gradients has been reported by some researchers. Other researchers have failed to confirm the existence of these gradients.

The validity of Darcy's law for the range of applied hydraulic gradients considered in the study was assessed. The equilibrium inflow rates determined during the hydraulic conductivity tests are presented in Figure 5.12(a). The equilibrium outflow rated determined during the hydraulic conductivity tests are presented in Figure 5.12(b).

For all specimens, a proportional relationship was observed between hydraulic flux and hydraulic gradients. The water flow velocities for highly compacted bentonite specimens were observed to be significantly lower than specimens with lower compaction dry densities. As the overall trend observed was linear in the case of inflow and outflow, it was concluded that Darcy's law was valid for the applied hydraulic gradients considered.

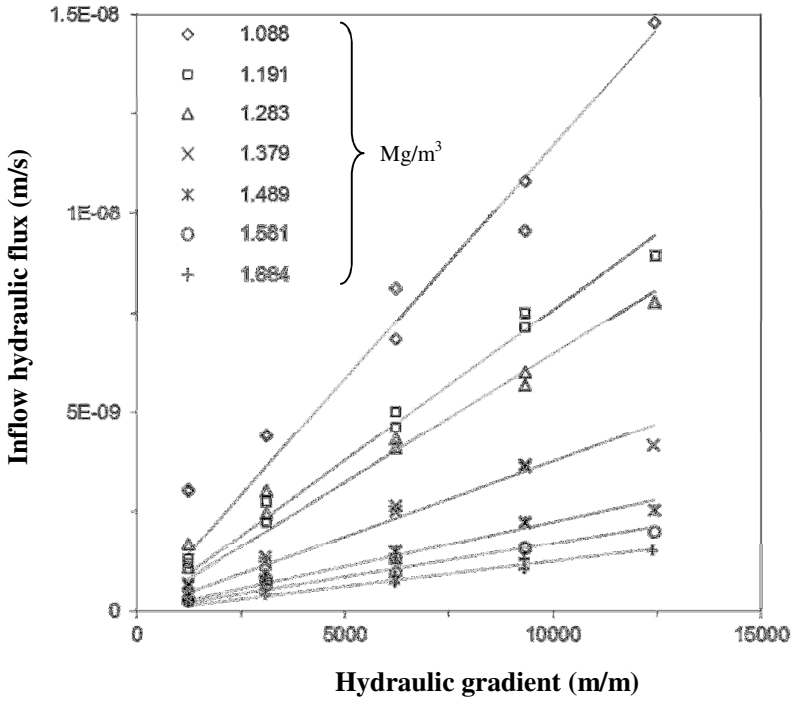

Figure 5.12(a) - Relationship between hydraulic gradient and inflow flux determined during hydraulic conductivity tests

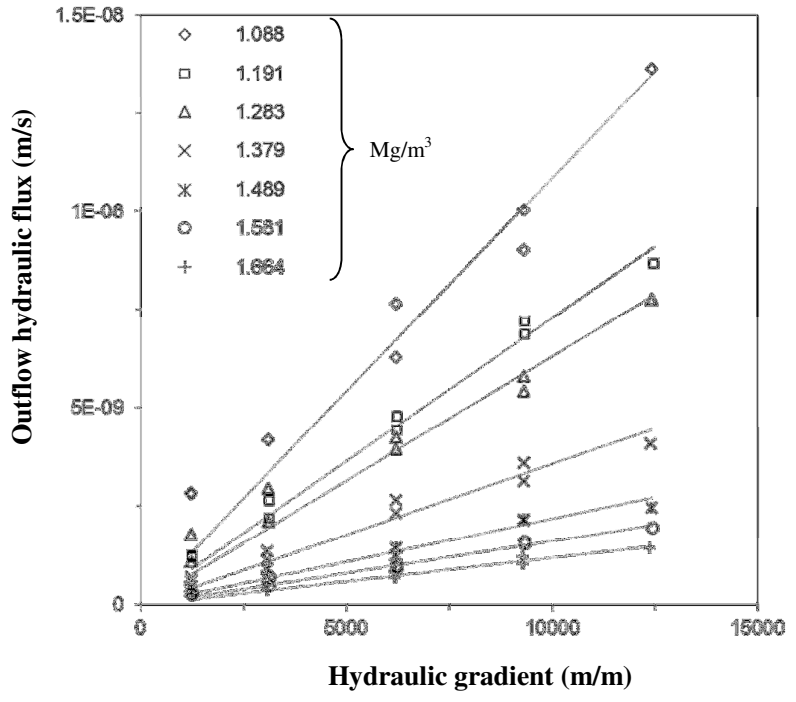

Figure 5.12(b) - Relationship between hydraulic gradient and outflow flux determined during hydraulic conductivity tests

From Darcy's law, the hydraulic conductivity is defined as the proportionality constant between the hydraulic flux and the applied hydraulic gradient. A linear relationship is observed between hydraulic flux and hydraulic gradient, with the gradient taken to be the hydraulic conductivity. In the case of the inflow and outflow fluxes determined for each dry density, a 'best-fit' line was added, as shown in Figures 5.12(a) and 5.12(b). This line passed through the origin. The hydraulic conductivity of each of the specimens was then determined in the case of the inflow and outflow hydraulic fluxes. The values calculated for each specimen are shown in Table 5.4.

Table 5.4 - Saturated hydraulic conductivities determined for the compacted bentonite specimens considered in this study

Dry density (Mg/m^3)	Hydraulic conductivity calculated from inflow flux *Figure 5.12(a)* (m/s)	Hydraulic conductivity calculated from outflow flux *Figure 5.12(b)* (m/s)
1.088	1.17×10^{-12}	1.09×10^{-12}
1.191	7.59×10^{-13}	7.30×10^{-13}
1.283	6.49×10^{-13}	6.31×10^{-13}
1.379	3.76×10^{-13}	3.58×10^{-13}
1.478	2.26×10^{-13}	2.18×10^{-13}
1.582	1.72×10^{-13}	1.62×10^{-13}
1.684	1.26×10^{-13}	1.21×10^{-13}

The hydraulic conductivity was found to decrease as the dry density increased. This is in agreement with that reported in the literature (Pusch, 1982; Dixon et al., 1999; Cho et al., 1999). The hydraulic conductivities calculated from the inflow and outflow rates were

observed to differ slightly. The differences between the hydraulic conductivities calculated from inflow and outflow rates were found to be less than 7% for all dry densities considered.

5.3 Expulsion of exchangeable cations during hydraulic conductivity tests

5.3.1 Inflow and outflow samples taken between hydraulic conductivity tests

The expulsion of exchangeable cations was determined throughout the hydraulic conductivity tests conducted on compacted saturated bentonite specimens. Five of the compacted saturated bentonite specimens were considered. The specimens considered were those prepared with dry densities of 1.191, 1.283, 1.379, 1.581 and 1.664 Mg/m^3.

The specimens were initially saturated. Once the swelling pressure had equilibrated, a fluid sample from the influent and effluent was taken. The first hydraulic conductivity test was then commenced. The influent and effluent was sampled once the inflow and outflow rates had equilibrated. In turn, the nine hydraulic conductivity tests were carried out. The influent and effluent was sampled after each test.

Approximately 30 ml of fluid was sampled from the influent and effluent after each hydraulic conductivity test. The inflow and outflow fluid pressures were maintained at 20 kPa. Care was taken to avoid fluid loss from the pipe. The experimental system was then prepared for the next hydraulic conductivity test.

The fluid samples taken were analysed using inductively coupled plasma optical emission spectrometry (ICP-OES). The concentration of calcium (Ca^{2+}), magnesium (Mg^{2+}), potassium (K^{+}) and sodium (Na^{+}) ions was determined in mg/l. These cations were found previously to be present within the MX80 bentonite. The concentration of anions in the fluid samples was not considered, as any movement of ions from the bentonite-water system will maintain electro-neutrality (Higashihara et al., 2008).

As the volume of fluid and concentration of cations present within the inflow and outflow systems were known, the mass of each species of exchangeable cation within the inflow and outflow systems was calculated. The initial masses of exchangeable cation were determined from the cation exchange capacity of the MX80 bentonite, as presented in Chapter 3. The total percentage loss of exchangeable cations from the compacted bentonite specimen to the adjacent water reservoirs at the end of the hydraulic conductivity testing programme for each specimen considered was calculated.

5.3.2 Total loss of exchangeable cations from the compacted bentonite specimens

Figure 5.13 shows the total percentage cation expulsion of exchangeable cations for the compacted saturated bentonite specimens considered in this study. The greatest total percentage of initial exchangeable cations lost from the specimen was observed to be sodium ions. The total percentage of initial calcium, magnesium and potassium ions expelled were similar for all dry densities considered. In all cases, the total percentage of initial exchangeable cations lost during the hydraulic conductivity tests were observed to decrease.

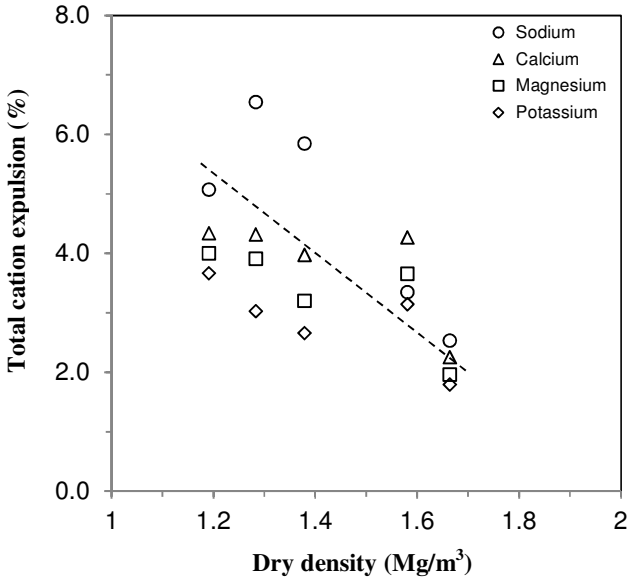

Figure 5.13 - Total percentage of exchangeable cations expelled during hydraulic conductivity tests

As the compaction dry density of the bentonite specimen increases, the inter-platelet spacing is reduced. The closer proximity of the platelets to one another result in the exchangeable cations within platelet interlayer being held more tightly as the dry density increases, and as such, are less likely to be able to exit the bentonite-water system. As such, the total percentage of initial cations observed to have been expelled from the compacted bentonite system would be expected to decrease, as the dry density increases.

It was observed that generally less than 6% of exchangeable cations have been lost from the system during the hydraulic conductivity tests. Tadza (2011) reported that 6 - 11 % of exchangeable cations were lost from the bentonite-water system during suction measurements using PEG solutions. Overall, as a small percentage of the initial exchangeable cations within the compacted bentonite system were lost, the finial cation exchange capacity of the compacted bentonite specimens were approximately that prior to the start of the tests.

As such, it would be expected that there would be no effect on the hydraulic conductivity determined throughout the testing programme. The small total percentage of exchangeable cations lost is supported by the relationships between hydraulic flux and hydraulic gradient presented in Figure 5.12, which show that no significant change of the hydraulic conductivity was observed.

5.4 Compressibility behaviour of compacted saturated bentonite

5.4.1 Experimental programme

Compacted specimens of MX80 bentonite were prepared at the air-dry water content (8%). The compressibility behaviour of five specimens was considered at increasing compaction dry densities. The targeted and actual dry densities of the prepared specimens are provided in Table 5.5.

Table 5.5 - Targeted and actual dry densities of compacted bentonite specimens prepared for consolidation tests

Specimen	Targeted dry density (Mg/m^3)	Actual dry density (Mg/m^3)
1	1.350	1.345
2	1.450	1.436
3	1.550	1.537
4	1.700	1.683
5	1.850	1.821

Prior to the step-wise consolidation, the swell-load method was adopted (Sridharan et al., 1986), during which the specimens were allowed to saturate under an applied surcharge, before sequential consolidation within increasing applied pressures. Initial saturation of a preliminary specimen prepared to a compaction dry density of about 1.6 Mg/m^3 showed that under a surcharge pressure of 50 kPa, a significant testing period was required for the swelling potential to equilibrate. Given this, the specimens with initial compaction dry densities of 1.537, 1.683 and 1.821 Mg/m^3 were saturated under a surcharge of 100 kPa. The specimens with compaction dry densities of 1.345 and 1.436 Mg/m^3 were saturated under a surcharge of 50 kPa. Upon saturation, the compacted specimens exhibited volume change.

The step-wise consolidation of the specimens was commenced after the swelling of the specimen had stabilised. The saturated specimens were step-wise loaded from 100 to 800 kPa using standard conventional oedometers.

5.3.2 Swelling of compacted bentonite specimens under constant vertical load

The swelling potentials that developed in the specimen are shown in Table 5.6. The greatest swelling potentials were found to occur in specimens 1 and 2. This was due to the applied vertical pressure being only 50 kPa, compared to 100 kPa of the other specimens tested. For the specimens, the height of the compacted specimen was found to be almost doubled during the saturation of the specimen.

Table 5.6 - Swelling potentials determined during saturation of compacted specimens

Specimen dry density (Mg/m^3)	Surcharge (kPa)	Swelling potential (%)	Final dry density after swelling (Mg/m^3)
1.345	50	81.8	0.74
1.436	50	96.1	0.73
1.537	100	67.9	0.91
1.683	100	73.6	0.97
1.821	100	69.8	1.07

5.4.3 Compressibility behaviour of compacted saturated bentonite

The pressure-void ratio (e-log p) relationships for the compacted bentonite specimens considered are shown in Figure 5.14. The specimens prepared at compaction dry densities of 1.345 and 1.436 Mg/m^3 were found to have greater void ratios after swelling. This was attributed to the lower applied vertical pressure applied during saturation, resulting in greater swelling within the specimens. As the 1.345 and 1.436 Mg/m^3 specimens were permitted to swell to a greater extent, the platelets within the microstructure are thought to have better aligned themselves in a parallel manner, such that at higher pressures, these specimens demonstrated greater compressibility.

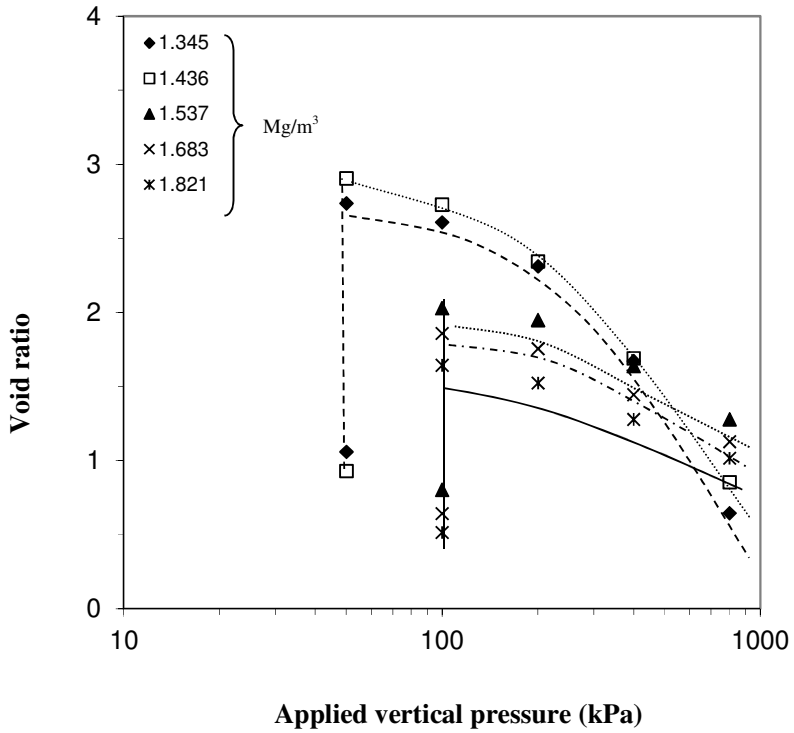

Figure 5.14 - Compressibility behaviour of MX80 bentonite

5.5 Comparison between saturated hydraulic conductivity determined experimentally and from compressibility behaviour

The coefficient of compressibility was calculated from the root-time (Taylor's) and log-time (Casagrande's) methods. The hydraulic conductivities were calculated from the coefficients of compressibility. The hydraulic conductivities determined in the rigid-walled permeameter was compared with that calculated hydraulic conductivity values. Figure 5.15(a) shows the hydraulic conductivities found in this study as a function of dry density. Figure 5.15(b) shows the determined hydraulic conductivities as a function of void ratio.

The range of dry densities and therefore void ratios that could be considered from saturated hydraulic conductivity tests and calculated from the compressibility behaviour was restricted by experimental limitations. It was not possible to produce compacted bentonite specimens at dry densities lower than 1.088 Mg/m^3 as the integrity of the specimen could not be maintained. The applied pressure during consolidation tests could not be increased higher than 800 kPa due to safety factors. The overlap between the two methods (between void ratios of 1 to 1.5) shows that the methods are comparable, but this cannot be confirmed in this study.

The hydraulic conductivities determined in this study were compared with that reported in the literature for compacted saturated bentonites permeated with water. Reasonable agreement was observed generally between this study and the hydraulic conductivities of different bentonites. Borgesson et al. (1996) presented the hydraulic conductivity of MX80 bentonite at increasing void ratios. The values determined in this study for MX80 bentonite show good agreement for the range of void ratios considered in this study.

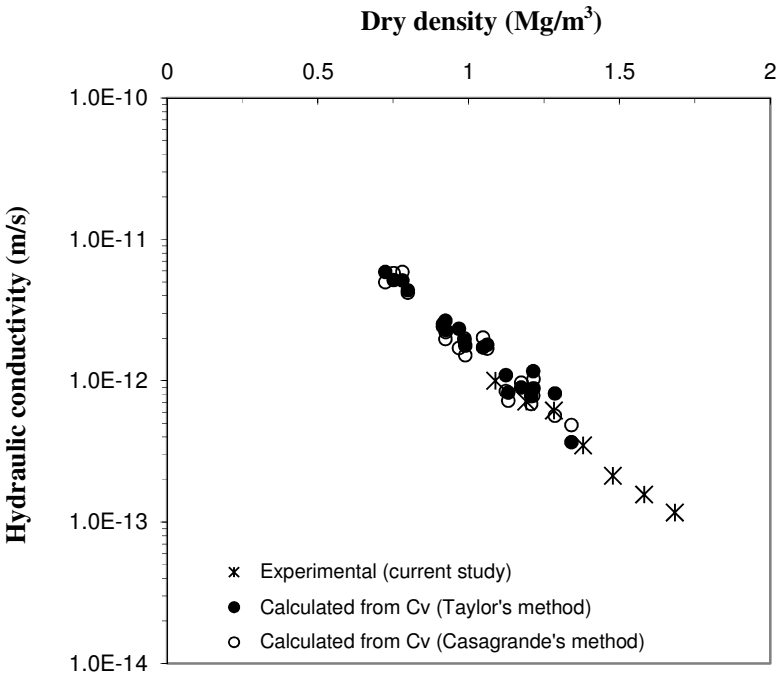

Figure 5.15(a) - Comparison of saturated hydraulic conductivity from hydraulic conductivity tests and consolidation behaviour as a function of dry density

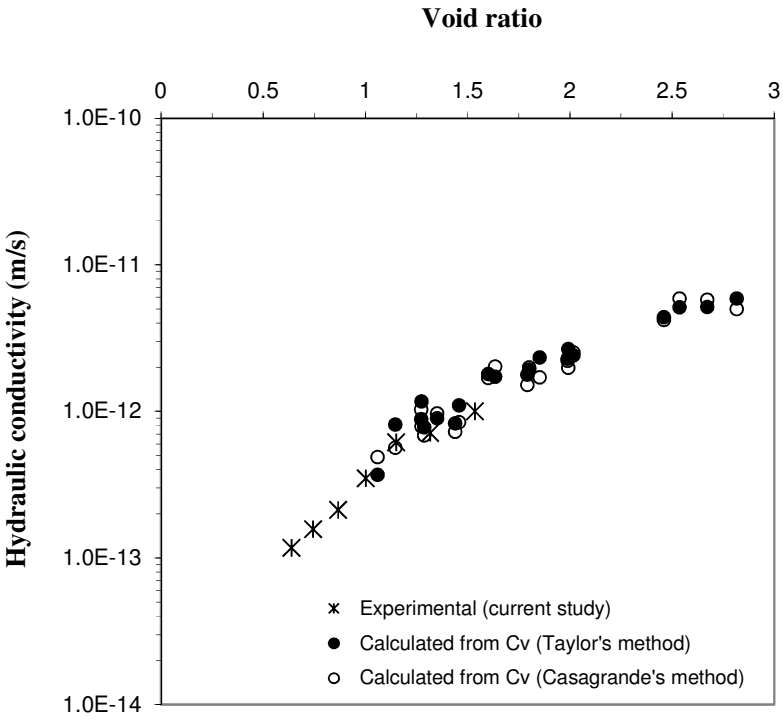

Figure 5.15(b) - Comparison of saturated hydraulic conductivity from hydraulic conductivity tests and consolidation behaviour as a function of void ratio

5.6 Concluding remarks

In this chapter, the hydraulic conductivities of compacted saturated MX80 bentonite were presented for a dry density range between 1.088 and 1.664 Mg/m^3. A high capacity fixed ring modified swelling pressure cell was used during the hydraulic conductivity tests. The compacted bentonite specimens were saturated with distilled de-aired water. The swelling pressures developed during hydration were monitored. The hydraulic conductivity tests were commenced once the swelling pressures were stabilised. The applied hydraulic gradients considered were between 1250 and 12500. These corresponded to pressure differentials between the inflow and outflow pressures of 100 to 1000 kPa. The actual inflow water volumes were calculated based on the system expansion at various water pressures. The hydraulic conductivity was determined from Darcy's law.

It was found that the inflow of water to the compacted bentonite specimen was greater than the outflow of water from the compacted bentonite specimen. The inflow volume was corrected to take into account the secondary expansion, and the corrected inflow and outflow volumes showed good compatibility. The water inflow and outflow rates were found to be about equal.

The influent and effluent to the compacted bentonite specimen was sampled after each hydraulic conductivity tests, to assess the loss of exchangeable cations from the bentonite-water system due to a number of transport processes, including diffusion and advection. Approximately 30ml of fluid was taken from the inflow and outflow pipe system after each test, which was subjected to ICP-OES analysis.

The compressibility behaviour of compacted bentonite was studied using a conventional oedometer. Compacted specimens were allowed to swell under an applied pressure of 50 or 100 kPa. The specimens were then step-wise loaded up to an applied vertical pressure of 800 kPa. Taylor's and Casagrande's method were used to calculate the hydraulic conductivity from the coefficient of compressibility.

The total percentage loss of exchangeable cations from the compacted bentonite specimen was then determined. It was found that less than around 6% of the initial exchangeable cations within the bentonite specimen were expelled during the hydraulic conductivity tests. No significant changes were therefore expected of the hydraulic conductivity of the specimen during the testing programme, which was confirmed through the step-wise increasing and decreasing of hydraulic gradient.

A linear relationship was noted between the hydraulic gradient and hydraulic flux calculated from the constant flow rates at the end of the hydraulic conductivity tests. This indicates that Darcy's law was valid for compacted bentonites in the range of hydraulic conductivities considered in this study. The calculated and measured hydraulic conductivities were found to decrease as the compaction dry density increased, in agreement with that reported in the literature.

CHAPTER 6

HYDRAULIC CONDUCTIVITY OF COMPACTED SAND-BENTONITE SPECIMENS

6.1 Introduction

Sand-bentonite or crushed rock-bentonite mixtures have been considered as suitable backfilling materials for deep geological repositories. The backfilling material is required to have similar hydraulic conductivity to that of the host rock (Villar, 2007). It has been reported that the hydraulic conductivity of sand-bentonite mixtures increased as the bentonite content of the mixture decreased (Sivapullaiah et al., 2000; Komine, 2008).

A number of researchers have determined the hydraulic conductivity of compacted sand-bentonite and crushed rock-bentonite mixtures at increasing compaction dry densities and increasing bentonite contents. Kenney et al. (1992) reported that the low conductivity of the sand-bentonite mixture was due to the continuation of the bentonite matrix within the specimen. Borgesson et al. (2003) found that heterogeneities in the crushed rock-bentonite mixtures were observed. Increased heterogeneities resulted in increasing hydraulic conductivity.

A number of bentonites have been considered during hydraulic conductivity tests on compacted sand-bentonite and crushed rock-bentonite mixtures. These include calcium bentonite (Prikryl et al., 2003), Nagayo clay (Watabe et al., 2011), Kunigel VI (Komine, 2004) and an Indian bentonite (Sivapullaiah et al., 2000). The hydraulic conductivity of compacted crushed rock-bentonite specimens using MX80 bentonite has only been reported previously by Borgesson et al. (2003).

The hydraulic conductivity of compacted sand-bentonite specimens determined at increasing compaction dry densities is presented in this chapter. The swelling pressures exhibited during saturation of the specimens are shown. The water inflow and outflow volumes are presented. The relationship between hydraulic gradient and hydraulic flux are shown for the compacted sand-bentonite specimens. The compressibility behaviour of compacted sand-bentonite mixtures is provided.

6.2 Saturated hydraulic conductivity of sand-bentonite mixtures

6.2.1 Experimental programme

Compacted sand-bentonite specimens were prepared at a ratio of 30% MX80 bentonite and 70% sand by mass. This ratio of sand to bentonite has attracted attention as a suitable composition for backfilling materials in radioactive waste disposal (Gunnarsson et al., 2004; Nirex, 2005). Prior to compaction, the mixture was thoroughly mixed, to limit the heterogeneities in the specimen. Table 6.1 shows the targeted and actual dry densities of specimens considered in this study.

Table 6.1 - Targeted and actual dry densities of sand-bentonite mixtures prepared

Specimen	Targeted dry density (Mg/m^3)	Attained dry density (Mg/m^3)
1	1.600	1.584
2	1.700	1.679
3	1.800	1.778

The hydraulic gradients applied corresponded with the pressure differentials considered during the hydraulic conductivity tests on saturated bentonite. The pressure differentials tested were 100 kPa, 250 kPa, 500 kPa, 750 kPa and 1000 kPa. These corresponded to hydraulic gradients between approximately 1250 and 12500. For each gradient applied, the test was terminated when the inflow and outflow rates were constant.

6.2.2 Saturation of compacted sand-bentonite specimens under constant volume conditions

The compacted sand-bentonite specimens were saturated with distilled de-aired water. The equilibrium swelling pressure was attained around 5000 minutes. Once the swelling pressures had stabilised, the hydraulic conductivity tests were undertaken. The equilibrated swelling pressures developed during saturation of the sand-bentonite specimens are shown in Figure 6.1.

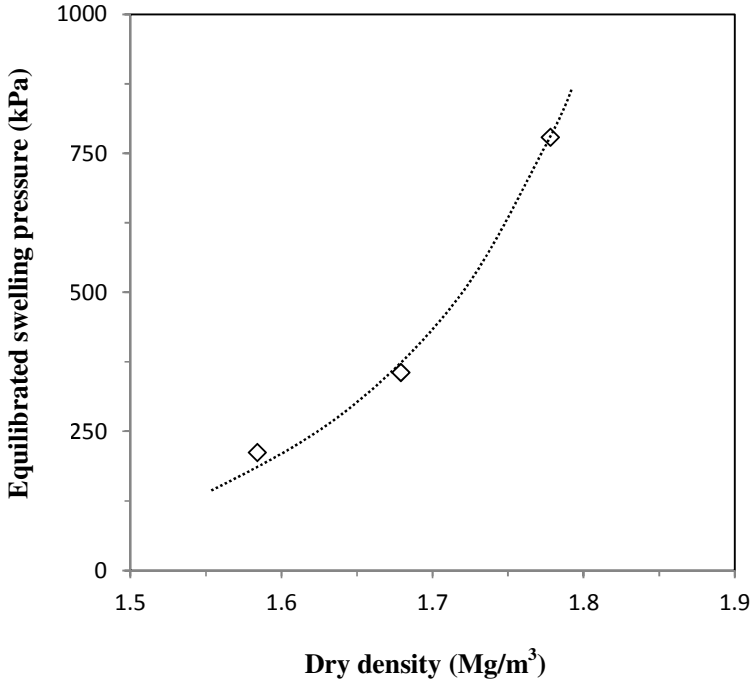

Figure 6.1 - Equilibrated swelling pressures prior to hydraulic conductivity tests for compacted sand-bentonite specimens

6.2.3 Measured inflow and outflow during hydraulic conductivity tests

Figures 6.2, 6.3 and 6.4 show the water inflow and outflow behaviour due to the applied hydraulic gradients for the specimens prepared with compaction dry densities of 1.584, 1.678 and 1.778 Mg/m^3 respectively. The water inflow volumes were corrected to account for secondary pipe expansion. The correction applied to the inflow as determined from Equation (4.1).

The inflow and outflow was observed to increase as the hydraulic gradient applied to the specimen was increased. For all tests carried out, the inflow and outflow rates equilibrated within about 1000 minutes of testing. Good compatibility was observed between the corrected inflow and outflow volumes for the majority of tests. The inflow and outflow rates were determined once steady flow conditions were observed for a minimum of 500 minutes. The calculated inflow and outflow rates from Figures 6.2, 6.3 and 6.4 are shown in Table 6.2. The outflow rate is also calculated as a percentage of the inflow rate.

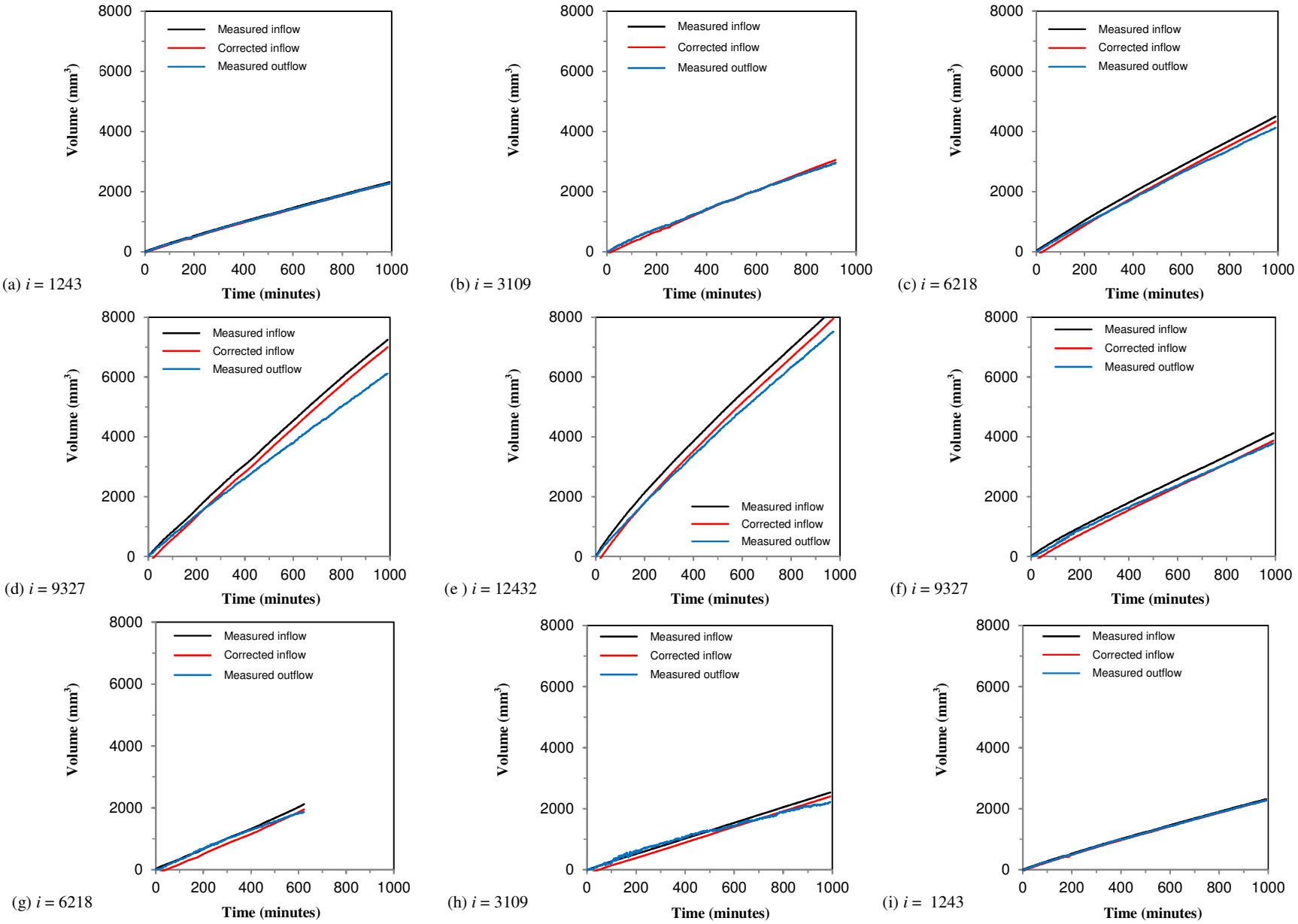

Figure 6.2 - Inflow and outflow behaviour determined for the 1.584 Mg/m^3 specimen

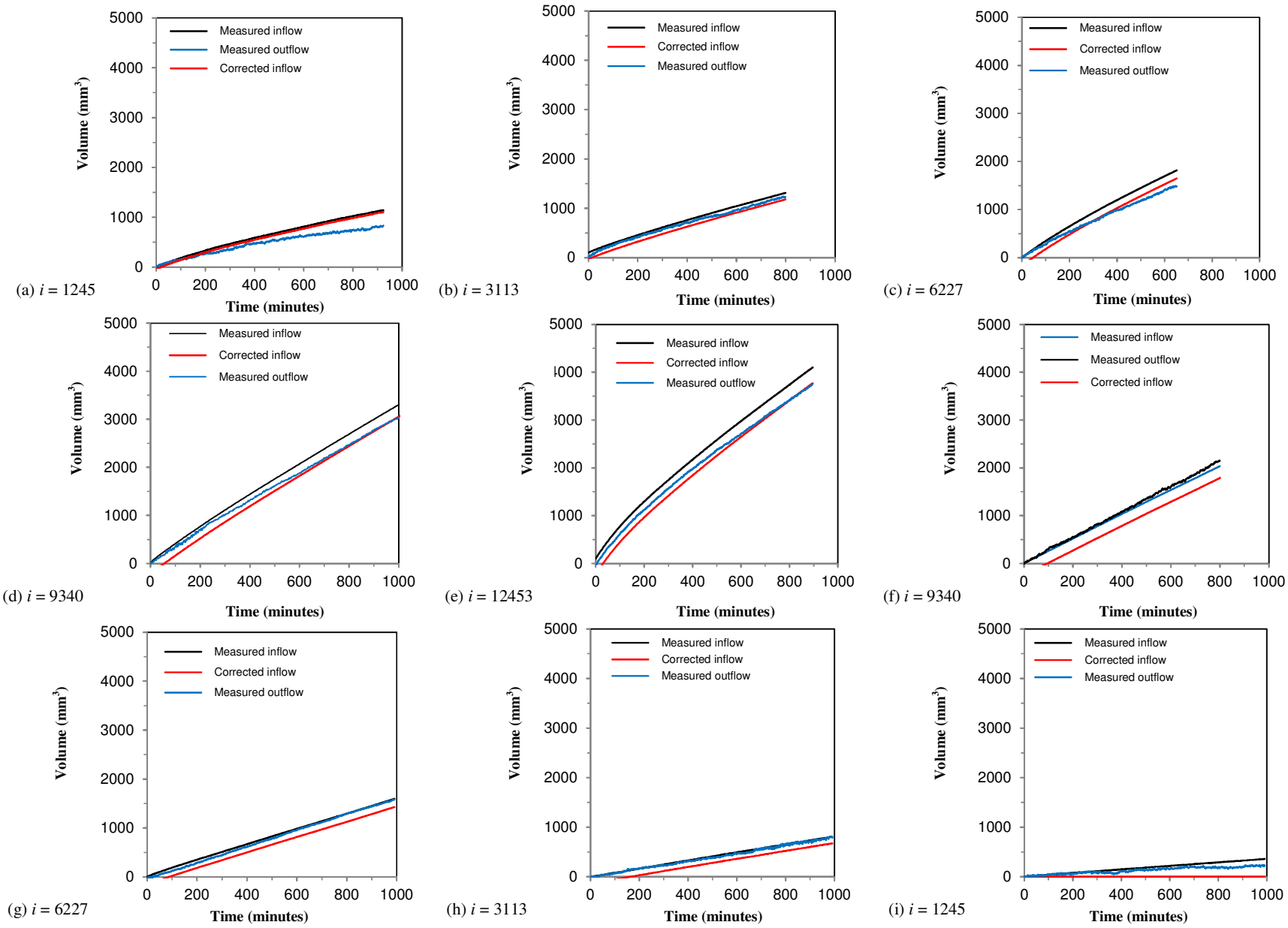

Figure 6.3 - Inflow and outflow behaviour determined for the 1.679 Mg/m^3 specimen

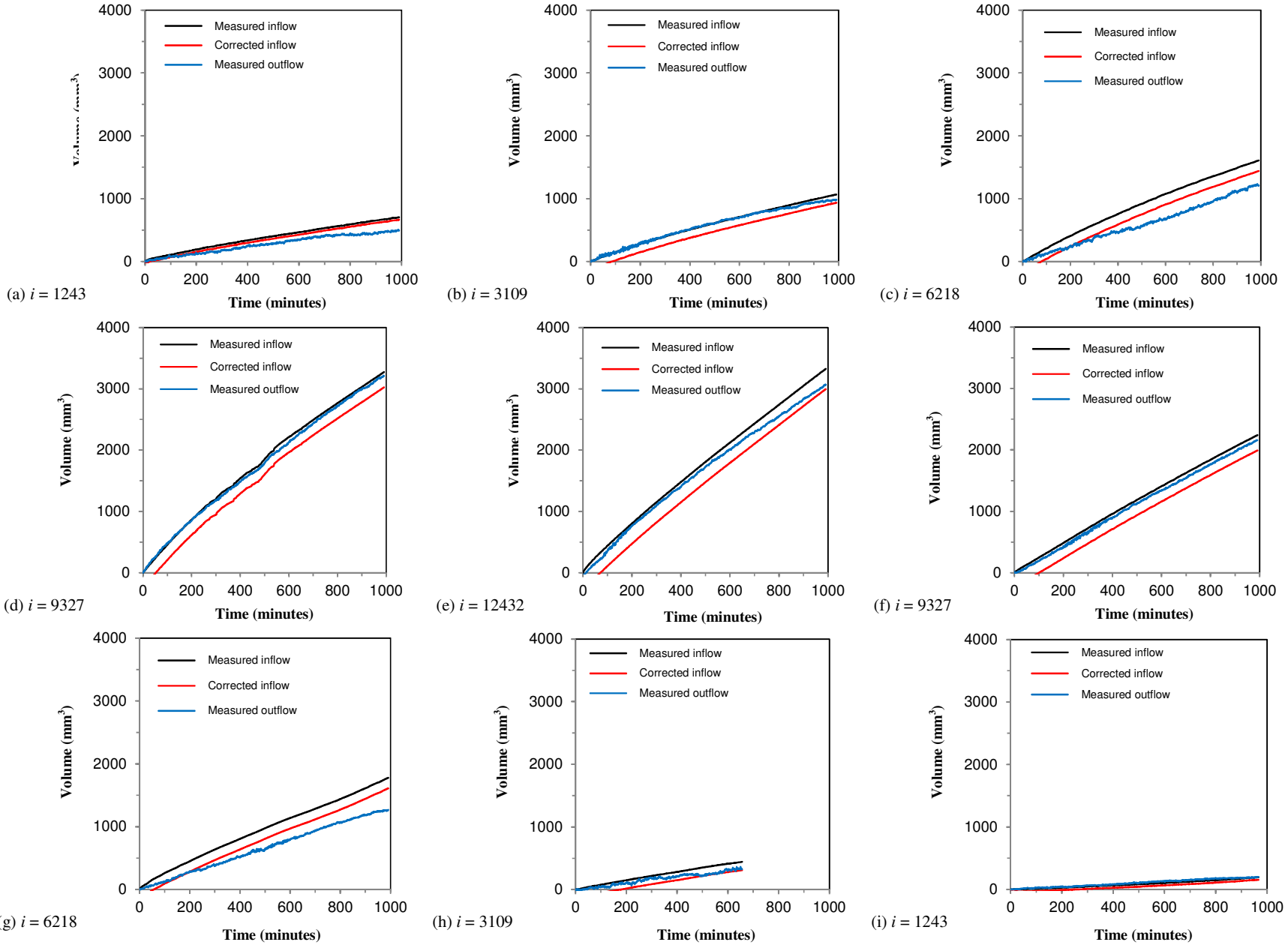

Figure 6.4 - Inflow and outflow behaviour determined for the 1.778 Mg/m^3 specimen

Table 6.2 - Equilibrated inflow and outflow rates determined during this study

Specimen	Dry density (Mg/m^3)	Test step	Pressure differential (kPa)	Hydraulic gradient (m/m)	Inflow rate (mm^3/min)	Outflow rate (mm^3/min)	Outflow as percentage of inflow (%)
1	1.584	a	100	1245	1.56	1.54	98.7
		b	250	3113	2.35	2.21	94.1
		c	500	6227	3.87	3.54	91.5
		d	750	9340	5.62	5.31	94.5
		e	1000	12453	7.09	6.77	95.6
		f	750	9340	4.61	4.59	99.6
		g	500	6227	2.83	2.71	95.8
		h	250	3113	2.15	1.45	67.4
		i	100	1245	1.64	1.57	95.7
2	1.679	a	100	1243	1.02	0.74	72.5
		b	250	3109	1.34	1.28	95.5
		c	500	6218	2.24	2.13	95.1
		d	750	9327	3.31	3.22	97.3
		e	1000	12432	3.95	3.55	89.9
		f	750	9327	2.68	2.66	99.3
		g	500	6218	1.72	1.68	97.7
		h	250	3109	0.85	0.78	91.8
		i	100	1243	0.45	0.43	95.5
3	1.778	a	100	1243	0.55	0.49	89.9
		b	250	3109	0.74	0.71	96.0
		c	500	6218	1.39	1.26	90.6
		d	750	9327	2.25	2.16	96.0
		e	1000	12432	3.12	2.65	84.9
		f	750	9327	2.06	1.99	96.6
		g	500	6218	1.58	1.47	93.0
		h	250	3109	0.65	0.63	96.9
		i	100	1243	0.25	0.22	92.1

The constant inflow and outflow rates determined from the hydraulic conductivity tests were found to be approximately equal. As with that observed from the hydraulic

conductivity tests on compacted MX80 bentonite, the outflow was generally observed to be between 95-100% of inflow. The differences between inflow and outflow rates were attributed to continuing secondary expansion of the system. This was supported by similar losses from both experimental programmes (compacted MX80 bentonite and compacted sand-bentonite specimens).

The inflow and outflow rates were observed to decrease as the dry density of the specimen increased. As the hydraulic gradient applied to the specimen increased, the inflow and outflow rates were also observed to increase.

6.2.4 Saturated hydraulic conductivity of compacted sand-bentonite

The inflow and outflow hydraulic fluxes were calculated from the equilibrated inflow and outflow rates and the cross-sectional area of the specimen. The relationships between inflow hydraulic flux and the hydraulic gradient during tests are presented in Figure 6.5(a). The relationships between outflow hydraulic flux and the hydraulic gradient during tests are shown in Figure 6.5(b). A linear relationship was observed between hydraulic gradient and hydraulic flux for each of the specimens considered.

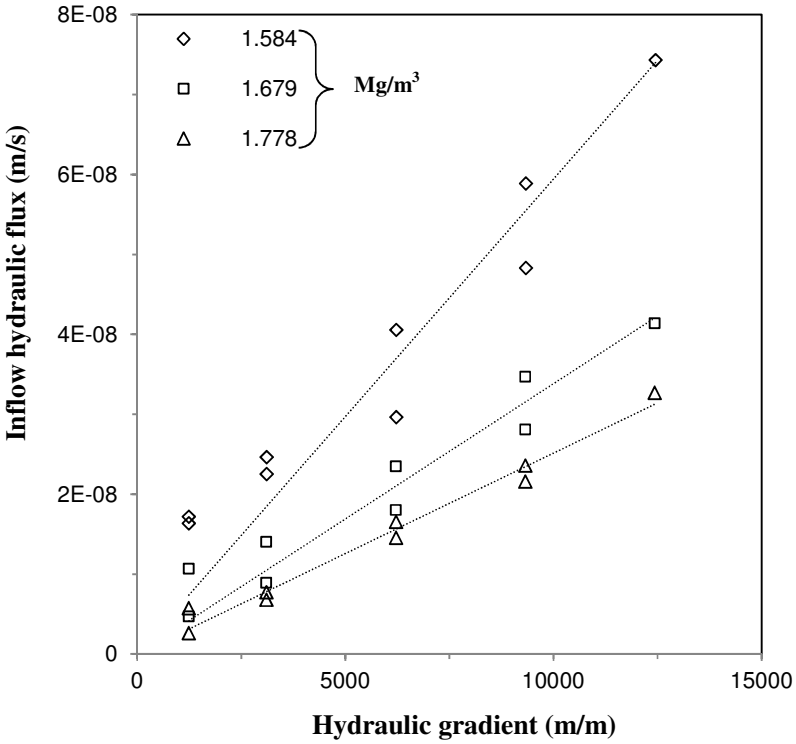

Figure 6.5(a) - Relationships between inflow hydraulic flux and hydraulic gradient determined during hydraulic conductivity tests

The hydraulic conductivity of the sand-bentonite specimens was determined using Darcy's law. The linear relationship observed between hydraulic flux and hydraulic gradient indicated that Darcy's law was valid, and so a proportional 'best fit' line was added for each specimen, passing through the origin. The hydraulic conductivity was then calculated from the gradient of the line. The hydraulic conductivity values determined are shown in Table 6.3.

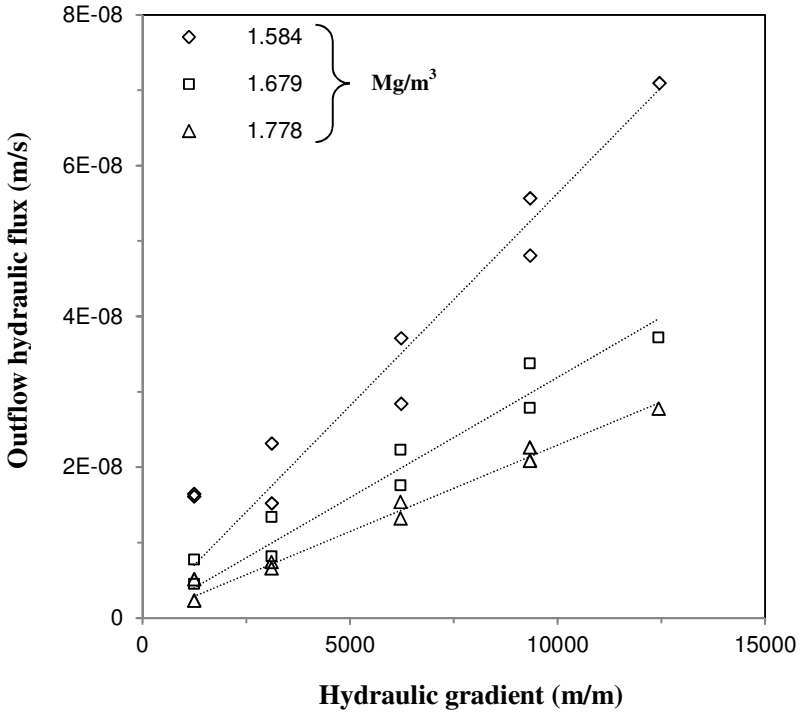

Figure 6.5(b) - Relationships between outflow hydraulic flux and hydraulic gradient determined during hydraulic conductivity tests

Table 6.3- Hydraulic conductivities calculated for compacted sand-bentonite specimens

Dry density (Mg/m^3)	Hydraulic conductivity from inflow flux *Figure 6.5(a)* (m/s)	Hydraulic conductivity from outflow flux *Figure 6.5(b)* (m/s)
1.584	5.94×10^{-12}	5.63×10^{-12}
1.679	3.38×10^{-12}	3.19×10^{-12}
1.778	2.51×10^{-12}	2.29×10^{-12}

The hydraulic conductivities of the tested specimens presented in Table 6.3 were found to decrease as the compacted dry density of the specimen increased. This is in agreement with that reported in the literature.

6.3 Compressibility of compacted sand-bentonite specimens

6.3.1 Experimental programme

Compacted sand-bentonite specimens were prepared at targeted dry densities between 1.5 and 1.8 Mg/m^3. The specimens were prepared from predetermined masses of sand and MX80 bentonite and mixed thoroughly prior to compaction. The details of the targeted and actual dry densities of the specimens are shown in Table 6.4.

Table 6.4 - Targeted and attained dry densities of specimens subjected to step-wise consolidation

Specimen	Targeted dry density (Mg/m^3)	Actual dry density (Mg/m^3)
1	1.500	1.497
2	1.600	1.582
3	1.700	1.680
4	1.800	1.785

The swell-load method (Sridharan et al., 1986) was adopted. Specimens were allowed to swell under an applied surcharge of 50 kPa, before being consolidated in a step-wise manner. Once the swelling of the specimens had equilibrated, the specimens were loaded in a step-wise manner. Applied vertical pressures of 100 kPa, 200 kPa, 400 kPa and 800 kPa were considered. The tests were terminated once equilibrium was reached.

6.3.2 Swelling of compacted sand-bentonite specimens under constant vertical load

Table 6.5 shows the swelling potentials of the compacted sand-bentonite specimens due to saturation with distilled water. The swelling potentials exhibited were observed to increase as the dry density of the specimen increased. The swelling potentials of sand-bentonite specimens were also observed to be considerably lower than those of compacted MX80 bentonite (shown previously in Table 5.6)

Table 6.5 - Swelling potentials determined during saturation of compacted specimens

Specimen dry density (Mg/m^3)	Surcharge (kPa)	Swelling potential (%)	Final dry density (Mg/m^3)
1.497	50	27.9	1.171
1.582	50	29.7	1.220
1.680	50	32.2	1.271
1.785	50	35.3	1.319

6.3.3 Compressibility behaviour of compacted sand-bentonite specimens

The pressure-void ratio (e-log p) relationships for the compacted sand-bentonite specimens considered are shown in Figure 6.6. The compression of the specimen under the applied vertical loads was observed to slightly decrease with an increase in the initial dry density of the specimen. The e-log p relationship was observed to be linear at applied vertical pressures greater than 100 kPa.

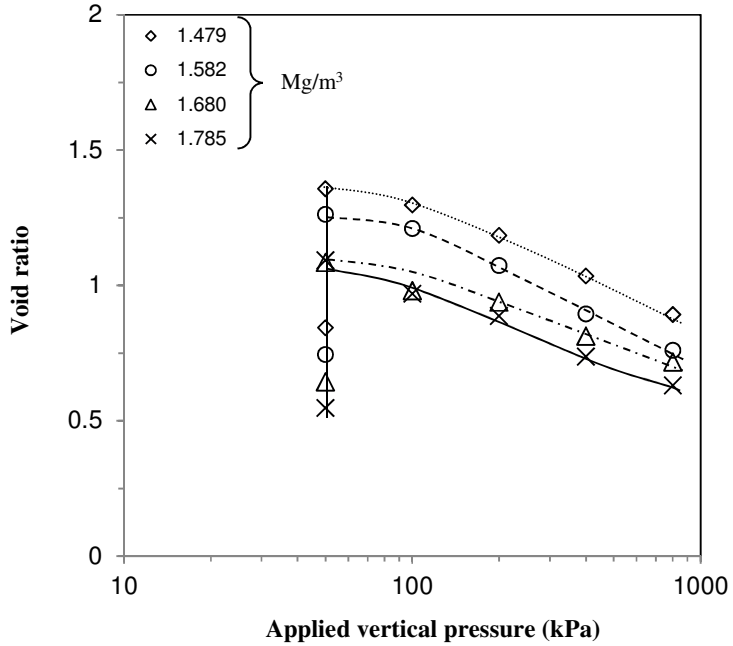

Figure 6.6 - Compressibility behaviour (e - log p) for compacted sand-bentonite specimens

The compressibility behaviour determined was compared with that reported by Sun et al. (2008) for compacted sand-bentonite mixture prepared with 30% Kunigel VI bentonite and 70% sand. The initial void ratio after swelling was greater in this study. This was attributed to the greater montmorillonite content of MX80 bentonite compared with Kunigel VI. The compressibility behaviour once saturated, however, was comparable to that of the results reported by Sun et al. (2008).

6.4 Comparison between saturated hydraulic conductivity determined experimentally and from compressibility behaviour

The compressibility behaviour of the compacted sand-bentonite specimens was used to calculate the saturated hydraulic conductivity. Taylor's and Casagrande's methods were used to determine the coefficient of compressibility through the root-time and log time procedures. The calculated hydraulic conductivities were then compared with those determined from the hydraulic conductivity tests. The hydraulic conductivity of compacted sand-bentonite mixtures as a function of dry density is shown in Figure 6.7(a). The relationship between void ratio and hydraulic conductivity is shown in Figure 6.7(b).

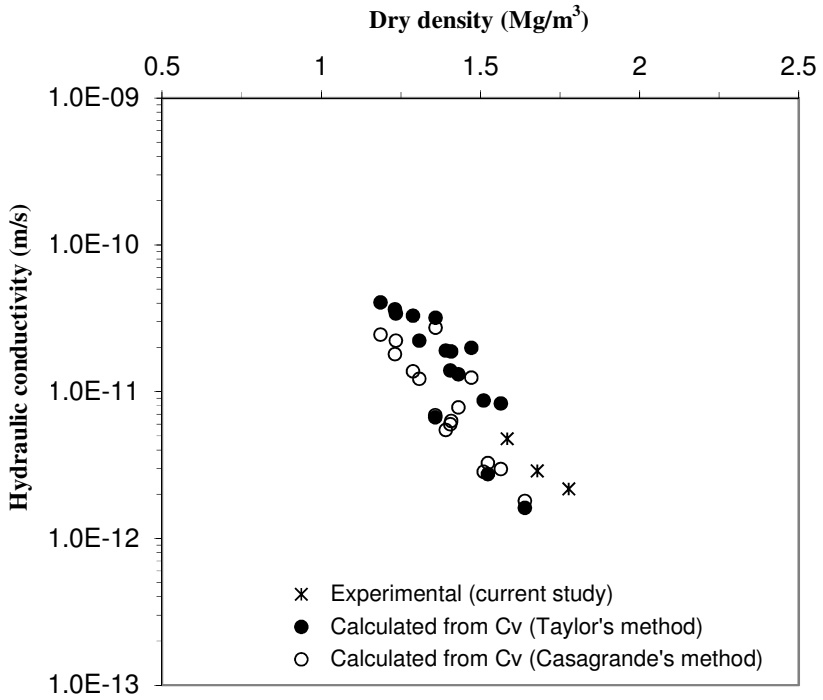

Figure 6.7(a) - Comparison of saturated hydraulic conductivity of compacted sand-bentonite mixtures as a function of dry density

The hydraulic conductivity was observed to decrease as the void ratio decreased (i.e. the dry density of the specimen increased). At overlapping void ratios, the hydraulic conductivities determined from hydraulic conductivity tests were comparable to those obtained from the compressibility behaviour of the compacted san-bentonite specimens.

Some scatter was observed in Figure 6.7 from the hydraulic conductivities calculated from the compressibility behaviour. This scatter is primarily attributed to the degree of accuracy of measurements taken during the consolidation of the compacted sand-bentonite specimens, as a significantly lesser degree of consolidation was observed than that of the compacted bentonite specimens. In addition, the potential for heterogeneities to be present within the sand-bentonite matrix may also have contributed to the scatter observed.

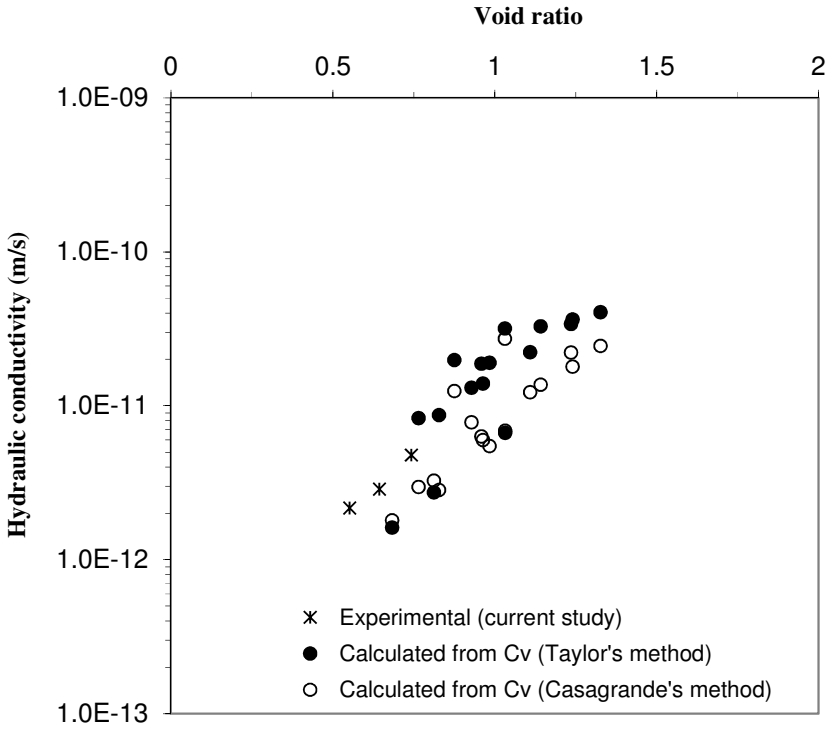

Figure 6.7(b) - Comparison of saturated hydraulic conductivity of compacted sand-bentonite mixtures as a function of void ratio

The hydraulic conductivity determined in this study was compared to experimental results in literature where 70:30 sand-bentonite specimens have been tested. Sivapullaiah et al. (2000) reported for a void ratio range between 1 - 2, the hydraulic conductivities of sand-bentonite mixtures decreased from 10^{-9} to 10^{-11} m/s. Gunnarsson et al. (2004), reported that for compacted sand-bentonite specimens prepared with compaction dry densities between 1.7 and 1.9 Mg/m^3, the saturated hydraulic conductivity determined decreased from 10^{-11} to 10^{-12} m/s.

The results obtained in this study are comparable to that reported in literature. The slight differences between the hydraulic conductivity determined in the current study and those reported in literature are due to the type of bentonite considered in the specimen. The results obtained by Borgesson et al. (2003) for mixtures comprised of MX80 bentonite and crushed rock are in reasonable agreement with that determined in this study.

6.5 Concluding remarks

The saturated hydraulic conductivities of compacted sand-bentonite specimens were presented in this chapter. The water inflow and outflow volumes under step-wise increasing and decreasing hydraulic gradients were shown. The hydraulic conductivity of compacted sand-bentonite specimens was calculated from Darcy's law. The compressibility behaviour of compacted sand-bentonite mixtures was also shown. The coefficient of compressibility was calculated at each test stage using Taylor's and Casagrande's methods. The hydraulic conductivities were calculated from the coefficients of compressibility.

As with the compacted bentonite specimens, the outflow rate was observed to be between 95 and 100% of the inflow rate for most cases. The correction of water inflow volumes to account for system expansion showed reasonable comparison with the measure water outflow volumes during the hydraulic conductivity tests.

The hydraulic conductivity of the specimens was found to decrease as the compaction dry density of the specimen increased. The hydraulic conductivities calculated from coefficients of compressibility showed a greater scatter than for compacted MX80 bentonite. This was attributed to measurement inaccuracies when determining the consolidation behaviour of the specimens, and to heterogeneities within the sand-bentonite mixture. The results obtained showed good agreement with that reported previously in literature.

CHAPTER 7

GAS PERMEABILITY OF COMPACTED BENTONITES

7.1 Introduction

The gas permeability of compacted bentonite is of particular importance in the disposal of municipal solid waste. Gas emissions from municipal landfill liners are primarily composed of methane and carbon dioxide produced from bacterial decomposition. The build-up of methane in landfill liners should be avoided due to its combustible nature.

Geosynthetic clay liners have been proposed as suitable cover materials for landfills. The landfill cover may not be fully saturated, depending on environmental factors.

Compacted bentonites are a constituent component of geosynthetic clay liners (Petrov et al., 1997; Lee and Shackelford, 2005). The hydraulic conductivity of geosynthetic clay liners has been widely investigated in the context of landfill liners. The gas permeability of unsaturated compacted bentonite has attracted limited attention. Didier et al. (2000) determined the gas permeability of compacted bentonites by nitrogen gas at water contents between 46 - 73%. An approximately linear relationship between air content and gas permeability was observed. Bouazza et al. (2004) established the effect of wet-dry cycles on the gas permeability of geosynthetic clay liners when saturated with de-ionised water and electrolyte solutions.

The gas permeability of compacted bentonites has been reported in literature for increasing water contents (Didier et al., 2000; Bouazza, 2002; Bouazza and Vangpaisal, 2003). A number of other aspects, including electrolyte concentration, have been considered. The gas permeability of compacted bentonites at low water contents has not been reported in the literature.

The objective of the chapter was to determine the gas permeability of compacted bentonite at the air-dry water content (8%). The gas permeabilities of compacted bentonite specimens were determined from the flow of nitrogen gas. An existing device commonly used for determining the gas permeability of concrete specimen was modified to allow for testing of compacted bentonite specimens. The pressure within the device was increased to the starting pressure, and the outlet valve was open. The rate of pressure reduction, the pressure decay within the device, was monitored regularly. The rate of pressure decay was plotted to produce pressure-decay curves for each of the initial pressures considered, for a range of compaction dry densities.

The gas permeabilities of the specimens were calculated from Darcy's law. The relationship between gas permeability and compaction dry density at the air-dry water content was established. The relationship between the gas permeability and hydraulic conductivity of the bentonite specimen was assessed.

7.2 Experimental programme

7.2.1 Specimen preparation

Compacted MX80 bentonite specimens were prepared with increasing compaction dry densities. The targeted and actual compaction dry densities of the specimens considered in the current study are presented in Table 7.1. Post-compaction, a 7.5 mm hole was drilled through the length of the specimen, described in Subsection 3.6.3.

Table 7.1 - Targeted and actual dry densities of the compacted specimens used in the study

Specimen	Targeted dry density (Mg/m^3)	Actual dry density (Mg/m^3)
1	1.400	1.391
2	1.500	1.489
3	1.550	1.536
4	1.600	1.605
5	1.650	1.637
6	1.700	1.692
7	1.750	1.739
8	1.850	1.832

Dry densities lower than 1.3 Mg/m^3 were not considered as the integrity of the compacted MX80 bentonite specimen could not be maintained while the central hole was drilled. Specimens prepared between 1.3 and 1.4 Mg/m^3 could not be tested as it was not possible to seal the top and bottom surfaces with petroleum jelly.

7.2.2 Testing programme

The testing procedure is provided in detail in Chapter 3. Prior to the start of each gas permeability test, the pressure within the gas permeability cell and the connecting gas reservoir was raised to the required starting pressure. The gas permeability experimental set-up considered during this study had not been previously used to determine the gas permeability of compacted bentonite, and so the range of initial pressures which could be considered was unknown. The initial pressure employed when determining the gas permeability of cast concrete specimens was 1 MPa (Gardner, 2005).

In the current study, the initial pressure was increased in a step-wise manner for each gas permeability test. Multiple tests were carried out on each specimen. The initial starting pressure considered was 100 kPa. The tests were carried out until the pressure in the gas permeability cell had reduced and stabilised. The lid was replaced and the next test was conducted at 200 kPa. The initial pressure was increased by 100 kPa for each test. The maximum initial pressure considered was 1 MPa. After each test was terminated, the lid of the gas permeability cell was removed and the specimen was inspected for cracks. If cracks were observed in the specimen, no further tests were conducted.

7.3 Determination of gas permeability from pressure-decay curves

7.3.1 Procedure for calculating gas permeability

The gas permeability can be determined from Darcy's law (Bouazza and Vangpaisal, 2003), assuming that steady state flow is present. However, in the case of the gas permeability tests carried out in this study, the specimen was not in steady state conditions.

For this study, it has been assumed that the rate of mass loss, and hence volume flow rate, are constant (as would be the case for steady state flow) at any instant, and so the gas permeability may be estimated for pressure intervals.

When the outflow valve on the gas permeability cell was opened, the gas pressure within the gas permeability cell decreased. The rate of pressure decrease in the gas permeability cell over time is referred to as the pressure decay curve. Pressure decay curves were obtained for each gas permeability test undertaken.

Selected parameters were required to determine the gas permeability following the procedure described by Gardner (2005). The half time of pressure decay ($t^{1/2}$) is the time taken for the pressure inside the gas permeability cell to reduce to half of the starting value (in minutes). The gradient of the initial pressure decay (a) was determined from the plot of log pressure against time. These parameters are shown schematically in Figure 7.1.

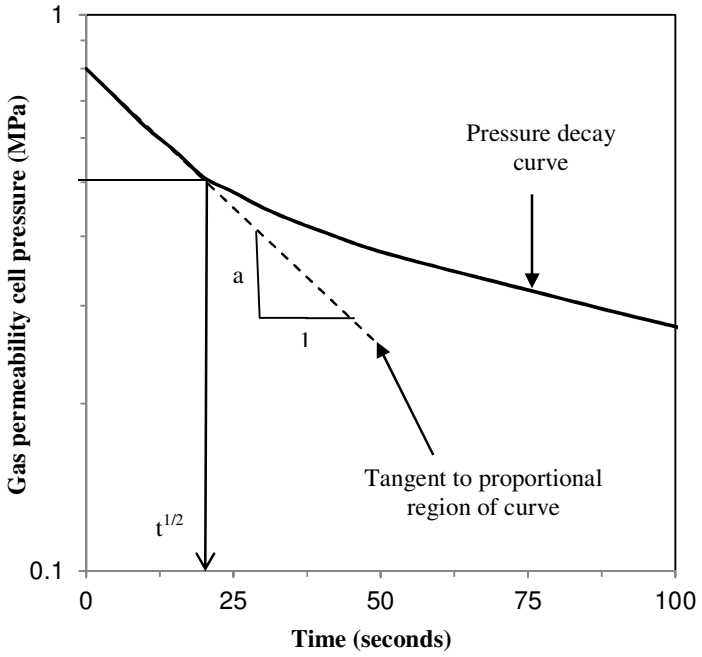

Figure 7.1 - Selected parameters from the pressure decay curves required to determine gas permeability

Martin (1986) carried out a series of tests to observe the pressure decay curve for concrete specimens. It was shown that the emperical relationship between relative pressure and time could be approximated by

$$p = 10^{1-at} \tag{7.1}$$

where p is the relative pressure (in bar), a is the initial gradient of the pressure-decay curve and t is the time (in seconds).

Using the ideal gas law, it can be shown that a loss of pressure from the system can lead to a loss of mass. In order to determine the rate of pressure loss from the system, the first order derivative of pressure, i.e. the rate of pressure decrease with respect to time, is required.

Firstly, the empirical relationship proposed by Martin (1986) required modification, to convert the pressure from bar to Pa. The relative pressure was also modified to give the absolute pressure. Equation (7.2) shows the modified empirical relationship for the pressure decay curves.

$$P = 10^{6.04-at} \tag{7.2}$$

where P is the absolute pressure (in Pa), a is the initial gradient of the pressure decay curve, and t is the time (in seconds).

To determine the rate of pressure decay, the modified empirical relationship between pressure and time shown in Equation (7.2) was differentiated. The first order derivative of Equation (7.2) with respect to time is stated in Equation (7.3).

$$\frac{dP}{dt} = -10^{6.04-at} a \ln 10 \tag{7.3}$$

The gas permeability tests carried out by Martin (1986) were all undertaken with an initial pressure of 1MPa (10 bar). As such, the rate of pressure decay stated in Equation (7.3) is valid for tests with an initial pressure of 1MPa. Following the form of the relationship stated by Martin (1986), the generalised empirical pressure decay relationships were obtained for the initial pressures considered during the experimental study;

$$P = 10^{(\log_{10} P_1)-at} \tag{7.4}$$

where P_1 is the absolute initial pressure within the gas reservoir, in Pa. The generalised rate of pressure decay was determined from Equation (7.4) to be;

$$P = -10^{(\log_{10} P_i) - at} aln10 \tag{7.5}$$

For each test, once the rate of pressure decay had been determined, the rate of mass loss was calculated from the ideal gas law. The ideal gas law is given as

$$Pv = mRT \tag{7.6}$$

where P is the gas pressure, v and m are the volume and mass of gas respectively, R is the individual gas constant (assumed to be 296.8 J/kg°K for nitrogen) and T is the temperature.

The volume of nitrogen gas contained with the gas permeability cell was determined as the sum of the volumes of each of the components of the testing apparatus. This included the cell itself, the gas reservoir, and the connecting pipework. The volume of nitrogen gas was calculated as

$$v_g = v_R + v_{ec} + v_p - v_b \tag{7.7}$$

where v_g is the volume of nitrogen gas lost during the gas permeability tests, v_R is the volume of the gas reservoir, v_{ec} is the volume of the empty gas permeability cell, v_p is the volume of the pipes connecting the gas reservoir to the gas permeability cell, and v_b is the volume of the compacted bentonite specimen.

In this study, v_R was determined to be 1.86×10^{-3} m^3. v_{ec} was calculated as 1.65×10^{-3} m^3. v_p was determined to be 1.62×10^{-5} m^3. v_b was 1.37×10^{-3} m^3. v_g was therefore calculated to be 2.15×10^{-3} m^3.

The volume of nitrogen gas present within the apparatus during each gas permeability test was 2.15×10^{-3} m^3. The individual gas constant and the temperature were assumed to remain constant through the experimental programme. The pressure decay during the gas permeability test resulted in a corresponding mass reduction. It follows therefore that the pressure decay rate was proportional to the rate of mass loss from the system, as shown in Equation (7.8).

$$v\frac{dP}{dt} = RT\frac{dm}{dt} \tag{7.8}$$

where $\frac{dm}{dt}$ is the mass loss rate during the gas permeability tests.

For each gas permeability test undertaken, the parameters a and $t^{1/2}$ were determined from the pressure-time relationship, as shown in Figure 7.1. The rate of pressure decay was then calculated from Equation (7.5), using a and $t^{1/2}$. The subsequent rate of mass loss was calculated from Equation (7.8). The flow rate of nitrogen gas through the specimen i.e. the volumetic rate at which gas volume left the system - was then calculated from Equation (7.9), using the density of nitrogen gas at the outlet (i.e at atmospheric pressure). The volume flow rate of gas through the specimen was calculated as

$$\frac{dm}{dt} = \rho\frac{dV}{dt} \tag{7.9}$$

where $\frac{dV}{dt}$ is the gas flow rate through the specimen, and ρ is the density of nitrogen gas.

Darcy's law describes laminar, viscous flow which is dependent on the properties of the permeating fluid. Dhir and Byars (1993) stated the following derivation of Darcy's Law to determine the gas permeability, which is independent of fluid properties

$$\frac{Q}{A} = -\frac{K}{\mu}\frac{dP}{dL} \tag{7.10}$$

where A is the cross-sectional area perpendicular to the direction of flow, K is the gas permeability, μ is the viscosity and $\frac{dP}{dL}$ is the pressure gradient in the direction of flow.

The modified version of Darcy's law stated in Equation (7.10) was solved by separation of the variables. The pressure differential was assumed to be the difference between the absolute inlet pressure to the specimen (the pressure within the gas reservoir) and the absolute outlet pressure (i.e. atmospheric). The gas permeability was found to be

$$K = \frac{Q\mu L}{A(P_1 - P_2)} \tag{7.11}$$

where L is the flow length, P_1 is the absolute inlet pressure and P_2 is the absolute outlet pressure .

Equation (7.11) is valid for steady state conditions. However, as the gas permeability tests were not carried out in steady state conditions, the volume flow rate Q varies with pressure P, due to the compressible nature of gas. At any given point,

$$PQ = P_1Q_1 = P_2Q_2 = \text{constant} = P_mQ_m, \quad (7.12)$$

where Q_1 is the volume flow rate at the inlet of the cell, P_2 is the absolute pressure at the outlet of the cell, Q_2 is the volume flow rate at the outlet of the cell, P_m is the mean pressure and Q_m is the mean volume flow rate. P_1, Q_1, P_2, Q_2 and P are known at any pressure interval, therefore substituting for Q from Equation (7.12) in Equation (7.10) and integrating, the gas permeability was expressed as

$$K = \frac{2\mu L P_2 Q_2}{A(P_1^2 - P_2^2)} \quad (7.13)$$

where all symbols have the meanings stated previously. In the current study, the volume flow rate at the outlet (Q_2) is assumed to be $\frac{dV}{dt}$, as determined from Equation (7.9).

7.3.2. Calculation of gas permeability in the current study

Gas permeability tests were carried out across a range of compaction dry densities. The pressure decay curve for each test was established. The half-life of pressure decay ($t^{1/2}$) and the gradient (a) were calculated from the pressure decay curves.

The pressure interval chosen for this work was from the initial pressure reading until the relative half pressure was reached. The pressure decay rate was calculated from Equation (7.5), based on the initial starting pressure of the test. The rate of mass loss was calculated from Equation (7.8). Once the rate of mass loss was determined, the gas permeability was calculated from Equation (7.13). The outlet pressure from the gas permeability cell, P_2, was

assumed to be atmospheric pressure. The gas permeability was calculated at the outflow of the gas permeability cell, at which the density of nitrogen was assumed to be 1.2506 kg/m^3. The flow length perpendicular to the direction of flow was calculated to be 0.0453 m. The cross-sectional area was calculated at the midway diameter of the specimen as 2.29 x 10^{-4} m^2.

The gas permeability tests carried out on the compacted MX80 bentonite specimens are presented in Table 7.2. The half time ($t^{1/2}$) and gradient of pressure decay (a) determined from the pressure decay curves are shown. The calculated rate of mass loss and volume flow rate are stated. The gas permeability calculated from each test is also presented.

Table 7.2 - Calculation of gas permeability from pressure decay curves

Dry density (Mg/m^3)	*Absolute starting pressure (MPa)*	*Half time of decay (s)*	*Gradient a*	*Rate of pressure loss x 10^4 (Pa/s)*	*Rate of mass loss x10^{-3} (kg/s)*	*Volume flow rate x10^{-3} (m^3/s)*	*Gas permeability K x10^{-13} (m^2)*
1.391	0.201	1.9	0.10	4.47	1.11	0.88	75.4
	0.301	1.3	0.17	9.44	2.33	1.87	84.9
	0.401	1.1	0.21	14.23	3.52	2.81	80.1
	0.501	1.0	0.28	20.34	5.03	4.02	78.6
	0.601	0.9	0.31	26.32	6.51	5.20	74.2
1.489	0.301	3.2	0.05	2.40	0.59	0.47	40.4
	0.401	3.1	0.06	3.61	0.89	0.71	32.5
	0.501	3.0	0.09	5.58	1.38	1.10	31.4
	0.601	2.4	0.10	7.96	1.97	1.57	30.8
	0.701	2.2	0.13	10.86	2.69	2.15	30.6
	0.901	2.0	0.16	15.89	3.93	3.14	26.9
1.536	0.201	5.8	0.02	1.06	0.26	0.21	17.9
	0.301	5.4	0.02	1.44	0.36	0.28	13.0
	0.401	3.8	0.05	3.72	0.92	0.74	21.0
	0.501	3.1	0.06	5.41	1.34	1.07	20.9
	0.601	2.8	0.08	7.71	1.91	1.52	21.7
1.583	0.301	13.1	0.020	0.76	0.19	0.15	12.8
	0.401	11.1	0.018	1.05	0.26	0.21	9.4
	0.501	8.9	0.020	1.53	0.38	0.30	8.6
	0.601	7.0	0.025	2.31	0.57	0.46	8.9
	0.701	6.4	0.028	2.99	0.74	0.59	8.4

Table 7.2 - Calculation of gas permeability from pressure decay curves (continued)

Dry density (Mg/m^3)	*Absolute starting pressure (MPa)*	*Half time of decay (s)*	*Gradient a*	*Rate of pressure loss x 10^4 (Pa/s)*	*Rate of mass loss $x10^{-3}$ (kg/s)*	*Volume flow rate $x10^{-3}$ (m^3/s)*	*Gas permeability K $x10^{-13}$ (m^2)*
	0.401	12.2	0.008	0.44	0.11	0.09	7.5
	0.501	8.9	0.012	0.87	0.21	0.17	7.8
1.615	0.601	9.2	0.016	1.32	0.33	0.26	7.4
	0.701	6.7	0.022	2.17	0.54	0.43	8.4
	0.901	6.0	0.037	3.58	0.89	0.71	10.1
	0.301	16.0	0.011	0.51	0.13	0.10	8.6
	0.401	12.2	0.014	0.87	0.22	0.17	7.9
	0.501	9.8	0.016	1.29	0.32	0.25	7.2
1.677	0.601	8.9	0.023	1.99	0.49	0.39	7.7
	0.701	8.2	0.028	2.66	0.66	0.53	7.5
	0.801	7.0	0.037	4.23	1.05	0.84	7.2
	0.301	21.9	0.008	0.37	0.09	0.07	6.2
	0.501	15.6	0.013	1.13	0.28	0.22	4.4
1.739	0.901	9.4	0.020	2.69	0.67	0.53	4.6
	1.10	11.1	0.031	3.56	0.88	0.70	4.0
	0.301	29.1	0.006	0.28	0.07	0.05	4.7
	0.401	31.1	0.007	0.39	0.10	0.08	3.5
1.832	0.501	36.7	0.007	0.45	0.11	0.09	2.5
	0.701	33.3	0.008	0.70	0.17	0.14	2.0
	0.901	32.7	0.009	0.95	0.23	0.19	1.6

Several factors were observed to affect the half time of pressure decay. Firstly, at higher compaction dry densities, the half time of decay increased. At the highest dry densities considered (1.832 Mg/m^3), the half time of decay was an order of magnitude greater than that observed in the case of the specimen with compaction dry density of 1.391 Mg/m^3. Secondly, the half time of decay reduced as the starting pressure of the test increased. The half time of decay was found to halve from the lowest to the highest starting pressure applied to the specimen.

The pressure decay rate, the rate of mass loss and the volume flow rate were all observed to decrease as the dry density of the specimen increased, but to increase as the initial starting pressure of the test was increased.

The relationship between the compaction dry density of the specimen and the calculated gas permeability is shown in Figure 7.2. The relationship between the void ratio of the specimen and the gas permeability is presented in Figure 7.3.

Gas permeability values between 8.5×10^{-12} and 1.6×10^{-13} m^2 were determined in the current study. The gas permeability was observed to decrease as the compaction dry density increased, and to increase as the void ratio of the specimen increased.

The determination of gas permeability of compacted bentonite at the low water contents is scarce in literature. Bouazza and Vangpaisal (2003) reported that the gas permeability determined for water contents of less than 20% was about 10^{-11} m^2. The compaction dry densities of the samples tested were at the lower end of the range

considered in the current study; nevertheless, the gas permeability values determined in this study are comparable.

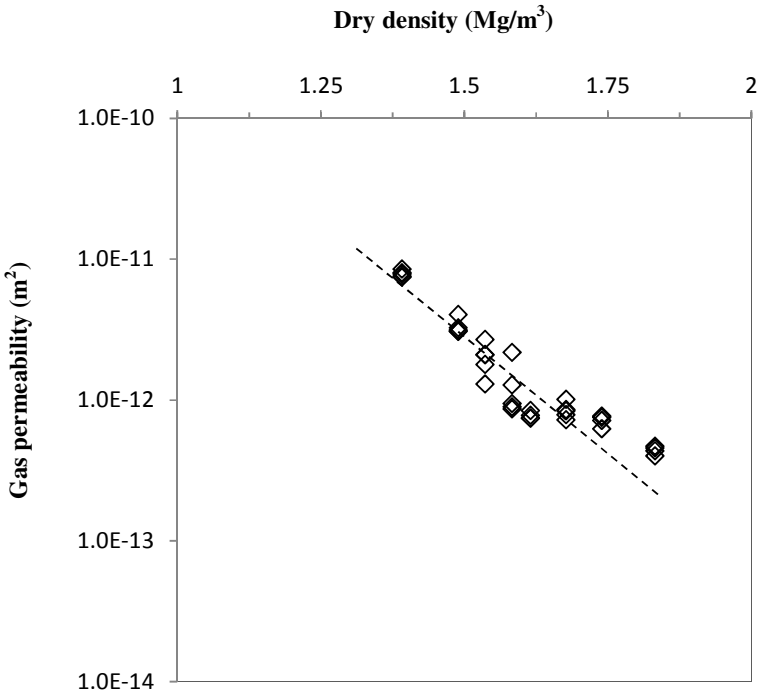

Figure 7.2 - The relationship between compaction dry density and gas permeability for compacted MX80 bentonite specimens at the air-dry water content

Some scatter was observed in the gas permeability calculated for each compacted MX80 specimen. This is thought to be due to gas slippage, a non-Darcian effect associated with gas flow in porous media (Rushing et al., 2004).

Klinkenburg (1941) reported the existence of the layer of gas molecules adjacent to the pore wall where molecule-wall collisions occurred. The increased collisions can cause increased molecule acceleration. Slippage can be significant when determining the gas

permeability by standard laboratory tests (Eates and Fulton, 1956). The correction of gas flow velocities to account for slippage was not within the scope of this study.

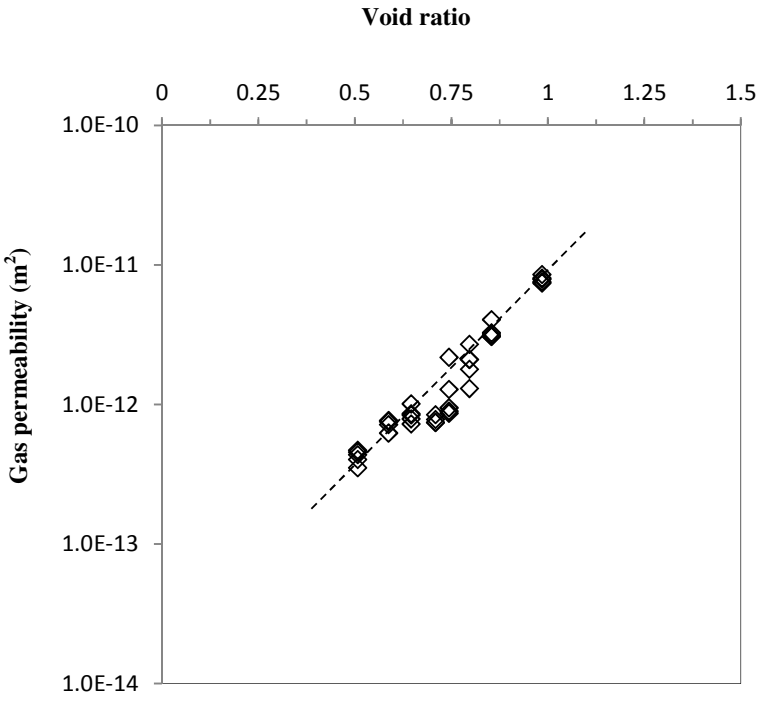

Figure 7.3 - The relationship between void ratio and gas permeability for compacted MX80 bentonite specimens at the air-dry water content

7.4 Determination of the hydraulic conductivity from the gas permeability

The gas permeability *K* determined in the current study provides a measure of the permeability of a porous material which is independent of the type of permeant. A theoretical relationship exists between K and the hydraulic conductivity, *k*, such that the ideal hydraulic conductivity of a material could be calculated. The relationship between the gas permeability and the hydraulic conductivity is provided in Equation (7.14).

$$K = k\frac{\mu}{\rho} \quad (7.14)$$

where k is the hydraulic conductivity, μ is the viscosity of water and ρ is the density of the water. The viscosity and density of water were assumed to be 0.00102 Pa.s and 977 kg/m^3 respectively (Handbook of Chemistry and Physics, 2006).

The gas permeabilities determined in this study were between 10^{-11} and 10^{-13} m^2. Using Equation (7.14), the ideal hydraulic conductivities calculated were found to range between 10^{-6} and 10^{-7} m/s.

The calculated values of hydraulic conductivity were found to be significantly greater than those determined previously in Chapter 5. Within the bentonite microstructure, discrete hydrate layers are absorbed to the platelet surfaces during hydration (Likos, 2004). The water molecules within these layers are tightly held to the platelet surface (van Olphen, 1963), leading to an increased viscosity within the immediate proximity of the platelet (Pusch and Yong, 2005).

Given the physico-chemical interactions taking place within the bentonite microstructure, it would be anticipated that flow through the bentonite would be retarded, and therefore the hydraulic conductivity would be expected to be reduced. The hydraulic conductivities calculated from the gas permeabilities determined in this study support this, as they are significantly higher than those determined experimentally. It is therefore not considered appropriate to determine the hydraulic conductivity of bentonite from the gas permeability.

7.5 Concluding remarks

Geosynthetic clay liners, comprised of compacted bentonite and geosynthetic layers, have been proposed as suitable materials for landfill covers and liners. During the lifetime of the landfill, gases will be generated due to bacterial degradation of the waste material. Methane is one such gas produced. The gas permeability of the landfill cover should prevent the build-up of methane in the landfill.

In the current study, the gas permeability of compacted bentonite at lower water contents was determined using nitrogen gas. Specimens were prepared with compaction dry densities between 1.39 and 1.83 Mg/m^3. A number of gas permeability tests were carried out on each specimen. The starting pressure of the test was increased in a step-wise manner until pressure cracks appeared in the compacted specimens. The maximum starting pressure considered as 1 MPa.

Pressure decay curves were produced from the gas permeability tests. The half time of pressure decay and the gradient of the time-log pressure behaviour were determined. The pressure decay rate was determined. The rate of mass loss and the volume flow rate were calculated from the rate of pressure decay. The gas permeabilities of compacted bentonite specimens were established.

The half time of pressure decay was observed to increase as the dry density of the specimen increased. A decrease in the half time of pressure decay was observed as the starting pressure of the test was increased. The gas permeabilities were observed to decrease as the compacted dry density of the specimens increased. Some scatter was

observed for the different gas permeability tests. This was attributed to the effect of gas slippage.

An attempt was made to use the gas permeabilities to calculate the ideal hydraulic conductivities of compacted bentonite. The hydraulic conductivity values determined were significantly greater than those determined experimentally. It was concluded that due to the physico-chemical effects within the bentonite water system, it was not appropriate to use the gas permeability to determine the hydraulic conductivity.

CHAPTER 8

ASSESSMENT OF THE HYDRAULIC CONDUCTIVITY OF COMPACTED SATURATED BENTONITE FROM VARIOUS MODELS

8.1 Introduction

The saturated hydraulic conductivity of a soil can be used to determine the flow of fluid under a hydraulic gradient. For low permeability soils, including compacted saturated bentonite, the experimental determination of hydraulic conductivity is time consuming. A number of experimental limitations can influence the measured hydraulic conductivity of the compacted saturated bentonites (Dixon et al., 1999).

The hydraulic conductivity of compacted saturated bentonite has been reported to be influenced by a number of factors, including compaction dry density, temperature, montmorillonite content, type of bulk fluid and predominant cation type. A review of the factors influencing the measured hydraulic conductivity was presented in Chapter 2.

Various models have been used to assess the hydraulic conductivity of compacted saturated bentonite. Olsen (1962) proposed the Cluster model to account for flow through the micro- and macro-pores of compacted saturated bentonite. This method was modified by Achari et al. (1999), using Gouy-Chapman diffuse double layer theory. Chapius and Aubertin (2003) reviewed the applicability of the Kozeny-Carman model for a number of soils previously reported in literature. Komine and Ogata (1999) and Komine (2004) proposed a model for calculating hydraulic conductivity in compacted bentonite based the swelling potential. The hydraulic conductivity of compacted bentonite can also be determined from the compressibility behaviour, as considered previously in this study.

The objectives of the chapter are threefold. Firstly, existing models will be used to determine the saturated hydraulic conductivity of compacted MX80 bentonite. Secondly, a new saturated hydraulic conductivity model will be proposed. Finally, the existing and proposed models will be compared with the experimentally determined saturated hydraulic conductivity.

In this chapter, existing hydraulic conductivity models are presented. These are the Kozeny-Carman model and the parallel plate model proposed by Komine (2004). The saturated hydraulic conductivity model proposed in this study in presented. The parameters of compacted MX80 bentonite required for each of these models are stated. The calculated

hydraulic conductivity behaviour is compared with that determined experimentally. Conclusions are drawn on the accuracy of the models in calculating the saturated hydraulic conductivity behaviour.

8.2 Models available to assess the hydraulic conductivity of compacted saturated bentonite

The models used to determine the saturated hydraulic conductivity of compacted bentonite in the current study are presented here. A review of the implementation of these models reported in literature has been presented previously.

8.2.1 Kozeny-Carman model

The Kozeny-Carman model is derived from Poisuelle's Law of flow through a bundle of parallel flow tubes (Mitchell and Soga, 2005). The model was presented by Kozeny (1927) and later modified by Carman (1937; 1956). The Kozeny-Carman equation is stated as

$$k_h = \left(\frac{\gamma_p}{\mu_p}\right)\frac{1}{k_0 T^2 S_0^2}\left(\frac{e^3}{1+e}\right) \tag{8.1}$$

where k_h is the hydraulic conductivity, γ_p is the density of the permeating fluid, μ_p is the viscosity of the permeating fluid, S_0 is the wetting surface per unit volume of particles and e is the void ratio.

8.2.2 Hydraulic conductivity determined from the model proposed by Komine (2004)

The determination of hydraulic conductivity from Komine (2004)'s approach is modified from the method proposed by Komine and Ogata (1999). The swelling strain of montmorillonite was stated as

$$\varepsilon_{sv}^{*} = \frac{V_v + V_{sw}}{V_m} \tag{8.2}$$

where ε_{sv}* is the swelling strain of montmorillonite, V_v is the volume of voids within the bentonite, V_{sw} is the swelling deformation under constant vertical pressure and V_m is the volume of montmorillonite within the bentonite.

Komine (2004) calculated the swelling strain of montmorillonite (ε_{sv}*) from the increase in swollen inter-platelet distance. The half distance between two montmorillonite platelets for each exchangeable cation species considered was determined from

$$d_i = \frac{\varepsilon_{sv}^{*}}{100}\{t + (R_{ion})_i\} + (R_{ion})_i \tag{8.3}$$

where d_i is the half distance between two platelets for exchangeable cation i (in m), t is the thickness of the montmorillonite platelet (in m) and R_{ion} is the non-hydrated radius of the exchangeable cation (in m).

The hydraulic conductivity was determined for each cation type considered from Equation (8.4). The weighted average of the individual hydraulic conductivities was calculated from Equation (8.5).

$$k_i = \frac{\gamma_{aw}}{12\mu_{aw}}(2d_i)^2 \quad (8.4)$$

$$k = \frac{1}{B}\sum_i [B_i k_i] \quad (8.5)$$

where k_i is the hydraulic conductivity determined for each exchangeable cation species (in m/s), γ_{aw} is the density of adsorbed water within the montmorillonite platelets (in Pa/m), μ_{aw} is the viscosity of adsorbed water within the montmorillonite platelets (in Pa.s), B is the cation exchange capacity (in meq/100g) and B_i is the individual exchange capacities for the exchangeable cation species considered (in meq/100g).

The ratio between density (γ_{aw}) and viscosity (μ_{aw}) of adsorbed water was calculated

$$\frac{\gamma_{fw}}{\mu_{fw}} = \frac{1}{R}\frac{\gamma_{aw}}{\mu_{aw}} \quad (8.6)$$

where R is an empirical factor, γ_{fw} is the density of free water (in Pa/m) and μ_{aw} is the viscosity of free water (in Pa.s). R has been reported as 14 for silty sands and 79 for bentonite (Sato, 1971), based on empirical fitting of previous experimental results. Both14 and 79 have been included in the calculations presented by Komine (2004).

8.2.3 Hydraulic model proposed in the current study

When compacted bentonite is allowed to saturated, diffuse double layers form between individual clay platelets (van Olphen, 1963; Tripathy et al., 2004; Mitchell and Soga, 2005). The development of diffuse double layers is accompanied by a subdivision of

platelet stacks (Saiyouri et al., 2004). At high water contents, the number of unit layers per unit stack in sodium bentonite was reported to reduce from 350 to 10 (Saiyouri et al., 2004). The increased micro-porosity in compacted saturated bentonite is accommodated by a reduction in the macro-porosity. Bourg et al. (2006) reported that the macro-porosity in compacted bentonite is fully eliminated as the compaction dry density is increased to 1.8 Mg/m^3. It was assumed in the model proposed in this study that the flow in compacted saturated bentonites predominantly occurs between platelets, as the flow channels through macro-pores are not present due to the degree of compaction.

Parallel plate flow was used to model the hydraulic conductivity of compacted saturated bentonites. Parallel plate flow is considered to be appropriate for modelling flow through compacted bentonite as the clay platelets are infinite in the *a* and *b* directions (Grim, 1953). The *c* spacing between platelet layers can be determined from the degree of saturation of the bentonite and the inter-platelet spacings determined for discrete hydrate layers (Saiyouri et al., 2000). The velocity profile between two parallel plates is shown in Figure 8.1.

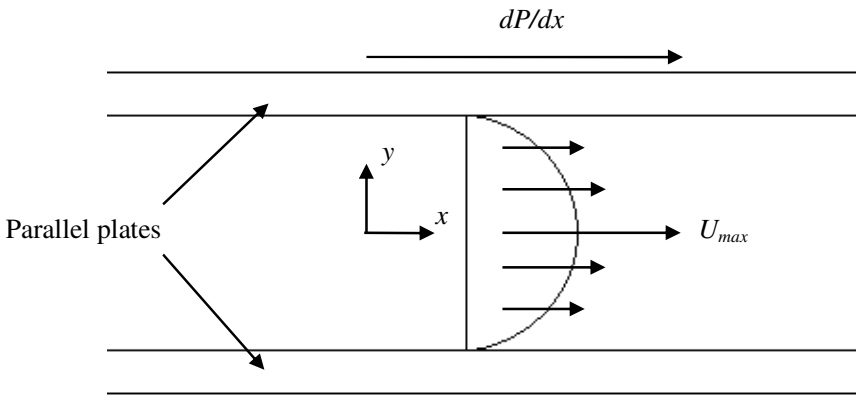

Figure 8.1 - Velocity flow profile between parallel plates (from Nalluri and Featherstone, 2001)

The velocity profile between parallel plates is determined from Equation (8.7) (Nalluri and Featherstone, 2001). The maximum velocity is found at the midpoint between the two plates.

$$\frac{\partial P}{\partial x} = \mu \frac{d^2 U}{dy^2} \tag{8.7}$$

where *dp/dx* is the pressure gradient, μ is the viscosity of the fluid and *U* is the velocity.

The state of water in the interlayer pores is complex. Fixed hydrate layers are adsorbed to the platelet surface due to crystalline swelling (Likos, 2004). Up to 4 hydrate layers have been reported at being present between platelets prior to the formation of diffuse double layers. The mobility of the first hydrate layer in sodium bentonite was stated as 30% (Kemper et al., 1964).

Pusch and Yong (2005) presented the water viscosity at increasing distances from the platelet surface. This is reproduced in Figure 8.2.

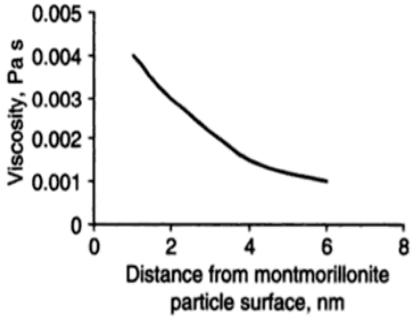

Figure 8.2 - Viscosity of pore water at increasing distance from the platelet surface (from Pusch and Yong, 2005)

The decrease in the pore water viscosity observed from Figure 8.2 was linearly approximated up to distances of 4 nm from the platelet surface was approximated by Equation (8.8).

$$\mu = 0.005 - 909091y \tag{8.8}$$

where μ is the pore water viscosity (in Pa.s), and y is the distance from the montmorillonite surface (in m).

The velocity profile was determined between the platelet surface and the half platelet spacing distance, d. The viscosity approximated from Equation (8.8) was substituted into Equation (8.7). The velocity profile was determined by integrating Equation (8.7) twice with respect to y, and rearranging for U. Using the known boundary conditions that the velocity at the platelet surface is zero, the velocity profile (between $y = 0$ and $y = d$) was calculated as

$$U = 200\frac{dP}{dx}\left((y + 5.5x10^{-9})\ln(0.005 - 909091y) - y\right) + C_1 y + C_2 \tag{8.9}$$

$$C_1 = \frac{dP}{dx}\left(\frac{1}{2(0.005-909091d)} - 200\left((d + 5.5x10^{-9})\ln(0.005 - 909091d) - d + 2.91x10^{-8}\right)\right) \tag{8.10}$$

$$C_2 = 3.205\frac{dP}{dx} \tag{8.11}$$

where dP/dx is the pressure gradient and d is the half platelet separation distance (in m)

The average velocity between the two platelets (u) was calculated from Equation (8.12).

$$u = \frac{\int_0^d U dy}{d} \quad (8.12)$$

Using Darcy's law, the hydraulic conductivity was calculated from

$$k = \frac{u}{i} \quad (8.13)$$

where k is the hydraulic conductivity, u is the average fluid velocity and i is the hydraulic gradient.

8.3 Calculation of hydraulic conductivity from the various models

8.3.1 Calculation of hydraulic conductivity from the Kozeny-Carman model

The Kozeny-Carman model describes the relationship between hydraulic conductivity and void ratio. In the current study, the hydraulic conductivity was calculated at assumed void ratios. The density of water at 298°K was assumed to be 977 kg/m^3 (Handbook of Chemistry and Physics, 2006). The viscosity of water at 298°K was assumed to be 0.00102 Pa.s (Handbook of Chemistry and Physics, 2006).

Carman (1956) reported that the k_0T^2 is equal to 4.8 ± 0.3 for uniform spheres. Mitchell and Soga (2005) stated that k_0 is equal to 2.5, and T is equal to √2. In the current study, k_0T^2 was assumed to be 5, taking the values reported by Mitchell and Soga (2005). The wetted surface area, S_0, was calculated from the specific surface area of the bentonite

determined previously. It was assumed that all platelet surfaces within the bentonite had been fully hydrated. The specific surface area of the MX80 was determined to be 640 m^2/g.

The Kozeny-Carman model has been used by a number of authors. Dixon et al. (1999) reported good agreement between the Kozeny-Carman model and the experimental hydraulic conductivity determined for bentonite. Schaap and Lebron (2001) stated that only macroscopic data was necessary to predict the hydraulic conductivity of soils using the Kozeny-Carman model. Chapius and Aubertin (2003) reported that the Kozeny-Carman model can be used with confidence for hydraulic conductivity values between 10^{-1} and 10^{-11} m/s. The hydraulic conductivities determined experimentally were observed to be between 1/3 and 3 times that calculated from the Kozeny-Carman model (Chapius and Aubertin, 2003). Carrier (2003) stated a number of limitations of the Kozeny-Carman model. In fine grain soils, such as bentonites, the physio-chemical forces are not taken into account.

8.3.2 Calculation of hydraulic conductivity from Komine (2004)'s approach

The hydraulic conductivity was calculated from Komine (2004)'s approach using the swelling potentials of the five compacted bentonite specimens considered during consolidation. The swelling potentials of the specimens were assumed. The parameters used in determining the hydraulic conductivity from Komine (2004)'s model are shown in Table 8.1. The density and viscosity of water was that assumed previously.

Table 8.1 - Properties used for calculating the hydraulic conductivity from Komine (2004)'s model

Parameter	Value	Comments
Thickness of platelet (t)	0.96 nm	
Montmorillonite content (C_m)	76 %	
Non-hydrated radius of calcium ion	0.100 nm	From Alther (2004)
Non-hydrated radius of magnesium ion	0.072 nm	
Non-hydrated radius of potassium ion	0.138 nm	
Non-hydrated radius of sodium ion	0.102 nm	
Calcium exchange capacity	31.9	
Magnesium exchange capacity	9.1	
Potassium exchange capacity	1.6	
Sodium exchange capacity	45.7	
Total cation exchange capacity	88.3	
R	14, 79	From Komine (2004)

The value of *R* has been reported as 79 for bentonite clay and 14 for silty clay (Sato, 1971). Komine (2004) considered both 14 and 79 when determining the hydraulic conductivity of compacted bentonite. Komine (2004) reported good agreement between the experimental values obtained with the hydraulic conductivity calculated using $R = 79$.The value of *R* applied is an empirical correction factor for the hydraulic conductivity calculated. Significant differences in hydraulic conductivity were calculated based on the two values considered.

8.3.3 Calculation of hydraulic conductivity from the model proposed in this study

The hydraulic conductivity calculated for a range of void ratios using the proposed model. For each void ratio assumed, Equation (8.14) was used to calculate *d* in each case.

$$e = G\gamma_w Sd \tag{8.14}$$

where *G* is the specific gravity of bentonite solids, *S* is the specific surface area and *d* is the half-distance spacing between platelets.

Once *d* was determined for each void ratio, the velocity profile between the platelets was determined from Equation (8.9). The average velocity, *u*, was then determined from Equation (8.12), and the hydraulic conductivity for each void ratio was determined from Equation (8.13).

The proposed model does not consider the effect of interacting diffuse double layers on the viscosity of fluid. The relationship between viscosity and distance from the platelet surface reported by Pusch and Yong (2005) did not consider a secondary platelet and the influence of the platelet on the viscosity. It was assumed in the current model that the viscosity of water between the platelet surface and the midway distance was that reported by Pusch and Yong (2005). It would be expected the viscosity would be greater if these additional forces were considered, which would reduce the calculated hydraulic conductivity.

An example calculation is given here. The void ratio of the bentonite was determined to be 0.88. Using Equation (8.14), the interplatelet spacing, d, was found to be 5 x 10^{-10} m.

The velocity profile of flow through the inter-platelet space was determined from Equation (8.9) as a function of y, the distance from the platelet surface. This relationship was then integrated to determine the average velocity within the inter-platelet region from Equation (8.2). The average velocity was determined to be 2.17 x 10^{-8} m/s. The average hydraulic conductivity was determined from Equation (8.3) and found to be 4.6 x 10^{-12} m/s.

8.4 Comparison of the models used to assess the hydraulic conductivity of compacted saturated bentonite

The saturated hydraulic conductivity was calculated for the models considered in this study. The saturated hydraulic conductivity was calculated for void ratios between 0 and 4. For the Kozeny-Carman model, and the model proposed in this study, the hydraulic conductivity was calculated for an assumed void ratio. For Komine (2004)'s method, the hydraulic conductivity was calculated from the previously determined swelling potential.

Figure 8.3 shows the comparison between the hydraulic conductivity models used in this study and the saturated hydraulic conductivity determined experimentally. The results obtained through hydraulic conductivity tests and from the compressibility behaviour of the compacted bentonite specimens are shown. The models considered in this study shown varying agreement with the experimental values determined.

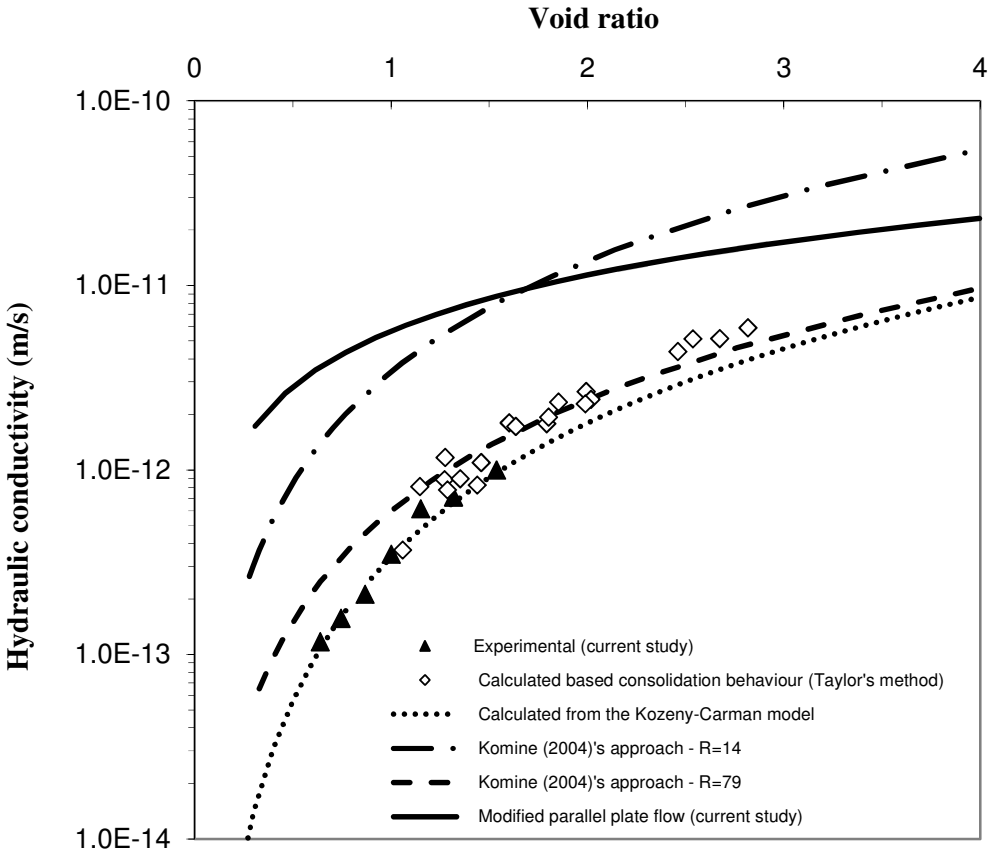

Figure 8.3 - Comparison of prediction models with experimentally determined hydraulic conductivity

The Kozeny-Carman model can be seen to best predict the hydraulic conductivity behaviour of compacted saturated bentonite, with a close agreement observed across the range of void ratios considered. The good agreement observed between the Kozeny-Carman model and the experimental results of this study supports the conclusions of Chapius and Aubertin (2003) that the Kozeny-Carman model is appropriate in determining the hydraulic conductivity of compacted saturated bentonite.

The hydraulic conductivities determined by Komine (2004)'s approach were found to differ significantly. This was primarily due to the R value used in calculation. Using R = 79, a

reasonable agreement was observed between the calculated hydraulic conductivity and the experimental results, although the calculated hydraulic conductivity was greater. The values calculated when $R = 14$ were significantly higher than the experimental results. The results calculated from Komine (2004)'s method were limited by the swelling potential tests conducted. Further tests were not considered as part of the experimental programme.

The model proposed in this study was not found to show good agreement with the experimental results obtained. The calculated hydraulic conductivity determined was greater than that observed experimentally. As previously discussed, a key limitation of the proposed model is that the effect of interacting diffuse double layers on water viscosity is not considered. The water within the inter-platelet region would be affected by forces from both platelets, not just the one considered in this study. The resultant effect of interacting diffuse double layer would be expected to reduce the hydraulic conductivity determined. Due to time constraints, this was not considered in the current study.

8.5 Concluding remarks

The hydraulic conductivity of compacted saturated bentonite was calculated from various hydraulic conductivity models. The Kozeny-Carman model was used to determine the hydraulic conductivity for a range of void ratios. Komine (2004)'s approach was used to calculate the hydraulic conductivity from the swelling pressures previously determined. A new model for determining the hydraulic conductivity of compacted saturated bentonite was proposed based on parallel plate theory. The proposed model was described in the chapter.

The available models were used to assess the hydraulic conductivity of compacted saturated MX80 bentonite. The Kozeny-Carman model was found to be in good agreement with the experimental results obtained. The hydraulic conductivities determined from Komine (2004)'s method varied significantly, due to the R value used in calculation. The calculated values were found to be in reasonable agreement with experimental values when R = 79, but were significantly larger when R = 14. The proposed model showed did not adequately assess the saturated hydraulic conductivity, and provided hydraulic conductivity values that were consistently greater than those measured. These differences were primarily attributed to the effect of the interacting diffuse double layer not being considered.

CHAPTER 9

CONCLUSIONS

The objective of this thesis was to (i) experimentally determine the saturated hydraulic conductivity of compacted bentonites and sand-bentonite mixtures used in geoenvironmental applications and (ii) to verify the applicability of various existing models used to assess the hydraulic conductivity for compacted bentonites.

A commercially available MX80 bentonite and Leighton Buzzard sand was used during the investigation. The properties of the bentonite including the grain size distribution, Atterberg limits, cation exchange capacity and specific surface area were determined from standard laboratory tests. Some differences were noted between the material properties of the

MX80 bentonite found in this study and those reported in the literature. The differences in the properties are attributed to the differences in the specific surface area and the cation exchange capacity, particularly the percentage of sodium.

The hydraulic conductivities of compacted bentonite specimens were determined for a dry density range of 1.088 to 1.664 Mg/m^3. The hydraulic conductivities of compacted sand-bentonite specimens prepared with 70% sand and 30% bentonite were determined for a dry density range of 1.584 to 1.778 Mg/m^3. The compaction dry densities of bentonite and sand-bentonite mixtures tested were similar to those considered in the literature for geoenvironmental applications.

A high capacity fixed ring modified swelling pressure cell was used during the hydraulic conductivity tests. The cell was similar to rigid-walled permeameters used previously in the literature for determining the hydraulic conductivity of compacted bentonite and sand-bentonite mixtures. The cell accompanied two high precision pressure-volume controllers that enabled the application of predetermined hydraulic gradients under constant head conditions.

The water inflow and outflow volumes were monitored by the pressure-volume controllers. The resolution of pressure and volume of the controllers used was 1 kPa and 1 mm^3 respectively. Fluorinated ethylene propylene pipes were used to connect the pressure-volume controllers to the hydraulic conductivity cell. Expansion of the inflow system due to applied water pressures between 45 and 1200 kPa was considered for calculating compatibility between inflow and outflow water volumes during hydraulic conductivity tests.

The compacted bentonite and sand-bentonite specimens were hydrated with distilled de-aired water. The swelling pressures developed during the hydration process were monitored. The hydraulic conductivity tests commenced once the swelling pressures were equilibrated. Pressure differentials (i.e. the differences in water pressures between the inflow and outflow sides) between 100 kPa and 1000 kPa were applied to the compacted specimens during the hydraulic conductivity tests. The applied hydraulic gradients varied between approximately 1250 and 12500.

For each specimen, the applied hydraulic gradient was increased to the maximum value and then decreased in a step-wise manner. At each applied hydraulic gradient, an equilibrium condition was considered to be reached when the water inflow and outflow rates were constant for a predetermined period of time. After each applied hydraulic gradient, fluid samples from the inflow and outflow reservoirs were analysed to explore (i) the type and amount of each cation expelled from the specimens and (ii) the influence of initial dry density and applied hydraulic gradient on the type and amount of exchangeable cations expelled.

The actual inflow water volumes were calculated based on the system expansions at various applied water pressures (i.e. applied hydraulic gradients). The hydraulic conductivities of the compacted bentonite and sand-bentonite specimens were calculated from Darcy's law.

The compressibility behaviour of compacted bentonite and sand-bentonite specimens was studied using a conventional oedometer. Compacted specimens were allowed to swell under an applied pressure of either 50 or 100 kPa. The specimens were step-wise loaded up to a vertical pressure of 800 kPa. Taylor's and Casagrande's methods were used to calculate the

coefficient of compressibility (C_v), from which the hydraulic conductivities could be calculated.

The gas permeability of compacted bentonite specimens prepared at the air-dry water content (8%) was experimentally determined. Nitrogen gas as used during the gas permeability tests. Specimens were prepared at a range of compaction dry densities and placed within the gas permeability cell. The initial pressure to which the tests were carried out was increase from 0.1 MPa to 1 MPa.

The saturated hydraulic conductivity of compacted bentonites was assessed using three existing models, such as the Kozeny-Carman model and the model proposed by Komine (2004). A model based on parallel plate flow was proposed in this thesis. The proposed model considered the viscosity of water in the inter-platelet region and its influence on the hydraulic conductivity of compacted saturated bentonites. The results from the proposed model were compared with the existing models. The results obtained from the various models were compared with the measured hydraulic conductivities of compacted bentonites.

Based on the findings reported in this thesis, the following conclusions are drawn.

1. During the hydraulic conductivity tests, the inflow volume of water to the compacted bentonite specimens was found to be greater than the outflow volume of water from the specimens. The difference between inflow and outflow water volumes was attributed to the expansion of the measuring system (the connecting pipes and the water reservoir). The correction of the inflow volume due to system expansion produced a closer correlation between inflow and outflow volumes.

2. The equilibrated inflow and outflow rates were found to be comparable for applied hydraulic gradients between about 1250 and 12500. Previous authors have typically considered either the inflow or the outflow rate when determining the hydraulic conductivity of compacted bentonite. This approach, however, has been reported to potentially introduce error (Chapius, 2012). The findings of this study indicated that the inflow rate was approximately equal to the outflow rate, and either can be used to calculate the hydraulic conductivity.

3. A linear relationship was noted between the hydraulic gradient and the hydraulic flux calculated from the constant flow rates (at the end of the hydraulic conductivity tests). This indicated that Darcy's law was valid for the range of hydraulic gradients considered, and is in good agreement with that generally reported in the literature.

4. The hydraulic conductivity of compacted saturated bentonite decreased as the compaction dry density increased. The measured hydraulic conductivity decreased from 1×10^{-12} m/s to 4×10^{-13} m/s with an increase in dry density from 1.088 to 1.664 Mg/m^3. The hydraulic conductivity test results in this study are in good agreement with those reported in literature for similar bentonites.

5. The hydraulic conductivity of compacted 70:30 sand-bentonite was found to be greater than the hydraulic conductivity of compacted sand-bentonite mixtures was found to decrease from 5×10^{-12} to 2×10^{-12} m/s as the dry density was increased from 1.584 to 1.779 Mg/m^3. The hydraulic conductivity test results are comparable to those reported in literature for similar compacted sand-bentonite mixtures prepared at the ratio considered in this study.

6. An expulsion of ions occurred during the hydraulic conductivity tests. The ions were found in both inflow and outflow fluid reservoirs. The expelled exchangeable cations (Ca^{2+}, Mg^{2+}, K^{+} and Na^{+}) were found to be less than about 6% from the compacted bentonite specimens. The percentage of exchangeable cations expelled was found to decrease as the compaction dry density of the bentonite increased. Limited studies on the expulsion of exchangeable cations from compacted bentonite during the application of a hydraulic gradient have been reported in the literature. The relatively low percentage of initial cations expelled from the specimen were found to not have an effect on the hydraulic conductivity determined through the testing programme.

7. The gas permeability of MX80 bentonite at air-dry water content was determined, and was found to decrease as the compaction dry density increased. For dry densities between 1.379 and 1.832 Mg/m^3, the gas permeability decreased from about 8×10^{-12} to 1×10^{-13} m^2. Limited studies exist within the literature at low volumetric water contents; the gas permeability of specimens with water contents less than 20% are of the order of magnitude of those determined in the current study.

8. The hydraulic conductivities of compacted bentonite calculated from the gas permeability results were found to be significantly greater than the measured hydraulic conductivities of the compacted saturated specimens. The differences between measured and calculated hydraulic conductivities were attributed to the swelling caused by physico-chemical forces affecting the flow of water in compacted saturated bentonite.

9. The hydraulic conductivities of compacted bentonite calculated from the Kozeny-Carman model were in good agreement with the measured hydraulic conductivities of compacted saturated bentonite. The hydraulic conductivities calculated from the model proposed by Komine (2004) were found to differ from the measured hydraulic conductivities.

10. The hydraulic conductivity model proposed in the study was not found to satisfactorily establish the hydraulic conductivity of compacted bentonite when compared with the measured hydraulic conductivities. The hydraulic conductivities determined from the proposed model were noted to be greater than those determined experimentally primarily due to assumptions made about the water viscosity in the model.

To further the research undertaken in the current study, a number of areas have been identified as requiring further research.

The chemical testing on the influent and effluent during hydraulic conductivity tests indicate that ions within the bentonite-water system can be expelled. However, the potential for ions to be expelled under long-term testing conditions has not been investigated. It is considered that further study on the long-term expulsion effects, in particular regarding the transport mechanisms controlling the expulsion of ions from the bentonite water system, may better inform the microstructure of the saturated bentonite, and the location of exchangeable cations.

Coupled processes are known to be present within the bentonite-water system. The presence of a hydraulic gradient across the specimen may lead to the development of additional coupled effects, such as streaming potential. Consideration of these effects can lead to a better understanding of the effect of hydraulic gradient, and the induced secondary potentials developed.

The proposed model for determining the hydraulic conductivity proposed in this study is limited by the determination of the inter-layer viscosity. While attempts to quantify the increased viscosity have been reported (Pusch and Yong, 2005), the combined effect of interacting diffuse double layers has not been fully captured. It is felt that refinement of the proposed model, taking into account this and other phenomena, will lead to better agreement with the hydraulic conductivity results determined experimentally.

References

Achari, G. Joshi R.C. Bentley L.R. and Chatterji S. (1999). Prediction of the hydraulic conductivity of clays using the electric double layer theory. *Canadian Geotechnical Journal*, 36, 783-792.

Ahn, H.-S. and Jo, H.Y., (2008). Influence of exchangeable cations on hydraulic conductivity of compacted bentonite. *Applied Clay Science* 44, 144–150

Al-Mukhtar, M., Qi, Y., Alcover, J-F. and Bergaya, F. (1990). Oedometric and water-retention behaviour of highly compacted unsaturated smectites. *Canadian Geotechnical Journal*, 36 (4), 675-684.

Almani, Z.A., Pathan, A.F.H. and Memon, A.A. (2013). Heavy metal diffusion through soft clay under high hydraulic gradients. *Mehran University Research Journal of Engineering & Technology*, 32(2), 307-318

Alonso, E.E., Olivella, S. and Arnedo, D. (2006). Mechanisms of gas transported in clay barriers. *Journal of Iberian Geology*, 32(2), 175-196.

Alther, G. (2004). Some practical observations on the practical use of bentonite. *Environmental and Engineering Geoscience*, 10(4), 347-359.

ASTM D 4943-08 (2008). Standard test methods for shrinkage factors of soils by the wax method.

ASTM E 104-85 (1998). Standard Practice for Maintaining Constant Relative Humidity by Means of Aqueous Solutions.

Bag, R. (2011). Coupled thermo-hydro-mechanical-chemical behaviour of MX80 bentonite in geotechnical applications. PhD thesis.

Baille, W., Tripathy, S. and Schanz, T. (2010). Swelling pressures and one-dimensional compressibility behaviour of bentonite at large pressures. *Applied Clay Science*, 48, 324-333.

Barbour S.L. and Fredlund, D.G. (1989). Mechanisms of osmotic flow and volume change in clay soils. *Canadian Geotechnical Journal*, 26, 551-562.

Bennett C.L, Tripathy S. and Thomas H.R. (2012). Wetting characteristics of compacted bentonites at large applied suctions. *Unsaturated Soils: Research and Applications*, 1, 229-234.

Benson C.H. and Daniel D.E. (1990). Influence of clods on hydraulic conductivity of compacted clay. *ASCE Journal of Geotechnical Engineering*, 111(8), 123 1-1248.

Bolt, G. H. (1956). Physico-chemical analysis of the compressibility of pure clays. *Géotechnique*, 6(2), 86–93.

Borgesson, L., Chijimatsu, M., Fujita, T., Nguyen, T.S., Rutqvist, J and Jing L. (2001). Thermo-hydro-mechanical characterisation of bentonite-base buffer material by laboratory tests and numerical back analyses. International Journal of Rock Mechanics and Mining Sciences, 38, 95–104

Borgesson, L., Johannesson, L. E. and Gunnarsson, D. (2003). Influence of soil structure heterogeneities on the behaviour of backfill materials based on mixtures of bentonite and crushed rock. *Applied Clay Science*, 23, 121–131.

Borgesson, L., Karnland, O. and Johannesson, L.E. (1996). Modeling the physical behaviour of clay barriers close to saturation. *Engineering Geology*, 41, 127-144.

Bouazza, A. (2002). Geosynthetic clay liners. *Journal of Geotextiles and Geomembranes*, 20(1), 3-17.

Bouazza, A. and Vangpaisal, T. (2003). An apparatus to measure gas permeability for geosynthetic clay liners. *Journal of Geotextiles and Geomembranes*, 21(2), 85-101.

Bouazza, A., Vangpaisal, T. and Jefferis, S. (2006). Effect of wet-dry cycles and cation exchange on gas permeability of geosynthetic clay liners. *Journal of Geotechnical and Geoenvironmental Engineering*, 132(8), 1001-1018.

Bourg, I. C., Sposito, G. and Bourg A.C.M. (2006). Tracer diffusion in compacted water-saturated bentonite. *Clays and Clay Minerals*, 54, 363.

Boynton S.S. and Daniel D.E. (1985). Hydraulic conductivity tests on compacted clay. *Journal of Geotechnical Engineering*, ASCE, 109(4), 465-478.

Bradbury M.H. and Baeyens B. (2003). Porewater chemistry in compacted re-saturated MX-80 bentonite. *Journal of Contaminant Hydrology*, 61, 329-338

BS 1377-2 (1990). Soils for civil engineering purposes. Part 2: Classification tests. *British Standards Institution*.

Bucher, F., and Müller-Vonmoos, M. (1989). Bentonite as a containment barrier for the disposal of highly radioactive waste. *Applied Clay Science*, 4(2), 157–177.

Carman P.C. (1937). Fluid flow through granular beds. *Institute of Chemical Engineers, London*. 15, 150-166.

Carman P.C. (1956). Flow of gases through porous media. *Butterworths Scientific Publications*, London.

Carrier III W.D. (2003). Goodbye, Hazen; Hello, Kozeny-Carman. *Journal of Geotechnical and Geoenvironmental Engineering*, 129(11): 1054-1056.

Cerato A. B. and A. J. Lutenegger (2002). Determination of surface area of fine grained soils by the ethylene glycol monoethyl ether (EGME) method. *ASTM Geotechnical Testing Journal*, 25 (3), 315-321.

Chan, H. and T C. Kenney (1973). Laboratory investigation of permeability ratio in New Liskeard varied soil. *Canadian Geotechnical.Journal*, 10(3), 453-472.

Chapuis R.P. (1989). Sand-bentonite liners: predicting permeability from laboratory tests. *Canadian Geotechnical Journal*, 27, 47–57.

Chapuis R.P. (1990). Sand–bentonite liners: field control methods. *Canadian Geotechnical Journal*, 27, 216–223.

Chapius, R. P. (2012). Predicting the saturated hydraulic conductivity of soils: a review. *Bulletin of Engineering Geology and the Environment*. 71 (3), 401 - 434.

Chapius, R.P. and Aubertin, M. (2003). On the use of the Kozeny-Carman equation to predict the hydraulic conductivity of soils. *Canadian Geotechnical Journal*, 2003, 40(3), 616-628

Cho W.J. Lee J.O. and Chun K.S. (1999). The temperature effects on hydraulic conductivity of compacted bentonite. *Applied Clay Science* 14, 47-58.

Choi, J.-W. and Oscarson, D.W. (1996). Diffusive transport through compacted Na- and Ca-bentonite. *Journal of Contaminant Hydrology*, 22, 189-202.

Dananaj, I., J. Frankovska, and I. Janotka. 2005. The influence of smectite content on microstructure and geotechnical properties of calcium and sodium bentonites. *Applied Clay Science*, 28, 223–232.

Daniel, D.E. (1989). A note on falling-headwater, rising tailwater permeability tests. *ASTM Geotechnical Testing Journal*, 12(4), 308-310.

Daniel, D.E. (1994). State-of-the-art: Laboratory hydraulic conductivity tests for saturated soils. *ASTM STP* 1142.

Daniel, D.E., Koerner, R.M., Bonaparte, R., Landreth, R.L., Carson, D.A., and Scranton, H.B. (1998). Slope stability of fourteen full-scale field test plots containing geosynthetic clay liners. *Journal of Geotechnical and Geoenvironmental Engineering*, 125(7), 628-637.

Darcy, H. (1856). Les fontaines publiques de la ville de Dijon. *V. Dalmont*, Paris, 590-594.

Davis, S.N. (1969). Flow through porous media. New York, Acadamic Press.

Delage, P., Howat, M. and Cui, Y.J. (1998). The relationship between suction and swelling properties in a heavily compacted unsaturated clay. *Engineering Geology*, 50(1), 31-48

Delage P., Marcial D., Cui Y.J. and Ruiz, X. (2006). Ageing effects in the compacted bentonite: a microstructure approach. *Géotechnique*, 56(4), 291-304.

Delage, P., Romero, E.E. and Tarantino, A. (2008). Recent developments in the techniques of controlling and measuring suction in unsaturated soils. *Proceeding of 1st European conference on Unsaturated soil*, Toll, D., Gallipoli, D., Wheeler, S. (eds), 33-52.

Dhir, R.M. and Byars, E.A. 1993. Pulverized fuel-ash concrete: intrinsic permeability. *ACI Materials Journal*. 90(6), 571-580.

Didier, G., Bouazza, A. and Cazaux, D. (2000). Gas permeability of geosynthetic clay liners. *Journal of Geotextiles and Geomembranes*, 18(2), 235-250.

Dixon, D.A. and Gray, M.N. (1985). The engineering properties of buffer material. *Technical report TR-350*, Underground Research Laboratory, Atomic Energy of Canada Limited, Pinawa MB, Canada.

Dixon D., Chandler, N., Graham J., and Gray M.N. (2002). Two large-scale sealing tests conducted at Atomic Energy of Canada's underground research laboratory: the buffer-container experiment and the isothermal test. *Canadian Geotechnical Journal*, 39: 503– 518.

Dixon, D.A., Graham, J. and Gray, M.N. (1999). Hydraulic conductivity of clays in confined tests under low hydraulic gradients. *Canadian Geotechnical Journal*, 36, 815-825.

Estes, R.K., Fulton, P.F., 1956. Gas slippage and permeability measurements. *Transactions of the American Institute of Mining and Metallurgical Engineers* 207(12), 338-342

Environment Agency (2011). Using geosynthetic clay liners in landfill engineering. Technical Report.

FEP Handbook, 2009. Available online at http://www.rjchase.com/fep_handbook.pdf (Accessed 21st February 2013).

Fleureau, J.M., Verbrugge, J.C., Huergo, P.J., Correia, A.G. and Kheirbek-Saoud, S. (2002). Aspects of the behaviour of compacted clayey soils on drying and wetting paths. *Canadian Geotechnical Journal*, 39, 1341-1357.

Fredlund D.G. and Rahadjo, H. (1993). Soil mechanics for unsaturated soils, John Wiley and Sons, Canada.

García-Gutiérrez, M., Cormenzana, J.L., Missana, T., Mingarro, M. and Molinero, J. (2006). Overview of laboratory methods employed for obtaining diffusion coefficients in FEBEX compacted bentonite. *Journal of Iberian Geology,* 32(1), 37-53.

Gardner, D.R. (2005). Experimental and numerical studies on the gas permeability of concrete. PhD thesis.

Gens, A., Guimaraes do N. L., Garcia-Molina, A., Alonso, E. E. (2002). Factors controlling rock-clay buffer interaction in a radioactive waste repository. *Engineering Geology*, 64, 297–308.

Gilbert, R.B., Fernandez, F. and Horsfield, D.W. (1996). Shear strength of reinforced geosynthetic clay liner. *Journal of Geotechnical Engineering*, 122(4), 259-266.

Grim, R.E. (1968). Clay mineralogy. 2nd ed. McGraw-Hill, New York.

Gunnerson, D., Borgesson, L., Keto, P., Tolppanen, P. and Hansen, J. (2004). Backfilling and closure of the deep repository. *SKB Technical Report*, TR-04-53.

CRC Handbook of Chemistry and Physics (1996), 77th ed. Lide, D.R., Ed.; CRC Press: Boca Raton, FL

Harrington, J.F. and Horseman, S.T. (1997). Gas migration in clay. In *PEGASUS - Project on the effect of gas in underground storage facilities for radioactive waste. Proceedings of a workshop, Mol, Belgium.* 28-29 May 1997.

Heilman, M.D., Carter, D.L. and Gonzalez, C.L. (1965). The ethylene glycol monoethyl ether (EGME) technique for determining soil-surface. *Soil Science*, 100(6), 409-413.

Horseman, S.T., Harrington, J.F., Sellin, P., 1999. Gas migration in clay barriers, *Engineering Geology*, 54, 139-149.

Iverson, B.V., Schjonning, P., Poulsen, T.G. and Moldrup, P. (2001). In-situ, on-site and laboratory measurements of soil air permeability: boundary conditions and measurement scale. *Soil Science*, 166, 97-106.

Japan Nuclear Cycle Development Institute (1999). H12: project to establish the scientific and technical basis for HLW disposal in Japan: supporting report 2 (respiratory design and engineering technology). Japan Nuclear Cycle Development Institute, Tokyo.

Jo H., Katsumi T,. Benson C.H. and Edil T. (2001). Hydraulic conductivity and swelling of non-prehydrated GCLs permeated with single-species salt solutions. *Journal of Geotechnical and Geoenvironmental Engineering* 127(7): 557-567.

Jo, H., Benson, C., Shackelford, C., Lee, J., and Edil, T. (2005). Long-term hydraulic conductivity of a non-prehydrated geosynthetic clay liner permeated with inorganic salt solutions. *Journal.of Geotechnical and Geoenvironmental Engineering,* 131(4),405-417.

Karnland, O., Olsson, S., Nilsson, U. and Sellin, P. (2007). Experimentally determined swelling pressures and geochemical interactions of compacted Wyoming bentonite with highly alkaline solutions. *Physics and Chemistry of the Earth*, 32, 275-286.

Kemper, W.D., Maasland, D.E.L. and Porter, L.K. (1964). Mobility of water adjacent to mineral surfaces. *Proceedings of the Soil Society of America*, 28(2), 164-167.

Kenney T. C., van Veen W. A., Swallow M. A. and Sungaila M. A. (1992). Hydraulic conductivity of compacted bentonite-sand mixtures. *Canadian Geotechnical Journal*, 29, 364-374.

Kleppe, J.H and Olson, R.E. (1985). Desiccation cracking of soil barriers. *Hydraulic barriers in soil and rock*, ASTM STP 874, 263-275.

Klinkenberg, L. J. (1941). The permeability of porous media to liquids and gases, *American Petroleum Institute*, *Drilling and Productions Practices*, 200–213.

Komine, H. and Ogata, N. (1994). Experimental study on swelling characteristics of compacted bentonite. *Canadian Geotechnical Journal*, 31(4), 478–490.

Komine, H. (2004). Simplified evaluation on hydraulic conductivities of sand-bentonite mixture backfill. *Applied Clay Science*, 26, 13-19.

Komine H. (2008). Theoretical equations on hydraulic conductivities of bentonite-based buffer and backfill for underground disposal of radioactive wastes. *Journal of Geotechnical and Geoenvironmental Engineering*, 134(4): 497-508.

Komine, H. (2010). Predicting hydraulic conductivity of sand-bentonite mixture backfill before and after swelling deformation for underground disposal of radioactive wastes. *Engineering Geology*, 114, 123-134.

Komine H. and Ogata N. (1999). Experimental study on swelling characteristics of sand-bentonite mixture for nuclear waste disposal. *Soils Foundation*, 39(2), 83–97.

Kozeny J. (1927). Ueber kapillare Leitung des Wassers im Boden. Sitzungsberichte Wiener Akademie, 136(2a): 271–306.

Krahenbuehe, F., Stoeckli, H.F., Brunner, F., Kahr, G and Muller-Vonmoos, M. (1987). Study of the water bentonite system by vapour adsorption, immersion calorimetry and X-ray techniques: micropore volumes and internal surface area, following Dubinin's theory. *Clay and Clay Minerals,* 22, 1-9.

Lai, T.M and Mortland, M.M. (1968). Cationic diffusion in clay minerals: orientation effects. *Clays and Clay Minerals*, 16, 129-136.

Laird D.A. (2006). Influence of layer charge on swelling of smectites, *Applied Clay Science*, 34, 74-87.

Lambe T. W. (1954). The Permeability of Fine-Grained Soils. Permeability of soils, *ASTM,STP*, 163, 55-67.

Lambe T.W. and Whitman R.V. (1969) Soil mechanics. John Wiley & Sons, New York.

Lee J. and Shackelford C.D. (2005). Impact of bentonite quality on hydraulic conductivity of geosynthetic clay liners. *Journal of Geotechnical and Geoenvironmental Engineering*, 131(1), 64–77.

Leroy, P., Revil, A., and Coelho, D. (2006). Diffusion of ionic species in bentonite, *Journal of Colloid and Interface Science*, 296, 248-255.

Li,X., Zhang, L.M and Fredlund, D.G. (2009). Wetting front advancing column test for measuring unsaturated hydraulic conductivity. *Canadian Geotechnical Journal*, 46(12), 1431-1445

Likos W.J. (2004). Measurement of crystalline swelling in expansive clay. *Geotechnical Testing Journal*, 27(6): 1-7

Lloret A. Romero E. Villar M.V. (2004) *FEBEX II Project Final report on thermo-hydromechanical laboratory tests.* Publicacion Tecnica ENRESA 10/04, Madrid, 180 pp.

Loll, P., Moldrup, P., Schjønning, P., & Riley, H. (1999). Predicting saturated hydraulic conductivity from air permeability: Application in stochastic water infiltration modelling. *Water Resources Research*, 35(8), 2387–2400.

Loiseau, C., Cui, Y.J and Delage, P. (2002). The gradient effect on the water flow through a compacted swelling soil. *Proc. 3rd Int Conf Unsaturated Soils, UNSAT'2002 Recife, Brazil, Balkema*, vol. 1, 395–400

Low P.F. (1980). The swelling of clay: II montmorillonites. *Soil Science Society of America Journal*, 44(4), 667-676.

Lutz J.F. and Kemper W.D. (1959). Intrinsic permeability of clay as affected by clay-water interaction. *Soil Science*. 88, 83-90.

Lydon, F.D. 1993. The relative permeability of concrete using nitrogen gas. *Construction and Building Materials*. Vol. 7, No. 4, pp.213-220.

Manjanna, J., Kozaki, T., and Sato, S. (2009). Fe(III)-montmorillonite: Basic properties and diffusion of tracers relevant to alteration of bentonite in deep geological disposal. *Applied Clay Science*, 43, 208-217.

Marcial, D., Delage, P. and Cui, Y.J. (2002). On the high stress compression of bentonites. *Canadian Geotechnical Journal*, 39, 812–820.

Martin, G.R. 1986. A method for determining the relative permeability of concrete using gas. *Magazine of Concrete Research*. Vol. 38, No. 135, pp.90-94.

Madsen, F.T. (1998). Clay mineralogical investigations related to nuclear waste disposal. *Clay and Clay Minerals* 33, 109-129.

Mata C., Romero E. and Ledesmana A. (2002). Hydro-chemical effects on water retention in bentonite-sand mixtures. *Proc. 3rd Int. Conf. on Unsaturated Soils*, UNSAT 2002,Vol. 1, pp. 283-288.

Mering, J. (1946). On the hydration of montmorillonite. Trans. Faraday Soc., 42, B205-B219.

Mesri, G. (1973). One dimensional consolidation of a clay layer with impeded drainage boundaries. *Water Resources Research*, 9(4), 1090-1093

Mesri, G. and Olsen, R.E. (1971). Consolidation characteristics of montmorillonite. Géotechnique, 21(4), 341–352.

Miller, R. H., and Low, P. F. (1963). Threshold gradient for water flow in clay systems. *Proceedings of the Soil Science Society of America*, 27(6), 605–609.

Miller, R. H., Overman, A. R., and Peverly, J. H. (1969). The absence of threshold gradients in clay-water systems. *Soil Science Society of America Proceedings,* 33(2), 183–187.

Mitchell, J.K. and Soga, K (2005). Fundamentals of soil behaviour. 3rd ed., John Wiley, New York.

Molera, M. and Eriksen,T. (2002). Diffusion of $^{22}Na^{+}$, $^{85}Sr^{2+}$, $^{134}Cs^{+}$ and $^{57}Co^{2+}$ in bentonite clay compacted to different densities: experiments and modeling. *Radiochimica Acta*: 90, 753-760.

Montes-H G., Duplay J., Martinez L. and Mendoza C. (2003). Swelling-shrinkage kinetics of MX80 bentonite. *Applied Clay Science*, 22, 279-293.

Montes-Hernandez, G., Duplay, J., Geraud, Y. and Martinez, L. (2006). Several textural properties of compacted and cation-exchanged bentonite. *Journal of Physics and Chemistry of Solids*, 67, 1769-1774.

Müller-Vonmoos, M. (1986). Bentonit und radioaktive Abfälle. *Neue Zürcher Zeitung* (Forschung und Technik)

Müller-Vonmoos, M., and Kahr, G. (1983). Mineralogische Untersuchungen von Wyoming Bentonit MX-80 und Montigel. Nagra Technischer Bericht 83-12.

Mundell, J.A. and Bailey, B. (1985). The design and testing of a compacted clay barrier layer to limit percolation through landfill covers. *Hydraulic Barriers in Soil and Rock*, ASTM STP 874, 246-262.

Muurinen, A. and Tournassat, C. (2011). Sorption and diffusion of Fe(II) in bentonite. *Posiva Working Report* 2011-09.

Nalluri, C. and Featherstone, R.E. (2001). Civil Engineering Hydraulics. Wiley-Blackwell; 4th Edition

Nirex (2005). Outline design for a reference repository concept for UK high level waste/spent fuel. Technical Note 502644.

Olivella, S. & Alonso, E. E. (2008). Gas flow through clay barriers. *Geotechnique*, 58(3), 157–176.

Olson R.E. and Daniel D.E. (1981) Measurement of the hydraulic conductivity of fine grained soils. *Permeability and Groundwater Contaminant Transport*. ASTM STP 746, 18-64.

Olsen H.W. (1962). Hydraulic flow through saturated clays. *In Proceedings of the 9th National Conference on Clays and Clay Minerals,* pp. 131–160.

Olsen, H. W. (1969). Simultaneous fluxes of liquid and charge in saturated kaolinite. *Proceedings of the Soil Society of America,* 33(3), 338-344.

Oscarson, D.W. (1994). Surface diffusion: is it an important transport mechanism in compacted clays? *Clay and Clay Minerals*, 42(5), 534-543.

Petrov, R.J., Rowe, R.K., Quigley, R. M. (1997). Selected factors influencing GCL hydraulic conductivity. *Journal of Geotechnical and Geoenvironmental Engineering*, 123(8), 683-695.

Prikryl, R., Ryndova, T., Bohac, J. & Weishauptova, Z. (2003). Microstructures and physical properties of 'backfill' clays: comparison of residual and sedimentary montmorillonite clays. *Applied Clay Science*, 23, 149-156.

Pusch, R. (1982). Mineral-water interactions and their influence on the physical behaviour of highly compacted Na bentonite. *Canadian Geotechnical Journal*, 19, 381-387.

Pusch, R. (1999). Microstructural evolution of buffers. *Engineering Geology*, 54, 33-41.

Pusch, R. (2001). The microstructure of MX-80 clay with respect to its bulk physical properties under different environmental conditions. *SKB Technical Report, TR-01-08*.

Pusch, R., Ranhagen, L. and Nilsson., K. (1985). Gas migration through MX80 bentonite. *SKB Technical Report,* TR-85-36.

Pusch R, and Schomburg, J. (1999). Impact of microstructure on the hydraulic conductivity of undisturbed and artificially prepared smectite clay. *Engineering Geology*, 54, 167–172.

Pusch R. and Yong R.N. (2006). Microstructure of smectite clays and engineering performance. Taylor & Francis, London. pp. 94–97.

Rao N.S. and Mathew P.K. (1995) Effect of exchangeable cations on hydraulic conductivity of marine clay. *Clays and Clay Minerals*. 43(4), 433 - 437.

Riley, H. and Ekeberg, E. (1989). Ploughless tillage in large-scale trials: studies of soil chemistry and physical properties. *Norsk Landbrugsforskning*, 3, 107-115.

Romero E., Gens A. and Lloret A. (2003). Suction effects on a compacted clay under non-isothermal conditions. *Géotechnique*, 53(1), 65-81.

Ross, C and Shannon, E.V. (1926). The minerals of bentonite and related clays and their physical properties. *American Ceramic Society*, 91,77-96.

Rushing, J. A., Chaouche, A.and Newsham,K.E. (2004). A mass balance approach for assessing basin-centered gas prospects: Integrating reservoir engineering, geochemistry and petrophysics, in *J. M. Cubitt, W. A. England, and S. Larter, eds., Understanding petroleum reservoirs: Toward an integrated reservoir engineering and geochemical approach: Geological Society (London) Special Publications*, 237, p. 370–390.

Saiyouri, N., Hicher, P. Y. and Tessier, D. (1998). Microstructural analysis of highly compacted clay swelling. *Proceedings of 2nd international conference on Unsaturated Soils*, Beijing, 1, 119–124.

Saiyouri, N., Hicher, P. Y. and Tessier, D. (2000). Microstructural approach and transfer water modelling in highly compacted unsaturated swelling clays. *Mechanics of Cohesive Frictional Material*, 5, 41–60.

Saiyouri N, Tessier, D. and Hicher P.Y. (2004). Experimental study of swelling in unsaturated compacted clays. *Clay and Clay Minerals*, 39, 469-479.

Samper, J., Zheng, L., Montenegro, L., Fernandez, A.M. and Rivas, P. (2008). Coupled thermo-hydro-chemical models of compacted bentonite after FEBEX in situ test. *Applied Geochemistry*, 23, 1186-1201.

Sato, K. 1971. On an effect of absorbing water for micro-seepage. *Journal of Japan Society of Civil Engineers*, Vol. 187, 67-77.

Sato, T., Watanabe, T., and Otsuka, R. (1992)/ Effect of layer charge, charge location, and energy change on expansion properties of dioctahedral montmorillonites. *Clays and Clay Minerals*, 40, 103-l13.

Sauzeat E, Villieras T F, Francois M, et al. (2001). Characterisation mineralogique, cristallochimique et textural de l'argile MX80 (in French).

Schanz, T. and Tripathy, S. (2009). Swelling pressure of a divalent-rich bentonite: Diffuse double-layer theory revisited. *Water Resources Research*, 45

Schanz, T., Khan, M.I. and Al-Badran, Y. (2013). An alternative approach for the use of DDL theory to estimate the swelling pressure of bentonites. *Applied Clay Science*, in press.

Shackelford, C.D. and Daniel, D.E. (1991). Diffusion in saturated soil. *American Society of Civil Engineering*, 117(3)

Shackelford, C. D. and Javed, F. (1991). Large-scale laboratory permeability testing of a compacted clay soil. *Geotechnical Testing Journal*, 14(2), 171-179.

Shackelford, C.D., Benson, C.H., Katsumi, T., Edil, T.B. and Lin, L. (2000). Evaluating the hydraulic conductivity of GCLs permeated with non-standard liquids. *Geotextiles and Geomembranes*, 18, 133-161.

Shainberg, I. and Kemper, W. D. (1966) Electrostatic forces between clay and cations calculated and inferred from electrical conductivity: *Clays & Clay Minerals* 14, 117-132.

Siemens, G. and Blatz, J.E. (2007). Development of a hydraulic conductivity cell apparatus for bentonite soils. *Canadian Geotechnical Journal*, 44, 997-1005.

Singh P. N. and Wallender W. W. (2008). Effects of Adsorbed Water Layer in Predicting Saturated Hydraulic Conductivity for Clays with Kozeny–Carman Equation. *Journal of Geotechnical and Geoenvironmental Engineering,* 134(6), 829.

Singh, R.M. (2007). An Experimental and Numerical Investigation of Heat and Mass Movement in Unsaturated Clays. PhD Thesis.

Sivapullaiah P. V. Sridharan A. and Stalin V. K. (2000). Hydraulic conductivity of bentonite-sand mixtures. *Canadian Geotechnical Journal*, 37, 406–413.

SMC Pneumatics Tubes and Fittings Information Sheet. Available online at http://www.smcpneumatics.com/pdfs/smc/70FITTING.pdf (Assessed on March 3rd 2013).

Sridharan, A. and Jayadeva, M.S. (1982). Double layer theory and compressibility of clays. *Géotechnique*, 32 (2), 133– 144.

Sridharan A., Rao, A.S. and Sivapullaiah P.V. (1986). Swelling pressure of clays. *ASTM Geotechnical Testing Journal*, 9(1), 24-33.

Stewart D.I., Studds P.G. and Cousens T.W. (2003). The factors controlling the engineering properties of bentonite-enhanced sand. *Applied Clay Science* 23, 97-110.

Studds P.G., Stewart D.I., and Cousens T.W. (1998). The effects of salt solutions on the properties of bentonite-sand mixtures. *Clay and Clay Minerals*, 33, 641-660.

Sun, A., Cui, H.B. and Sun W.J. (2009). Swelling of compacted sand bentonite mixtures. *Applied Clay Science*, 43, 485-492.

Swartzen-Allen, S.L. and Matijevic, E. (1974). Surface and Colloid Chemistry of clays. *Chemical Reviews*, 74(3), 385-400.

Tadza, M.Y.M. (2011). Soil-water characteristic curves and shrinkage behavior of highly plastic clays: An experimental investigation. PhD thesis.

Tanai, K., Kanno, T. and Gallé, C. (1997). Experimental study of gas permeabilities and breakthrough pressures in clays. In: Scientific *Basis For Nuclear Waste Management Boston* (eds W.J. Gray And I.R. Triay), MRS Symposia Proceeding Vol. 465,1003–1010.

Tang, A.M., Cui, Y.J. and Le, T.T. (2008). A study on the thermal conductivity of compacted bentonites. *Applied Clay Science*, 41, 181-189.

Thomas, H.R., Rees, S.W. and Sloper, N.J. (1998). Three-dimensional heat, moisture and air transfer in unsaturated soils. *International Journal of Numerical and Analytical Methods in Geomechanics*, 22(2), 75-95.

Thomas, H.R., Cleall, P.J., Chandler, N., Dixon, D. and Mitchell, H.P. (2003). Water infiltration into a large-scale in-situ experiment in an underground research laboratory. *Géotechnique*, 53 (2), 207–224.

Tien. Y.M., Wu, P.L., Chuang, W.S and Wu, L.H. (2004). Micromechanical model characteristics of bentonite-sand mixtures. *Applied Clay Science*, 26, 489-498.

Torstenfelt, B., Andersson, K., Kipatsi, H., Allard, B. and Olofsson, U. (1982). Diffusion measurements in compacted bentonite, sodium bentonite. *Scientific Basis for Nuclear Waste Management* -/V, Elsevier, p. 295.

Tripathy, S. and Schanz, T. (2007). Compressibility behaviour of clays at large pressures. *Canadian Geotechnical Journal*, 44, 355-362.

Tripathy S., Sridharan A. and Schanz T. (2004). Swelling pressures of compacted bentonites from diffuse double layer theory. *Canadian Geotechnical Journal*, 41, 437-450.

Tripathy, S., Kessler, W. and Schanz, T. (2006). Determination of interparticle repulsive pressures in clays. *From Proceedings of the International Conference on Unsaturated Soils*, Arizona, United States of America.

van Olphen, H. (1963). An Introduction to Clay Colloid Chemistry: For Clay Technologists, Geologists and Soil Scientists. Wiley, New York.

Verwey, E.J.W. and Overbeek, J.Th.G. (1948). Theory of the stability of lyophobic colloids. Elsevier, Amsterdam.

Villar, M. (2005). Infiltration tests on a granite/bentonite mixture: Influence of water salinity. *Applied Clay Science*, 31, 96-109.

Villar, M. (2007). Water retention of two natural compacted bentonites. Clays and Clay Minerals, 55(3), 311-322.

Villar, M. and Gomez-Espina (2009). Report on thermo-hydro-mechanical laboratory tests performed by CIEMAT on FEBEX bentonite 2004-2008.

Villar, M.V. and Lloret, A. (2004). Influence of temperature on the hydro-mechanical behaviour of a compacted bentonite. *Applied Clay Science*, 26, 337-350.

Villar M.V. and Lloret A. (2007) Influence of dry density and water content on the swelling of a compacted bentonite. *Applied Clay Science*, 39, 38-49.

Watabe, Y., Yamada, K. and Saitoh, K. (2011). Hydraulic conductivity and compressibility of mixtures of Nagoya clay with sand or bentonite. *Geotechnique*, 61(3), 211-219.

Yong, R.N. (1999). Soil suction and soil-water potentials in swelling clays in engineered clay barriers. *Engineering Geology*, 54, 3-13.

Young, W.C. and Budynas, R.G. (2002). Roark's Formulas for Stress and Strain. McGraw-Hill; 7th Revised edition.

Zimmie, T.F., LaPlante, C.M. and Bronson, D. (1992). The effects of freezing and thawing on the permeability of compacted clay landfill covers and liners. *Environmental Geotechnology*, MA Usmen and Y.B, Acar (Eds), Balkema, Rotterdam, 213-217.